Investigating the role of ERp18 during Activation of UPR sensor ATF6α

Arvin Shedrach Pierre MSc (dist.)

Supervised by Profs Neil Bulleid and Cheryl Woolhead

Submitted toward fulfilment of the requirements for a degree of

Doctor of Philosophy (PhD) at the

School of Molecular Biosciences

College of Medical Veterinary and Life Sciences

University of Glasgow

March 2023

Abstract

Proteins destined for the cell surface membrane or secretion enter the secretory pathway via the ER. As the gateway to the secretory pathway, the endoplasmic reticulum is responsible for the folding and maturation of proteins to the native functional conformation. Physiological or pathological changes can create an imbalance between the protein folding load and capacity of the ER, a condition known as ER stress. The ER hosts stringent quality control mechanisms to maintain a suitable environment for the faithful folding of proteins. One such mechanism, the unfolded protein response (UPR), is primarily adaptive and maintains homeostasis by regulating translational and transcriptional networks that increase the folding capacity of the ER while reducing the burden. However, when ER stress persists the UPR can engage apoptotic mechanisms. Thus, unresolved ER stress can be deleterious and contributes to pathogenesis of diseases including neurodegenerative diseases, diabetes and cancers.

Transmembrane proteins Ire1α, PERK, and ATF6α mediate the UPR networks by detecting and responding to ER stress. These parallel pathways regulate pro-survival outcomes during acute ER stress. However, during chronic stress, Ire1α and PERK direct apoptotic outcomes frequently associated with disease. Presently, our understanding of the mechanisms of activation of Ire1α and PERK exceed that of ATF6α. Thus, there is ample room to increase our understanding of the mechanisms of ATF6α activation and function to exploit the pro-survival outcomes in the context of disease pathology.

ATF6α is repressed by interaction with BiP as part of regulatory complex. In response to ER stress, release from BiP and reduction of lumenal cysteine residues prelude its exit from the ER. Activation is achieved through trafficking to the Golgi where intramembrane proteolysis by S1P and S2P releases an active transcription factor that regulates transcription of target genes at the nucleus. Some aspects of ATF6α regulation remain unclear. There are three oligomeric states of ATF6α; a monomer and two dimers, but their contributions toward regulation or activation are yet to be elucidated. Modulation of ATF6α redox status is important for activation however, the exact role it plays remains unclear. Also unclear, is the role of ERp18, a small PDI-like protein which can reduce ATF6α and regulates trafficking by an unknown mechanism.

This thesis aimed to investigate how redox modulation contributes to the activation of ATF6α and identify roles for the different oligomeric states. In doing so, we interrogate ERp18 reductase activity to understand the mechanism by which it regulates trafficking. Finally, we investigate the contributions of putative binding residues S136 and T137 to ERp18 reductase activity. Our results showed that, during the initial stages of activation, the oligomeric status of ATF6α shifts from monomer to a disulfide stabilised dimer, designated 467D, in response to ER stress. This change was evaluated based on the relative abundance of the two redox forms in stressed compared to unstressed cells. We also showed that this dimer trafficked to the Golgi where S1P cleavage liberated dimeric lumenal domain. By overexpressing ERp18, we showed that it antagonised the formation of the dimer by reducing the interchain disulfide thereby regulating ATF6α trafficking to the Golgi. Mutation of Tyrosine-137 to Threonine (Y137T) within the proposed binding peptide of ERp18 affected its activity reductase activity in vitro but not in vivo. The S136D mutation had no discernible effect on ERp18 activity.

Our findings revealed that, following reduction of ATF6α cysteines, redox dependent dimerisation and ERp18 activity function as additional regulatory mechanisms in the early stages of ATF6α activation. From these findings we proposed a model in which the monomer is engaged during retention while 467D is involved in trafficking which is policed by ERp18 reduction. These findings have contributed to the understanding of ATF6α activation but also allude to further aspects of regulation that are yet to be elucidated.

Dedication

Dedicated to my late father Francis Anthony Christopher Pierre. Dad, my earliest memories of you are of us sitting at the dinner table at our old home in backstreet. That was the start of what translated into your tangible and unwavering support in all my endeavours right up to my decision to start a PhD. You created the foundation for all of my successes, and I dedicate them all to you. Though you are not physically here to celebrate with me, I know that you are eternally proud, even as I am eternally grateful.

Table of Contents

List of Tables

List of Figures

Acknowledgement

I am finally here! It has been a long journey getting through this phase of my research journey. Though difficulties arose from the hurricanes, Yorkers, and Googlies that life sent my way, I must say that I really enjoyed doing my PhD and I am grateful to be at this point. I consider myself extremely fortunate to have had support from a great number of persons at defining moments throughout my journey.

Firstly, I would like to thank the creator for giving me life, strength, and good health even amid a global pandemic. Many thanks to my parents Catherine and (the late) Francis Pierre for their eternal unwavering support in all my academic endeavours up to and including this PhD; you did well. And to the rest of my family; Japheth, Shem, Ava, Akim, Nerissa, Shemar, Jaiden, and Keisha, my co-workers at the T.A. Marryshow Community College, members of my church, Project Friends and Zamar who, in some way, supported me; I am forever grateful. It would be remiss of me not to thank some of my former teachers, at the Boca Secondary School, who were instrumental in establishing a sound academic foundation; Mr Martin Mitchell & Mrs. Sarona Abraham (former form teachers), Mr. Godfrey Lewis who cultivated my appetite for science, Mrs Pauline St. Paul (vice principal) and Mr. Victor Antoine (Principal) who recognised and nurtured my abilities.

Thanks to my supervisory team; Profs Neil Bulleid & Cheryl Woolhead and Dr Ojore Oka for giving me the opportunity to work on this project and for your tremendous support and guidance through my academic and my personal endeavours and trials. Neil, thanks for your mentorship and guidance within and out with the lab. I am fortunate to have benefited from your consistent outpouring of profound knowledge and experience. It was extremely beneficial to be able to knock on your door at any time with my questions. You always provided comprehensive and timely feedback especially with my writing assignments. Such a supervisory experience made it easy to enjoy the process of learning research. Special thanks to Ojay, my line manager, who also went above and beyond to keep me grounded being a mentor, counsellor, confident and friend. To the rest of the Bulleid lab, thanks for lending your expertise whenever I needed it. Thank you to other members of the academic and

administrative staff for your support. Thanks to MSc students Haoyi Wang, Adil Talati and Yuntian Wang who assisted with the insulin assay. Also, thanks to Paola Asprilla for your intangible contribution in supporting my research and mental health.

Thanks to following for scholarships and funding awards that made my study possible; the University of Glasgow and the college of MVLS, the diabetes association of Grenada and other funding bodies. And to everyone who supported me on this journey, thank you. You have cemented your place in my memories, and this is your victory as much as it is mine.

Author's Declaration

I declare that the work presented in this thesis is my own, that any contribution from others have been clearly indicated and referenced and that the work has not been otherwise submitted for any other academic qualification at the University of Glasgow or elsewhere.

Arvin Shedrach Pierre

March 2023

Definitions/Abbreviations

AD: Alzheimer’s disease

ADP: adenosine diphosphate

ADP: Adenosine diphosphate

ALS: Amyotrophic lateral sclerosis

AMS: 4-acetamido-4′-maleimidylstilbene-2,2′-disulfonic acid

APP: amyloid precursor protein

ASK1: apoptosis-signal-regulating kinase

ATF4: activating transcription factor 4

ATF6: activating transcription factor 6

ATP: adenosine triphosphate

ATP: Adenosine triphosphate

Aß: ßeta-amyloid

Baf A1: Bafilomycin A1

Bcl-2: B-cell lymphoma 2

BH3 - Bcl-2 homology domain 3

BiP: Immunoglobulin heavy-chain binding protein

BZIP: basic leucine zipper

CGN: cis-Golgi network

CNS: central nervous system

COPII: coat protein II

CSM: cell surface membrane

DCI: 3,4-dichloroisocoumarin

DMEM: Dulbecco's Modified Eagle Medium

DNA: Deoxyribonucleic acid

DSP: dithiobis succinimidyl propionate

DSP: dithiobis succinimidylpropionate

DTT: Dithiothreitol

DTT: dithiothreitol

EDTA: Ethylenediaminetetraacetic acid

EIF2α: α-subunit of eukaryotic initiation factor 2

ER: endoplasmic reticulum

ER: endoplasmic reticulum

ERAD: ER associated degradation

ERES: ER exit sites

ERGIC: ER-to-Golgi intermediate compartment

ERO1: Endoplasmic reticulum oxidase 1

ERp18: endoplasmic reticulum protein 18

ERSE: ER stress response element

ERSE: ER stress response elements

GLS: Golgi localisation signal

Hsp: heat shock protein

IMAC: immobilized metal affinity chromatography

IRE1: inositol requiring enzyme 1

KO: knockout

LAP: Lamin-associated proteins

LB: Lewy bodies

LD: lumenal domain

LN: Lewy neurites

MALDI-TOF: Matrix Assisted Laser Desorption/Ionization- Time of Flight

MANF: Mesencephalic astrocyte-derived neurotrophic factor

MAPK: mitogen activated kinases

NBD: nucleotide binding domain NEI: nucleotide exchange inhibitor

NEM: N-Ethylmaleimide

NF-Y: nuclear transcription factor

ORFS: Open reading frames

OST: oligosaccharyltransferase

PD: Parkinson’s disease

PDI: protein disulfide isomerase

PDIA5: protein disulfide isomerase A5

PDI-like proteins

PERK: PKR-like ER kinase

PROSPER: PROtease substrate SPecificity server

QC: Quality control

Rbd: Rhomboid

RIDD: regulated Ire1-dependent decay

Rip: regulated intramembrane proteolysis

RNA: Ribonucleic acid

ROS: reactive oxygen species

S1P: site 1 protease

S1P: site-1- protease

$S1P_i$: S1P inhibitor

S2P: site-2-protease

SBD: substrate binding domain

SDS: sodium dodecyl sulfate

SERCA: Sarco/endoplasmic reticulum Ca2+-ATPase

SREBP: sterol regulatory element-binding protein

TAD: transactivation domain

TBS: tris buffered saline

TCEP: tris 2-carboxyethyl phosphine

TG: thapsigargin

TGN: trans-Golgi network

TNBC: triple negative breast cancer

TPCK: tosyl phenylalanine chloromethyl ketone

TRAF2: tumour necrosis factor receptor associated 2

TrxR1: thioredoxin reductase 1

UPR: unfolded protein response

XBP1: X-box-binding protein 1

XBP1: X-box-binding protein 1

XBP1s: spliced X-box-binding protein 1

α Syn: α-Synuclein

Chapter 1. Introduction

Proteins, a major class of biomolecules, are important to correct cellular function. They are functionally diverse and can provide structure, participate in biochemical reactions, contribute to communication and signalling and immunity, regulate pH and fluid balance and can act as energy storage. The diversity of function directly relates to differences in structural design. While the manufacturing process is universal, the site of protein manufacture, cytoplasm or endoplasmic reticulum (ER), is largely determined by the destination of the protein. Quality control is an important feature of the manufacturing process given the close relationship between structure and function. This work focuses on aspects of the quality control mechanisms involved in the manufacture and export of proteins in the secretory pathway.

1.1 The secretory pathway

1.1.1 Overview

A significant proportion of proteins that are synthesised within the cell is targeted to the ER, the entry point to the secretory pathway. This includes proteins that are to be secreted into the extracellular milieu, embedded in the cell surface membrane (CSM) or transported to other intracellular compartments (Kaufman 1999). In addition to the rough endoplasmic reticulum (rough ER), the pathway includes the ER-to-Golgi intermediate compartment (ERGIC) and the Golgi. Each compartment contains factors to execute specific tasks which includes chaperones, foldases and factors involved in the sorting, packaging and transportation of cargo (Farhan and Rabouille 2011).

Intercompartment trafficking is an important and highly regulated process that ensures that proteins arrive to their intended final destinations. Differential coating of transport vesicles helps to regulate specificity. Proteins leaving the ER *en route* to the Golgi are normally packaged into vesicles coated with COPII proteins. Cargo moving from the Golgi to the CSM are differentially coated to distinguish them from cargo destined for the ER and endo-lysosomes which are coated with COP I and clathrin, respectively (Ford, Parchure et al. 2021) (Figure 1-1). These proteins enter the secretory pathway via the ER.

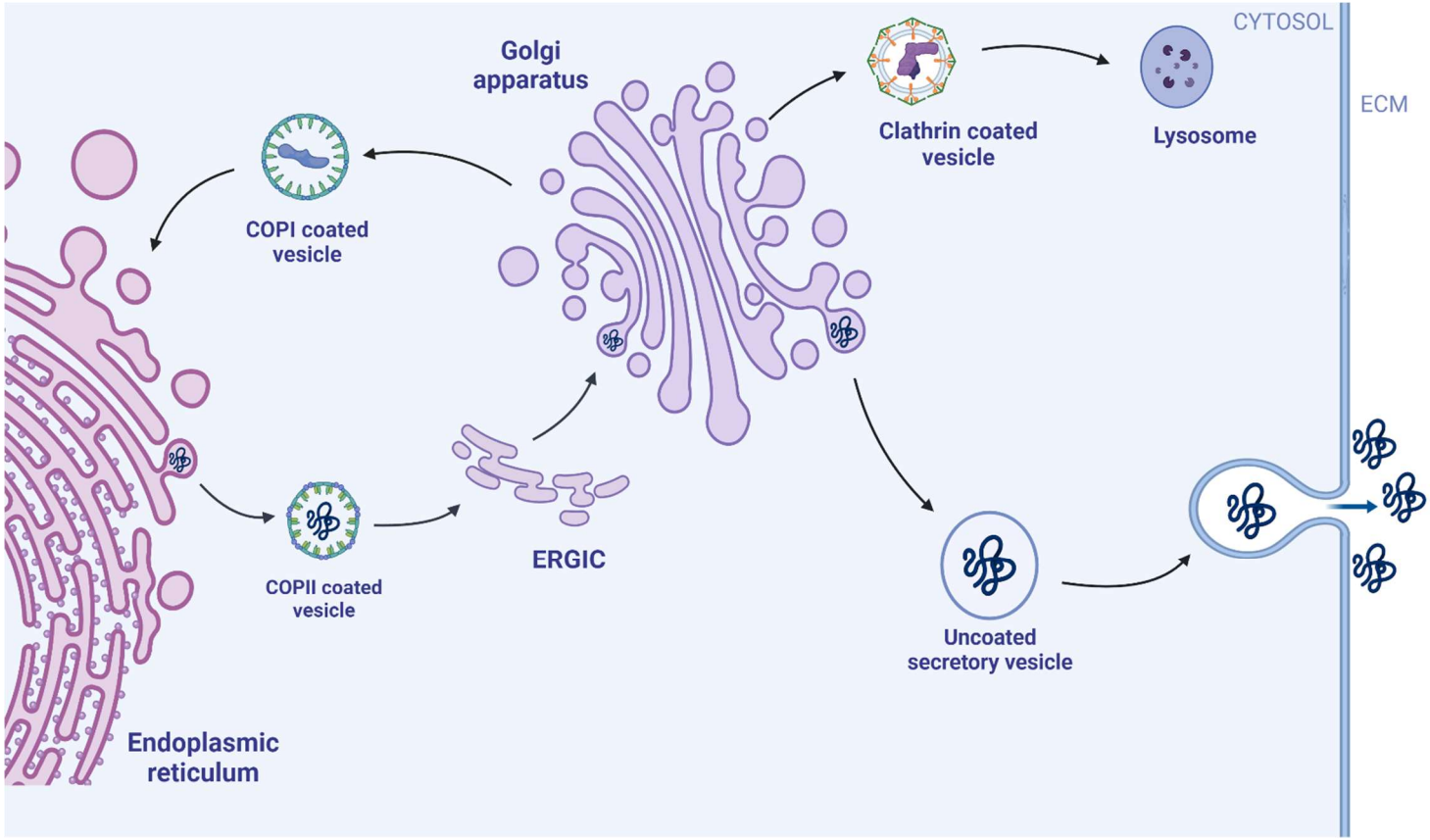

Figure 1-1 Transport of proteins along the secretory pathway.
Proteins synthesised in the ER are packaged into COPII coated vesicles and transported to the Golgi via the ERGIC. From the Golgi, they are packaged into uncoated vesicles to be secreted into the extracellular milieu. These vesicles are distinct from COPI coated vesicles which carry cargo from Golgi to ER and clathrin-coated vesicles which carry cargo to the lysosomes (Created with BioRender.com).

1.1.2 The Endoplasmic Reticulum

1.1.2.1 Structure and function of the ER

The ER is an extensive network of cisternae and membranous tubules that extend throughout the cytoplasm and are contiguous with the nuclear membrane. Despite continuity of the membrane system, the presence of unique proteins, such as Lamin-associated proteins 1 and 2 (LAP1 and 2), associated with the inner nuclear envelope defines it as a functionally distinct domain (Holmer and Worman 2001, Voeltz, Rolls et al. 2002). The ER contributes to various functions within the cell such as protein synthesis, lipid synthesis and storage, calcium storage and regulation, glucose and xenobiotic metabolism (Wilson and Hunt 2002, Rana 2020). The ER is also integrated into cellular homeostatic response mechanisms and maintains communication with various other organelles, such as the Golgi, endosomes, mitochondria, peroxisomes and lysosomes, through contact sites. These interactions feedback into essential roles to regulate function or to inform interactions with the cytoskeleton that can regulate ER distribution and dynamics (Voeltz, Rolls et al. 2002). Contact sites with the mitochondria, known as mitochondria-associated membranes (MAMs), create a structural communication link between the organelles to regulate ER Ca^{2+} homeostasis and integrate signalling to control cell survival mechanisms (Hayashi, Rizzuto et al. 2009).

Ultra-structurally, the ER is divided into the smooth ER (SER), which is more convoluted and tubular in structure, and rough ER (RER), which is more sheetlike and granular in appearance. As with the nuclear envelope, integral proteins associated with the smooth and rough ER define their physical and functional division into distinct domains. Given that lipid synthesis is a main function of the smooth ER, it is responsible for maintaining lipid membranes. Thus, the ER houses the sterol regulatory element-binding protein (SREBP) family involved in maintaining lipid homeostasis and the enzymes and other proteins involved in the biogenesis of components such as membrane phospholipids (Iddon, Wilkinson et al. 2001, Fagone and Jackowski 2009).

The major function of the rough ER is that of protein biogenesis, folding, modification, and export. This functional domain is primarily defined by the

presence of ribosomes, giving it a grainy appearance. Additionally, the presence of the Sec61 translocon facilitates translocation of newly synthesised polypeptides into the rough ER while a network of folding enzymes and quality control systems integrate to execute protein folding (Chen, Novick et al. 2013).

1.1.2.2 Protein biogenesis and folding in the rough ER

Derived from the nucleotide sequence in DNA, the linear sequence of amino acids must fold into a specific 3- dimensional shape to give rise to a functional protein. Based on the evidence that denatured proteins can be refolded in vitro, this process was thought to be completely spontaneous (Anfinsen 1973). However, it is well established that under physiological conditions in the ER, this process is accomplished with the assistance of molecular chaperones, chaperonins and protein folding enzymes (Hartl 1996, Kim, Hipp et al. 2013).

Folding of nascent polypeptides begins co-translationally at the rough ER but some proteins require various post translational modifications to completely fold. Ribosomes convert the information encoded in mRNA into the primary sequence of the protein. This process, known as translation, is initiated at ribosomes located in the cytoplasm. However, once the signal peptide, an N-terminal sequence of approximately 25 amino acids, is translated, it engages the signal recognition particle which targets the nascent chain and its attached ribosome(s), known as the ribosome-nascent chain complex, to the ER membrane (Ellgaard, McCaul et al. 2016). The presence of these ribosomes at the membrane gives the rough ER its characteristic grainy appearance.

As the nascent chain enters the lumen via the Sec61 translocon, the signal peptide is recognised and cleaved by the signal-peptidase complex. Chaperones will engage exposed hydrophobic sequences to shield them from the crowded hydrophilic ER environment, prevent aggregation and direct folding toward functional tertiary or quaternary conformations through modifications such as disulfide bond formation and N-glycosylation, among others.

1.1.2.3 Disulfide bond formation

The ER maintains a relatively oxidising environment which accommodates the introduction of disulfide bonds to stabilise the tertiary and quaternary structure of proteins and thus are critical to the final native conformation. These bonds are derived as a result of a covalent linkage between the sulfur atoms of two cysteine residues. Any two cysteines can potentially form a disulfide, therefore the formation of non-native disulfides, i.e., those not normally present in the correctly folded functional protein, is possible. Thus, disulfide formation begins co-translationally, but frequently involves the formation of non-native disulfides which must be resolved post-translationally for successful folding.

Oxidative protein folding involves different types of reactions namely, disulfide exchange (or oxidation), reduction and isomerisation. These reactions are catalysed by oxidoreductases of the protein disulfide isomerase (PDI) family which consists of one or more characteristic CXXC active site motifs each contained within a thioredoxin fold (Okumura, Kadokura et al. 2015). Cysteine residues within the active site of the enzymes facilitate the transfer of electrons to the substrate, in the case of reduction, or from the substrate during disulfide exchange.

1.1.2.4 PDI family

Many members of the PDI family have been identified which are involved in various functions within the ER (Bulleid and Ellgaard 2011). The founding member, PDI, is well characterised and has been shown to display chaperone activity in addition to disulfide exchange and isomerisation (Bulleid and Ellgaard 2011). It contains two catalytic thioredoxin like domains, **a** & **a'**, both containing a CGHC active site. In addition, two non-catalytic domains, **b'** and **b**, are responsible for substrate binding and structural integrity, respectively. The **a**, **a'** and **b** domains are required for disulfide exchange and isomerisation reactions (Ellgaard and Ruddock 2005). While some PDI enzymes exhibit broad substrate specificity, others are more restricted. Intrinsic factors affecting functional specificity within the family include the redox potential, location, and number, of CXXC active sites. Functional specificity may also be modulated by extrinsic factors such as interacting partners (Okumura, Kadokura et al.

2015). Despite this, there is significant functional redundancy within the PDI family which safeguards the integrity of disulfide bond formation and can complicate functional studies.

In order to oxidise a substrate, the enzyme will transfer the disulfide bond, present in its active site, to the substrate while the active site cysteines become reduced. Disulfide reduction/isomerisation requires the action of a reductase which reduces the substrate while itself becomes oxidised (Figure 1-2). In order to continue its function, the enzyme would need to regain its pre-catalytic state.

Regeneration of the pre-catalytic state of the active site can be carried out by pathways involving Ero1, H_2O_2, disulfide exchange among family members or shuttling reductive power from the NADPH/TrxR1 cytoplasmic pathway into the ER by a yet to be identified membrane protein (Araki, Iemura et al. 2013, Oka, Yeoh et al. 2015, Cao, Lilla et al. 2020).

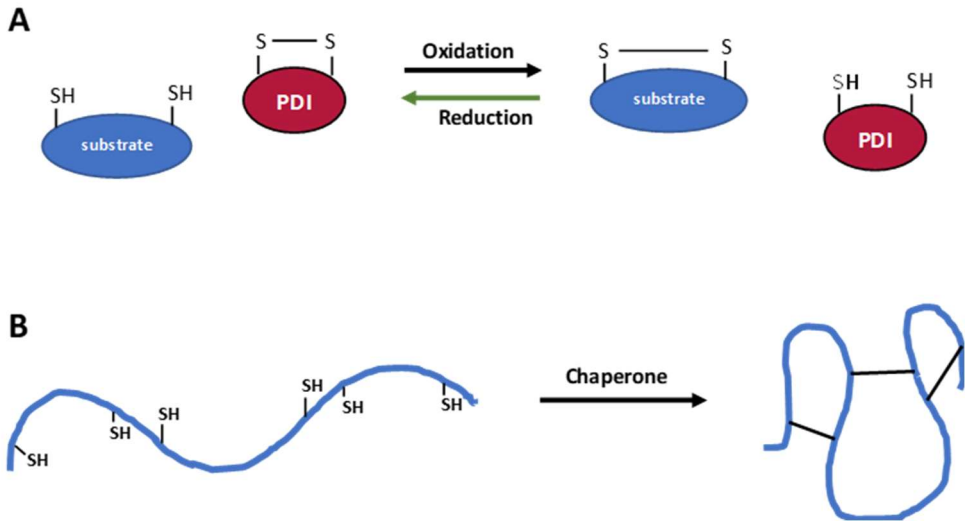

Figure 1-2 Schematic of disulfide exchange in oxidative protein folding.
(A) Disulfide exchange between substrate and PDI family members during protein folding. Oxidised PDIs can transfer disulfide bonds to the nascent chains. Non-native disulfides can be reduced by reductases. (B) Disulfide bonds (longer black lines) formed during chaperone assisted protein folding stabilise protein conformation.

1.1.2.5 N-linked glycosylation

Many proteins include a carbohydrate moiety as part of their final structure. The addition of the glycans, as they are called, promotes protein folding by facilitating the engagement of the calnexin/calreticulin chaperones and other factors important to maturation (Helenius and Aebi 2001). They also promote stability by shielding hydrophobic residues from the aqueous environment, thus preventing aggregation and enhancing secondary structure organisation (Imperiali and O'Connor 1999, Yamaguchi 2002) and facilitate functional engagement with interacting partners (Reily, Stewart et al. 2019).

The addition of the glycans usually occurs co-translationally with the transfer of a core of three glucose, nine mannose, and two N-acetylglucosamine residues ($Glc_3Man_9GlcNAc_2$) onto the asparagine residue of a Asn-Xaa-Ser/Thr sequon. The oligosaccharyltransferase (OST) catalysing the transfer may contain one of two isoforms of its catalytic subunit: STT3A or STT3B. STT3B-OST can post translationally glycosylate sequons missed during cotranslational glycosylation by STT3A-OST (Ruiz-Canada, Kelleher et al. 2009). As the glycoprotein matures, engagement with lectins facilitate the sequential removal of the 3 terminal glucose residues, which are not usually present in secreted proteins, by glucosidase I and II. This allows further modifications and the addition of other types of glycans that occur in a protein-dependent manner further along the secretory pathway (Hanson, Culyba et al. 2009, Thompson and Wakarchuk 2022).

1.1.3 ER to Golgi transport

Proteins that successfully achieve native conformation in the ER must be separated from ER resident proteins and packaged into coat protein II (COPII)–coated vesicles and trafficked to the Golgi. This occurs at functionally distinct domains known as ER exit sites (ERES) (Bannykh, Rowe et al. 1996). Cargo sorting is dependent on “localisation sequences” that are recognised by accessory or coat proteins. For example, ER lumenal proteins contain a KDEL (or KDEL-like sequence) that facilitates their retention (or retrieval) to the ER by interacting with the KDEL receptor (Cosson and Letourneur 1994). Similarly, motifs, such as Golgi localisation sequences can drive ER export, although they are not exclusively required (Barlowe 2003). Other factors contributing to

sorting stringency include folding status, which influences interactions with accessory/transport factors, and oligomeric status (Mezzacasa and Helenius 2002, Lee, Miller et al. 2004).

In addition to the cargo, COPII vesicles consist of an inner layer, composed of Sar1 (a GTPase) and sec23/24 adapter complex, and an outer layer containing sec13/Sec31 heterotetramers. Sar1 GTPase activity initiates coat assembly by recruiting components of the inner layer which in turn recruits the outer layer (Fath, Mancias et al. 2007). Budding, release of the COPII coated cargo, is thought to be controlled by the assembly of Sec16 on the membrane in concert with Sar1 activity (Watson, Townley et al. 2006). Vesicle movement toward the Golgi may occur via the ERGIC and is dependent upon movement of the cytoskeleton (Presley, Cole et al. 1997). At the Golgi, vesicles are tethered to and then fuse with the membrane to release their contents into the cisternae.

1.1.4 The Golgi apparatus

The Golgi apparatus is involved in the trafficking and post-translational modification of proteins received from the ER. Like the ER, flattened, cisternal, membranous structures make up the Golgi apparatus. However, unlike the ER, they are closely stacked and do not form a continuous reticular structure (see Figure 1-1). The Golgi cisternae are divided into distinct functional regions. The cis-Golgi network (CGN) receives vesicles with cargo, that originate from the ER, and shuttles them through the cis, medial and trans faces of the Golgi stack onto the trans-Golgi network (TGN). The CGN is also involved in recycling cargo to the ER (Gleeson 1998, Short, Haas et al. 2005). At the TGN, cargo is sorted and packaged into vesicles destined for export or the lysosomes (Griffiths and Simons 1986).

As proteins move through the Golgi networks, they undergo various post-translational modifications such as proteolytic processing, trimming and modification of N-linked glycan moieties and O-linked glycosylation (Potelle, Klein et al. 2015, Thompson and Wakarchuk 2022). These modifications, which determine structure and function or the subcellular localisation of the proteins, are important to cellular function (Potelle, Klein et al. 2015). For example, O-linked glycosylation requires a series of different O-glycosyltransferases that are

localised to the various compartments of the Golgi and has been identified as a key component of ABO blood group antigen and other cell signalling events (Reily, Stewart et al. 2019). O-glycosylation is distinct from ER localised N-linked glycosylation. It does not occur via *en bloc* carbohydrate transfer but by sequential addition of single monosaccharide units to Serine or Threonine residues using an oxygen-mediated glycosidic bond. Furthermore, the carbohydrate moieties added are much more variable to facilitate increased diversity of functions.

Proteolytic processing in the Golgi is an important modification that is involved in the regulation. This type of processing is seen in the regulation of sterol regulatory element-binding proteins and ATF6α in the management of membrane lipid content and unfolded proteins in the ER, respectively (Haze, Yoshida et al. 1999, Nohturfft, DeBose-Boyd et al. 1999). Proteolytic regulation of ATF6α is addressed in chapters 3 and 5.

1.1.5 ER quality control

1.1.5.1 ER stress

Productive protein folding is an error-prone process, and misfolded or unfolded proteins can often accumulate in response to various stimuli. The circumstance where the number of proteins that require folding exceeds the capacity of the cell to do so is referred to as ER stress (Walter and Ron 2011). This may occur under various physiological and pathological conditions. For example, glucose deprivation, inflammation or viral infections can all lead to ER stress (Nadanaka, Yoshida et al. 2006, Oslowski and Urano 2011). This can be particularly harmful and is associated with the progression of neurodegenerative diseases, metabolic disorders and cancers (Moenner, Pluquet et al. 2007, Matus, Glimcher et al. 2011, Cao and Kaufman 2013). To avert the deleterious effects of ER stress, the ER houses quality control elements that integrate into mechanisms such as ER associated degradation (ERAD) and the unfolded protein response (UPR) which are designed to maintain proteomic integrity.

1.1.5.2 BiP, master regulator of the ER

Chaperones represent a major class of quality control elements of which immunoglobulin heavy-chain binding protein (BiP), has been extensively characterised. The 78 kDa hsp70 was discovered non-covalently bound to antibody heavy chains thus preventing their secretion before assembly with the light chain (Haas and Wabl 1983). As an ER chaperone BiP recognises and binds to exposed hydrophobic regions of newly synthesised peptides which reduces chances of aggregation and misfolding (Knarr, Gething et al. 1995). Such sequences, e.g. SVFPLAP and HTFPAVL found in the antibody heavy chain domain 1 (C_H1), display increased binding affinities for BiP but are ordinarily buried in the native conformation and would normally escape BiP capture (Marcinowski, Rosam et al. 2013). Other major ER functions BiP include managing movement across the ER membrane during protein translocation and retrotranslocation and regulating the response to perturbations in ER homeostasis (Pobre, Poet et al. 2019).

BiP is composed of two domains connected by a conserved linker that transfers allosteric signals between the two domains. The highly conserved and predominantly helical nucleotide-binding domain (NBD) binds ATP or ADP to regulate the function of the substrate binding domain (SBD) composed of ß-sheets that define a cleft for binding substrates. An α-helical lid within the SBD regulates substrate access to the peptide binding cleft (Zhu, Zhao et al. 1996).

Canonical BiP-client interaction occurs via the substrate binding domain (SBD) in a cycle that is allosterically regulated by nucleotide interactions with the NBD (Figure 1-3). The nucleotide-bound state controls substrate engagement through conformational changes of the binding cleft as well as the position of the lid (Yang, Zong et al. 2017). When ATP is bound to the NBD, the two domains are docked together with the lid open allowing substrates to access the binding cleft. This is achieved with the assistance of cochaperones such as the J domain containing proteins. Hydrolysis of ATP leaves ADP occupying the NBD and signals undocking of the domains and closing of the lid to lock the substrate in place. Nucleotide exchange swaps ATP for ADP creating an open lid which facilitates substate release and further substrate engagement (Swain, Dinler et al. 2007, Bertelsen, Chang et al. 2009).

BiP function is further regulated by interactions with cofactors, including nucleotide exchange enhancers or inhibitors, or by reversible modifications that can modulate substrate affinity. Recent evidence has shown that, even with ATP bound to the NBD, substrate binding can be inhibited by a closed arrangement of the ß-sheets in the SBD. This state is thought to immediately follow ATP-mediated substrate release and is important in preventing the [same] substrate from re-engaging. In this model, the hsp40, ERdj3, stimulates the transition of the SBD from a closed to open conformation to allow a new substrate to engage (Yang, Zong et al. 2017). Other hsp40s which are known co-chaperones can promote BiP-substrate interactions, either by transferring substrates to BiP and/or stimulating ATPase activity leading to ADP-BiP with a tightly bound substrate (Laufen, Mayer et al. 1999). Substrate release is mediated by nucleotide exchange enhanced by exchange factors such as Grp170 and Sil1 (Behnke, Feige et al. 2015).

In order to efficiently cope with varying demands within its diverse roles and frequent changes in the ER environment, differential modification can interrupt BiP chaperone cycle to delineate different functional pools of BiP. These modifications allow responses to fluctuating demands to occur on a comparable time scale (Preissler, Rohland et al. 2017). Unmodified, BiP participates in its ADP/ATP chaperone cycle engaging with unfolded proteins in the monomeric form. Post-translational ribosylation with ADP, disrupts the chaperone cycle and creates a pool of latent BiP aggregates which can be de-ribosylated and activated in response to increase demands for BiP e.g., in conditions such as glucose deprivation (Carlsson and Lazarides 1983, Chambers, Petrova et al. 2012). An excessively oxidising ER environment similarly targets the chaperone cycle; however, this leads to modification of a cysteine residue which favours BiP holdase activity (Wang, Pareja et al. 2014, Wang and Sevier 2016).

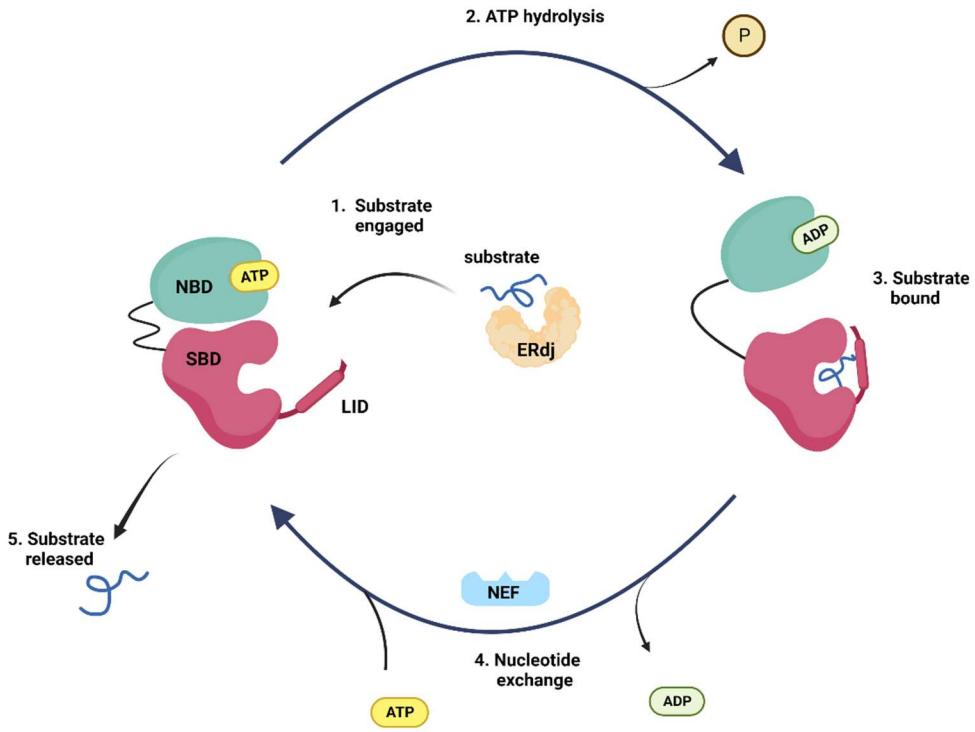

Figure 1-3 Nucleotide-regulated substrate engagement cycle of BiP.
(1) ATP binding to the NBD allows substrates to enter the binding site with assistance from ERdjs. (2) ATP hydrolysis and the release of the γ phosphate. (3) ADP occupies the NBD which creates conformational changes resulting in a closed lid to lock the substrate in place. (4) Nucleotide exchange returns BiP to an open lid conformational state in which substrate release (5) allows the cycle to resume. (Created with BioRender.com).

1.1.5.3 ERAD

A key aspect of ER quality control system is ER-associated degradation (ERAD). The actions of the UPR increases the folding capacity of the cell thus providing opportunity for proteins to refold properly. Proteins which fail to achieve native conformation are monitored and degraded by the ERAD system. The process involves recognition of the substrate that may reside in the ER lumen or membrane, transport of the substrate into the cytoplasm (retro-translocation) and ubiquitination facilitated by E3 ubiquitin ligase complexes. Ubiquitinated proteins are finally degraded by the 26S proteasome (Ruggiano, Foresti et al. 2014).

Substrate recognition within the ER must be finely tuned. Given, that terminally misfolded proteins are not exclusive substrates of the ERAD system, they must be clearly distinguished from folding intermediates and efficiently cleared to maintain ER function. In addition to the unusual exposure of hydrophobic

residues, substrate recognition may be based upon extended interactions with chaperones or differential N-glycan trimming. Unfolded domains of lumenal and membrane proteins present, and are recognised, variably. Parallel pathways facilitate the degradation of these proteins but the exact mechanisms of substrate recognition and division of labour among the ERAD pathways are still to be fully elucidated (Christianson and Carvalho 2022).

The membrane spanning E3 ubiquitin ligase itself is involved in substrate recognition and works in concert with factors that are involved in substrate recognition and transfer (Sato, Schulz et al. 2009). In mammals, the ER chaperone BiP, OS9 and XTP3-B all participate in substrate recognition while the Derlins transfer substrates to the HRD1 complex. The HRD1 complex itself can recognise substrates with misfolded membrane domains (Sato, Schulz et al. 2009, Ruggiano, Foresti et al. 2014).

Retrotranslocation, facilitated by the E3 complex, involves movement of the substrate across the ER membrane and into the cytoplasm. Ubiquitination of the substrate, through the actions of E1 and E2 enzymes, occurs as it enters the cytoplasm. Ubiquitination signals recruitment of p97 ATPase complex to the ER to extract the substrate from the ER membrane (Lemberg and Strisovsky 2021). The substrate is kept soluble for access by the proteasome by the action of a holdase complex that includes the chaperone Bag6 (Xu, Cai et al. 2012).

1.1.6 The unfolded protein response

The unfolded protein response (UPR) is a transcriptional and translational response that is engaged when the cell experiences ER stress. The primary goal of the UPR is to maintain the balance between the demand for new proteins and the manufacturing capacity of the cell. Perturbation of the balance leads to an accumulation of unfolded or misfolded proteins. Remedial signalling pathways are employed to effectively to reinstate the balance or proteostasis (Walter and Ron 2011).

The ER contains many chaperones, cochaperones and other enzymes involved in protein folding. Increasing their expression during the UPR improves the cell's ability to cope with increased demands. Simultaneously, decreasing

transcription and translation reduces the number of proteins entering the ER that would require folding. The protein folding load is further reduced by the removal of proteins that cannot be correctly refolded through increased expression of ERAD components. Additionally, increased phospholipid synthesis facilitates ER expansion. These immediate responses are designed to alleviate ER stress and restore homeostasis. However, prolonged ER stress can lead to apoptosis (discussed in section 1.1.6.4) (Schroder and Kaufman 2005, Schröder 2006).

These efforts are mediated by three transmembrane proteins: inositol requiring enzyme 1 (IRE1), PKR-like ER kinase (PERK) and activating transcription factor 6 (ATF6). They are involved in detecting ER stress and coordinate the response pathways. In such a system, transducer regulation represents an important feature to prevent constitutive activation and to tune the response to the level of perturbation. As part of the UPR, BiP maintains the transducers in an inactive state and releases them in the presence of ER stress. However, debate is still rife about the regulatory mechanism as well as its role in stress detection.

1.1.6.1 The Ire1α pathway

Ire1α is a type I transmembrane serine/threonine kinase, that has been conserved from yeast to metazoans (Acosta-Alvear, Karagöz et al. 2018). The N terminus protrudes into the ER lumen and serves as a sensory domain for ER stress. The cytosolic C terminus comprises of serine/threonine kinase and endoribonuclease (RNase) domains (Poothong, Sopha et al. 2010). The two isoforms Ire1α/ß are differentially expressed with the former being ubiquitously expressed in mammals (Walter and Ron 2011).

Ire1α is thought to be regulated by non-canonical interaction of the monomer with BiP via its NBD (Carrara, Prischi et al. 2015). Activation, through BiP release of the monomer, is believed to be triggered by the binding of unfolded proteins to BiP SBD during ER stress (Lee, Dey et al. 2008, Carrara, Prischi et al. 2015). However, there is also evidence in support of Ire1 activation being driven by direct interaction of its lumenal domain with unfolded proteins. Crystal structures of dimers of Ire-LD show a putative peptide binding groove that may engage unfolded proteins. Additionally, mutations of hydrophobic residues,

M229A-F265A-Y301A, within the putative peptide binding domain diminished Ire1 response suggesting its involvement in interacting with unfolded proteins. Further analysis showed that interaction with the dimers promoted oligomerisation which is thought to be important for activation (Gardner and Walter 2011).

Activation is propagated through dimerization and oligomerisation which leads to auto trans-phosphorylation of Ire1. Initial dimerisation allows monomers arranged in a face-to-face orientation to trans-phosphorylate. Allosteric changes induced allows association of dimers to produce an active complex (Prischi, Nowak et al. 2014, Siwecka, Rozpędek-Kamińska et al. 2021). This triggers the endoribonuclease activity which cleaves X-box-binding protein 1 (XBP1) mRNA, removing a 26-nucleotide intron, to produce the trans-activator, XBP1s, that targets genes involved in ER expansion and ER associated degradation (Siwecka, Rozpędek-Kamińska et al. 2021). Unspliced XBP1 mRNA encodes the protein XBP1u which is believed to accumulate and repress the UPR during recovery. Therefore, alternate splicing can tune the response by controlling the balance between activation and repression (Siwecka, Rozpędek-Kamińska et al. 2021)

Ire1α also reduces the protein folding load by degrading a subset of specific mRNAs by a process known as regulated Ire1-dependent decay (RIDD). Basal RIDD activity, which occurs in the absence of ER stress, is important for maintaining ER homeostasis by degrading some proteins. However, changes in RIDD activity may be controlled by the relative amounts of Ire1α and XBP1 mRNA. During ER stress, increased Ire1α activation cleaves and reduces the amount of XBP1 mRNA which causes increased RIDD activity (Tsuru, Imai et al. 2016). RIDD primarily degrades mRNAs that encode proteins targeted to the secretory pathway. Its function is cytoprotective, but it can induce cell death during chronic ER stress by degrading mRNA of genes that prevent apoptosis (Maurel, Chevet et al. 2014, Iurlaro and Muñoz-Pinedo 2016).

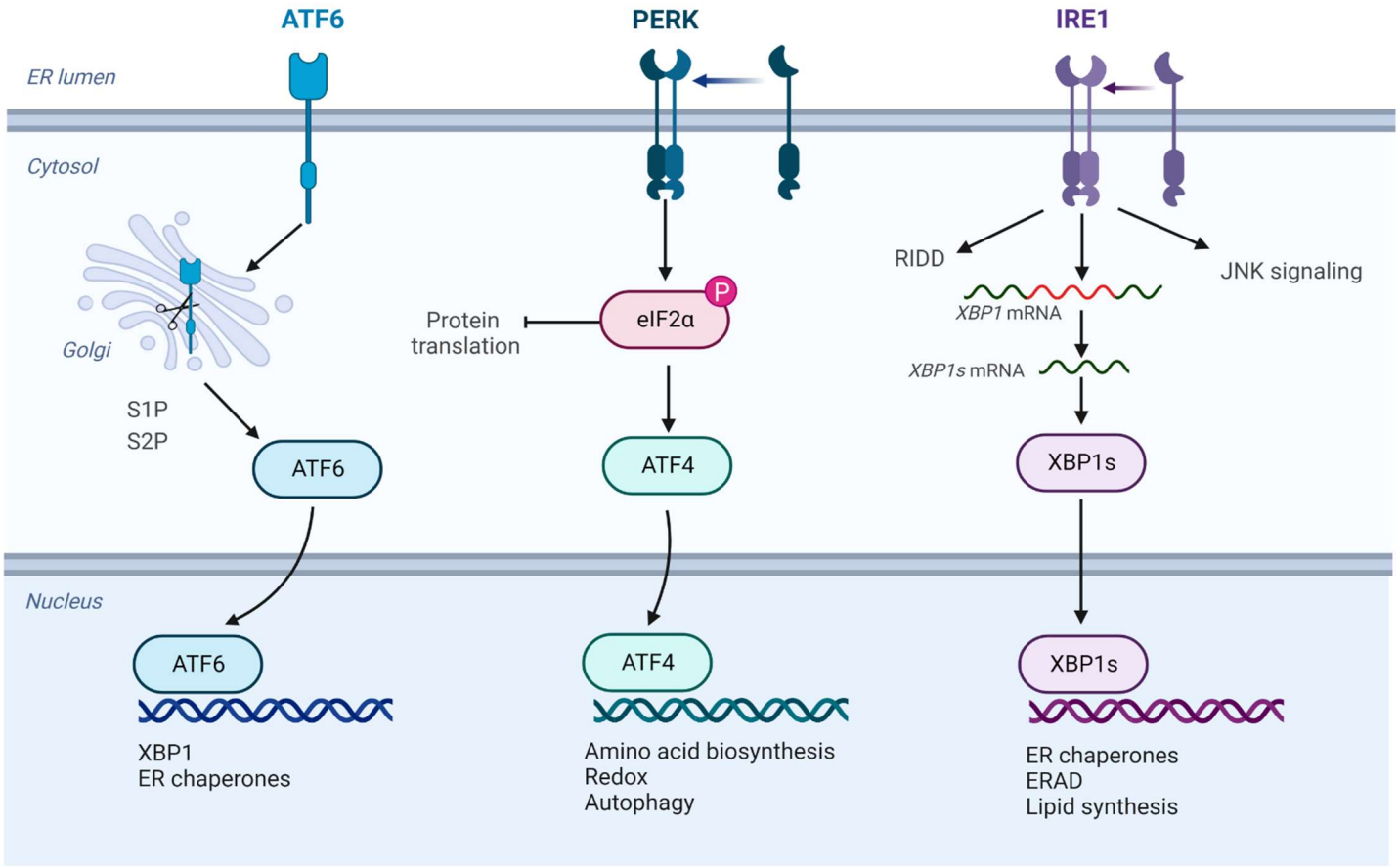

Figure 1-4 Signal transduction pathways in the UPR.
Homeostatic control of the UPR is executed by three transmembrane proteins IRE1, PERK and ATF6 which regulate a number of proteins involved in protein quality control as well as degrade specific mRNAs to reduce the protein folding burden on the cell (Reprinted from "UPR Signaling (ATF6, PERK, IRE1", by BioRender.com (2023). Retrieved from https://app.biorender.com/biorender-templates).

1.1.6.2 The PERK pathway

PERK, like Ire1, is a type I transmembrane protein. Dimerisation via the lumenal domain is believed to be regulated by interaction with BiP via its NBD (Carrara, Prischi et al. 2015). During ER stress, the cytoplasmic kinase domain is activated through release from BiP. Subsequent dimerisation leads to auto phosphorylation and phosphorylation of eIF2α which inhibits general translation and reduces ER influx of proteins (Harding, Zhang et al. 1999). Select mRNAs with short ORFS in the 5′-untranslated regions escape eIF2α mediated downregulation. One of these, the transcription factor ATF4, is induced during eIF2α phosphorylation and drives the expression of transcription factor C/EBP homologous protein (CHOP), a transcription factor that regulates the expression of components of the apoptotic pathway. It also upregulates the expression of growth arrest and DNA damage–inducible 34 (GADD34), a regulatory phosphatase subunit that dephosphorylates eIF2α to restore translation when ER stress is alleviated (Marciniak, Yun et al. 2004, Tsaytler, Harding et al. 2011).

1.1.6.3 The ATF6α pathway

1.1.6.3.1 The structure of ATF6α

Activating transcription factor 6 (ATF6) is synthesised as two isoforms of a type II transmembrane protein that exhibit important structural similarity but differ in size, abundance, and activity. ATF6ß is 110kDa and less abundant than the 90kDa ATF6α which has been identified as the more potent UPR transducer (Haze, Okada et al. 2001, Thuerauf, Morrison et al. 2004). ATF6α is the focus of this thesis.

ATF6α contains 670 amino acid residues and is divided into three functional domains. The transmembrane domain of ATF6α anchors the protein in the ER membrane with the N-terminal and C-terminal sections protruding into the cytoplasm and ER lumen, respectively. The C terminal lumenal domain is largely disordered and contains regulatory sequences and two cysteine residues (C467 and C618) that are important to ATF6 function (Figure 1-5A). These cysteines are conserved in ATF6ß. Like IRE1α and PERK, ATF6α lumenal domain functions as a stress detector. However, the mode of stress detection is different, and activation involves regulated intramembrane proteolysis (Rip) in the Golgi.

Unlike the other UPR transducers which bind to BiP NBD, ATF6α is regulated by lumenal sequences interacting with BiP SBD acting as canonical BiP substrate (Shen, Snapp et al. 2005, Carrara, Prischi et al. 2015).

The ATF6α lumenal domain has multiple BiP binding sites that interact with variable affinities. BiP interaction with amino acids 431 – 550 is stronger than interaction with amino acids 551 – 670. ER to Golgi translocation is signalled by two Golgi localisation sequences (GLS1 & 2) also located within the lumenal domain (Figure 1-5A). GLS1 spans amino acids 468 – 475 and GLS2 covers amino acids 476 – 500. Overlap between these two antagonistic targeting and regulatory sequences necessitates BiP release to expose the GLSs and induce translocation to the Golgi (Shen, Chen et al. 2002).

Lumenal cysteines, C467 and C618, control ATF6α redox state and are implicated in stress detection. They can form an intramolecular disulfide bonded monomer or intermolecular disulfides between equivalent residues to give rise to distinct dimers designated 618D and 467D shown in Figure 1-5B (Nadanaka, Okada et al. 2007, Oka, van Lith et al. 2019, Koba, Jin et al. 2020, Oka, Pierre et al. 2022). The identification of the reduced monomer in the Golgi during ER stress implicates redox change as a possible mechanism for stress detection (Haze, Yoshida et al. 1999, Nadanaka, Okada et al. 2007). However, the mechanistic details of stress detection are yet to be fully elucidated. For IRE1α and PERK, stress detection involves the sensing of unfolded proteins by BiP SBD as well as their lumenal domains (Carrara, Prischi et al. 2015). Hence, it is reasonable to anticipate that BiP is involved in stress detection but the fact that ATF6α binds the SBD of BiP suggests an alternative sensing domain that may involve at least one of its cofactors (Nadanaka, Okada et al. 2007, Pobre, Poet et al. 2019).

The cytoplasmic domain of ATF6α consists of a transactivation domain (TAD) and a basic leucine zipper (bZIP) domain which facilitates DNA binding and transcription of target genes. Release of the transcription factor is enabled by a Site-2 protease cleavage site located within the transmembrane domain. However, S2P cleavage is dependent on the activity of S1P which removes the majority of the lumenal domain. Thus, S1P cleavage represents an important regulatory feature (Haze, Yoshida et al. 1999).

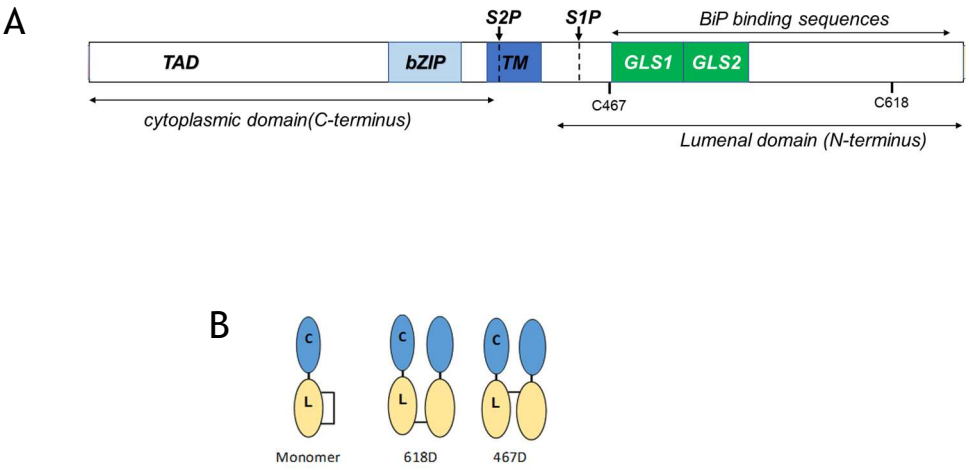

Figure 1-5 Schematic representation of ATF6α domain structure and oligomeric status. (A) The cytoplasmic domain contains basic leucine zipper (bZIP) and transactivation domains (TAD) while the lumenal domain contains Golgi localisation sequences (GLS1 & 2) an S1P cleavage site and cysteines. The construct used in this study contains HA and V5 tags on the C- and N-terminus, respectively. (B) ATF6α exist as one of three forms in the unstressed cell; a disulfide bonded monomer, or one of two dimers stabilised by intermolecular disulfides

Analysis of the promoters of its target genes revealed that they contain the consensus sequence of the cis-acting ER stress response elements ERSEI and II (CCAAT – N9 – CCACG). The CCAG motif of the ERSE is bound by ATF6α which, in conjunction with the binding of nuclear transcription factor NF-Y to the CCAAT motif, induces the transcription of UPR related genes including BiP, PDI and GRP94 (Ye, Rawson et al. 2000, Yoshida, Okada et al. 2000). The transcription domain of ATF6ß can also bind the ERSE elements, however it is not as potent and may function to inhibit transcriptional upregulation by ATF6α (Thuerauf, Morrison et al. 2004).

1.1.6.3.2 Mechanism of ATF6 activation

Activation of ATF6α is facilitated by its release from BiP, reduction of the lumenal cysteines and trafficking to the Golgi for proteolytic processing to release the active transcription factor occurs in the Golgi. ER stress causes BiP release and reduction of intra- and intermolecular disulfides. The reduced monomer is then packaged into COPII vesicles and trafficked to the Golgi. At the Golgi, cleavage by S1P and S2P release the soluble transcription factor that regulate transcription in the nucleus (Figure 1-6A). Trafficking to the Golgi is influenced by the redox status of the protein and regulated by the activity of ERp18 (Oka, van Lith et al. 2019). However, the precise mechanism by which ERp18 acts was not determined.

ERp18, also called ERp19 or ERp16, contains 172 amino acids and displays a characteristic thioredoxin fold (Figure 1-6); consisting of a four-stranded ß-sheet surrounded by α-helices. A single CGAC catalytic domain is located toward the N-terminus and an ER retention sequence (EDEL) at the C-terminus. Sequence alignments between ERp18 and other known proteins with at least one thioredoxin-like domain showed that it shares several conserved features with domains found in human PDI and is more closely related to PDI than thioredoxin (Rowe, Ruddock et al. 2009). A unique loop inserted within the thioredoxin fold has been identified as a potential binding site that may confer substrate specificity based on its hydrophobic nature, flexibility and proximity to the active site (Rowe, Ruddock et al. 2009). ERp18 has been shown to catalyse disulfide bond formation, reduction, and isomerisation (Jeong, Lee et al. 2008). It exhibits a more compact and stable structure in its reduced form, which suggests that it may function preferentially as an oxidase (Rowe, Ruddock et al. 2009).

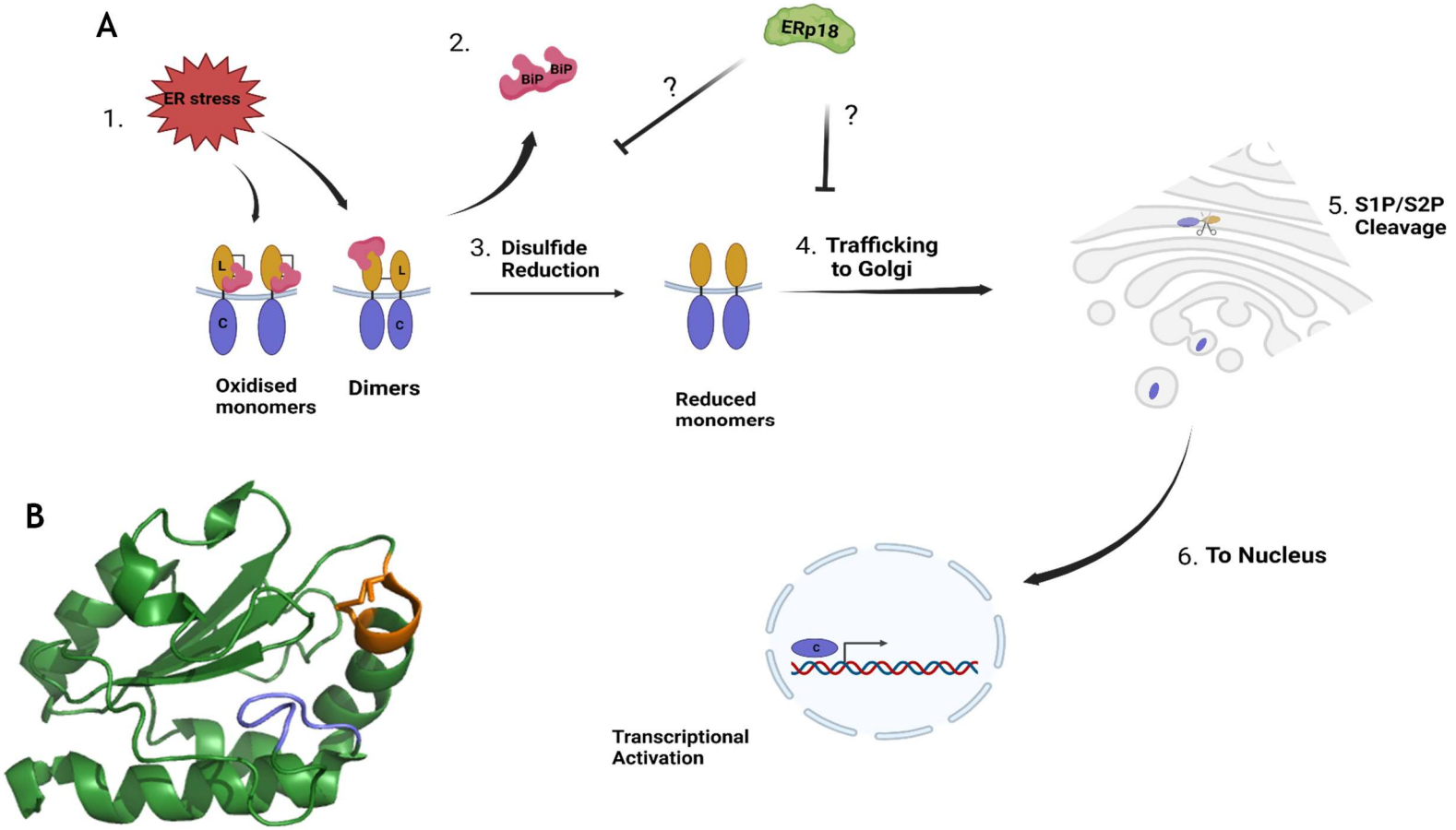

Figure 1-6 Activation of ATF6α and structure of ERp18

(A) Activation sequence of ATF6α. ER stress (1.) induces the release of BiP (2.) and reduction of cysteines (3.). Reduced monomer is then trafficked to the Golgi (4.) where it is cleaved by S1P and S2P (5.). The released transcription factor moves to the nucleus to regulate transcription (6.). The role of ERp18 in regulating trafficking is unclear (Created with BioRender.com). (B) PyMOL generated image of oxidised ERp18 (1SEN) showing the main thioredoxin fold in green and active site in orange. A loop inserted into the thioredoxin fold which is putatively involved in substrate binding is shown in blue.

1.1.6.4 Apoptotic UPR responses

The responses described so far are adaptive and designed to alleviate the stress and re-establish homeostasis. However, in response to persistent ER stress, apoptotic programs can be triggered through integration of signals out with the ER (Schröder and Kaufman 2006). Two apoptotic signalling pathways, intrinsic and extrinsic, are engaged by factors of the PERK and Ire1α pathways, respectively. During intrinsic signalling, in the background of prolonged ER stress, PERK phosphorylation of eIF2α drives ATF4 and CHOP expression to alternatively regulate members of the B-cell lymphoma protein 2 (Bcl-2) family (Youle and Strasser 2008). The Bcl-2 family is divided into anti-apoptotic proteins, pro-apoptotic proteins and Bcl-2 homology domain 3 (BH3)-only containing proteins (Szegezdi, Macdonald et al. 2009). CHOP expression induces the expression of pro-apoptotic genes while reducing the expression of anti-apoptotic genes. It also increases the expression of GADD34, which restores protein synthesis. However, in the context of persistent ER stress, continued misfolded increases oxidative stress leading to apoptosis. Calcium signalling and mitochondrial crosstalk play a crucial role in the intrinsic pathway. In response to apoptotic stimuli, Bcl-2 family members tethered to the ER and mitochondrial membranes are activated, cytochrome c moves into the cytosol and there is increased efflux of Ca^{2+} from the ER to cytoplasm (Szegezdi, Logue et al. 2006). Apoptosis via these changes is realised through the action of caspases 12, 3 and 9 (Sisinni, Pietrafesa et al. 2019).

While the extrinsic pathway is normally initiated by extracellular necrosis factors, the process can be induced through alternate activity of Ire1α via the c-JUN N-terminal kinase (JNK) pathway (Urano, Wang et al. 2000). Terminally, JNK signalling converges upon Bcl-2 family members to initiate the caspase cascade leading to apoptosis (Sisinni, Pietrafesa et al. 2019). The signalling pathways originates from the cytoplasmic domain of Ire1α recruiting tumour necrosis factor receptor associated 2 (TRAF2) protein. This initiates a series of events including the recruitment of apoptosis-signal-regulating kinase (ASK1), and activation of p38 MAPK, both members of the mitogen activated kinases (MAPKs) (Nishitoh, Saitoh et al. 1998). P38 MAPK phosphorylates CHOP and increases its transcriptional activity which converges upon the Bcl-2 family and

GADD34. Alternatively, these effects of Ire1α are proposed to result from overactive RIDD activity of hyperphosphorylated Ire1α (Papa 2012).

The UPR integrates internal and external stimuli to regulate pro-survival and pro-death mechanisms. While all three arms have pro-survival functions, the pro-death outcomes are dominated by Ire1α and PERK signalling which can act synergistically to execute apoptosis. Consequently, ER stress, and the resulting fate of cells, play a crucial role in disease onset and progression.

1.1.7 The UPR and Disease

Proteins are responsible for a myriad of intra- and extracellular functions that contribute to the overall health and wellbeing of the cell and organism. The stringent quality control mechanisms employed in the manufacture and export of proteins are paramount in maintaining health. Thus, the UPR, as a major QC mechanism, has been implicated in the pathologies of various classes of diseases (Wang and Kaufman 2016). For example, protein aggregation in neurodegenerative diseases point towards misfolding and a possible faulty quality control system as key to disease pathology (Brehme and Voisine 2016). On the contrary, plasticity of the UPR can contribute to diseases such as cancer in which the UPR is adapted to accommodate large increases in protein synthesis required to facilitate accelerated cell proliferation. Also, death of pancreatic ß cells due to persistent ER stress has been implicated in the onset and progression of diabetes (Rabhi, Salas et al. 2014). Consequently, much effort has been directed toward elucidating the link between the UPR and disease with the aim of developing novel therapeutic strategies. For the purposes of this thesis, discussions will be limited to three major classes of diseases, neurodegenerative and metabolic diseases, and cancer, that significantly affect populations of developing and developed countries.

1.1.7.1 The UPR and neurodegenerative diseases

Alzheimer's disease (AD) and Parkinson's disease (PD) are part of a group of progressive disorders characterised by loss of function within the central nervous system (CNS). The hallmark of accumulated misfolded protein is common to these diseases and as such they fall into the category of protein misfolding

diseases (PMDs) (Doyle, Kennedy et al. 2011). Given that the UPR is designed to preserve proteomic integrity and mitigate secretion of misfolded protein, it becomes prime suspect, alongside other ER QC mechanisms, in the cause and/or progression of neurodegenerative diseases. Therefore, it is being researched as a therapeutic target (Marciniak, Chambers et al. 2022).

Alzheimer's patients may present with extracellular deposits of ß-amyloid (Aß) protein or plaques in the CNS. Several different forms of Aß proteins are produced by cleavage of amyloid precursor protein (APP), including the amyloidogenic form Aß42, often found in plaques. Cleavage of APP is performed by proteolytic complexes ß- and γ-secretase. The IRE1/XBP1 axis has been implicated in the formation of Aß42 by regulating the expression of genes involved in the trafficking and processing of APP (Acosta-Alvear, Zhou et al. 2007). One APP-related target of XBP1 is UBQLN1, a negative regulator of the γ-secretase complex involved in cleaving APP to produce Aß42. It is proposed that downregulation of XBP1 decreases UBQLN1 activity leading overactive production of Aß peptides (Doyle, Kennedy et al. 2011). Additionally, Aß peptide accumulation may deplete ER Ca^{2+} and interrupt the functions of chaperones which increases ER stress. In a later study, it was found that stimulation of the IRE1 pathway increased the levels of APP and targeting IRE1/XBP1 axis contributed to reversal of AD symptoms in mouse models (Duran-Aniotz, Cornejo et al. 2017).

In the case of Parkinson's disease (PD), the accumulated misfolded protein is α-Synuclein (α Syn) occurring as Lewy bodies (LB) or Lewy neurites (LN) in neurons. Selective loss of dopaminergic (DA) neurons in the region of the brain involved in movement and muscle contraction control is the other major hallmark of PD. α Syn is ubiquitous in neurons, where it might be involved in lipid transport and membrane and vesicular remodelling (Burré, Sharma et al. 2018). Mutations in α Syn promote abnormal aggregation and PD progression. In addition, interconnectivity of neuronal circuits facilitate the transmission of the aggregates throughout the network increasing ER stress and inducing death (Ghemrawi and Khair 2020). Several models have been proposed for α Syn mediated induction of ER stress and cell death. In-cell proximity ligations revealed that direct interactions of α-Syn aggregates with SERCA

(Sarco/endoplasmic reticulum Ca^{2+}-ATPase) perturbed calcium processing. Progressive dysfunctions of disrupted Ca^{2+} metabolism was found to be fatal (Betzer, Lassen et al. 2018). Another model suggested that stress was induced by blocking ER to Golgi trafficking. The result of which attenuates ATF6α activation and its pro-survival activity thereby promoting apoptosis (Gitler, Bevis et al. 2008, Credle, Forcelli et al. 2015). These stress mechanisms converge on the PERK pathway as evidenced by activation of PERK related transcription factors ATF4 in response to glucose deprivation and the identification of phosphorylated PERK and eIF2α from the brains of PD patients (Hoozemans, van Haastert et al. 2007, Bellucci, Navarria et al. 2011).

1.1.7.2 The UPR and diabetes mellitus

Diabetes mellitus is a chronic metabolic disorder characterised by hyperglycaemia (high concentrations of glucose in the blood). The inability to regulate the level of glucose in the bloodstream may result from resistance to insulin and/or inability to produce sufficient insulin. Insulin is produced in the pancreas by specialised secretory ß-cells. Biosynthesis begins in the ER and is completed in the trans-Golgi. Cleavage of the signal peptide produces pro-insulin, from pre-proinsulin, which accumulates in the ER where it is folded, packaged into vesicles and trafficked to the Golgi. The final cleavage and associated processing to create mature insulin occurs in trans-Golgi vesicles which also contain the necessary enzymes (Steiner 2000).

The ER of ß-cells are well adapted to sustain high rates of synthesis, folding and secretion of large amounts of insulin required to maintain blood sugar levels. Thus, there is a significant potential for high levels of ER stress which can be easily exacerbated by other factors such as mutations leading to chronic ER stress (Papa 2012). Successful trafficking of proinsulin to the Golgi requires a native structure that is stabilised by 3 intramolecular disulfide bonds. Two mutations in the insulin 2 gene, Ins2C95S and Ins2C96Y that disrupt native disulfide bond formation, prevent trafficking of proinsulin leading to chronic ER stress in the Munich and Akita diabetic mouse models, respectively (Oyadomari, Koizumi et al. 2002, Herbach, Rathkolb et al. 2007). The mice experienced diminished insulin production due to loss of ß cells and exhibited symptoms of diabetes characterised as mutation-induced diabetes of youth (Ghosh, Colon-

Negron et al. 2019). Similar mutations that disrupt the folding of proinsulin have been identified in humans (Støy, Edghill et al. 2007).

Decrease in ß-cell mass, as has been frequently identified in diabetes, is thought to develop in two phases. In phase one, initial decrease may be caused by stress induced apoptosis due to increased demands caused by insulin resistance coupled with the accumulation of islet amyloid polypeptide. These are usually seen in type 2 diabetes (Westermark, Johnson et al. 1992, Sawaya, Sambashivan et al. 2007). In type 1 diabetes, the initial decrease stems from T-cell autoimmune attack. In phase 2, the remaining cells then become overworked as they try to compensate for the insulin deficit leading to further ß cell loss (Ghosh, Colon-Negron et al. 2019).

Loss of function mutations in the PERK arm of the UPR have been also been shown to create early infancy diabetic phenotypes (Delépine, Nicolino et al. 2000). However, the conditions are usually rare and the major contribution of the UPR to diabetes is through apoptosis of ß cells (Pandey, Mathur et al. 2019). The proposed mechanism is based on hyperactivation of Ire1α dependent mRNA decay (RIDD). It is believed that persistent, chronic ER stress in ß cells leads to hyperphosphorylation of Ire1 oligomer complexes. This reduces the specificity of RNase activity resulting in promiscuous decay of mRNAs and loss of proteins including ER chaperone and folding factors and proteins involved in maintaining redox balance terminating with apoptosis (Ghosh, Colon-Negron et al. 2019).

1.1.7.3 The UPR and cancer

Cancer encompasses a large group of diseases primarily characterised by uncontrollable proliferation of cells which often invade and eventually destroy surrounding tissues and organs. An adaptive UPR is necessary for cancers to cope with persistent ER stress, which is now being considered one of the many hallmarks of cancer. Sustained rapid growth of tumour cells leads to changes within the tumour microenvironment (TME) that can generate ER stress through metabolic and environmental pressures. These include limited availability of oxygen and nutrients, which usually result from poor vascularisation, coupled with increased demands on the transcriptional and translational machinery (Chen and Cubillos-Ruiz 2021). Hypoxia, the limited availability of oxygen, is

characteristic of solid tumours and is known to exacerbate disease progression and promote aggressiveness (Lv, Li et al. 2017). In the context of protein homeostasis, oxygen is required to facilitate post-translational disulfide formation and isomerisation reactions performed as a part of oxidative protein folding (Hudson, Gannon et al. 2015). In this way, hypoxia can cause ER stress by disrupting the folding process. Protein folding may also be disrupted by the availability of nutrients. Glucose, for example, is critical for the N-glycosylation required for productive folding of glycoproteins (Hanson, Culyba et al. 2009). Additionally, it is required as a source of ATP to drive important ER processes including for chaperone activity of BiP which is central to ER quality control (Wei and Hendershot 1995).

Unresolved ER stress would usually signal apoptosis. However, intrinsic cellular changes, such as mutations, are thought to be fundamental in driving mechanisms that promote tumorigenesis (Sisinni, Pietrafesa et al. 2019). Mutations represent one of the major contributors to the development of cancers with the usual suspects being genes involved in cell cycle regulation such as p21 (Parveen, Akash et al. 2016). However, genomic screens have identified somatic mutations within the genes for the UPR sensors IRE1, PERK and ATF6 that may be involved in oncogenic development (Greenman, Stephens et al. 2007). Sensors were found to exhibit distinct mutation profiles with variable distribution of mutation rates among tissues. Mutation rates of ATF6 and IRE1 were highest in gastrointestinal cancers, for both, and lowest in cancers of the nervous system and urological cancers, respectively. The highest and lowest mutations rates for PERK were identified in lung and cancers of the nervous system, respectively. However, PERK mutation rate was also considerably high in gastrointestinal cancers (Chevet, Hetz et al. 2015). These mutation profiles are indicative of the involvement of UPR sensors in specific cancers and may represent suitable targets for intervention. In support of this, UPR signalling has been validated as contributory to tumour survival and/or metastasis. For example, PERK signalling was found to be critical in the metastasis of triple negative breast cancers (TNBC) via a downstream transcription factor, CREB3L1, that regulates genes involved in deposition of ECM, and cell migration. Importantly, the downstream activity of CREB3L1 presented a potential therapeutic target that overcame the limitations of direct

PERK targeting in cancer treatment(Feng, Jin et al. 2017). Additionally, ATF6α was shown to interact with the DNA damage response machinery, thereby promoting pro-survival mechanisms in colon cancer (Benedetti, Romeo et al. 2022).

1.1.7.4 Emerging therapeutic strategies

The increase in understanding of the ER stress and the UPR along with their role in pathophysiology drives the emergence and development of health-related tools including small molecule inhibitors or activators, biomarkers as well as therapeutic targeting (Almanza, Carlesso et al. 2019). Several pharmacological modulators have been identified that target specific arms of the UPR.

Type I and type II (ATP-competitive) kinase inhibitors of Ire1α activate and inhibit the RNase domains, respectively. In addition to their use in elucidating allosteric signalling between the kinase and RNase domain (Feldman, Tong et al. 2016), their activity has been applied to treatment of cancer. For example, Sunitib inhibits cancer growth and is used in the treatment of kidney cancer (Jha, Polyakova et al. 2011). Another compound, Toyocamycin, targets Ire1α RNase activity and is being tested as a broader spectrum cancer treatment (Ri, Tashiro et al. 2012). Determination of Ire1α structures which informed conformational changes during activation and drug binding was instrumental in driving the discovery of novel inhibitors.

Direct PERK inhibitors, GSK2656157 & GSK2606414 have been identified and were shown to reduce tumour growth in mouse models. The former entered preclinical trials to treat pancreatic cancer and multiple myeloma. However, these compounds caused ß cell damage as seen in some forms of diabetes (Papa 2012, Atkins, Liu et al. 2013). Using small molecule inhibitors of PERK that target the GADD34 activity to prevent eIF2α dephosphorylation bypassed the cytotoxicity. Sephin1 binds the PP1R15A regulatory subunit of GADD34 which is stress inducible to extend the life of PERK signalling and was shown to have therapeutic benefits in ALS mouse models (Das, Krzyzosiak et al. 2015). A similar compound Raphin1 was shown to inhibit PPR15B (constitutive regulatory subunit of GADD34) to improve outcomes in a neurodegenerative disease mouse model (Krzyzosiak, Sigurdardottir et al. 2018).

The best example of molecules which specifically target the ATF6α pathways are Ceapins which prevent ATF6α trafficking (Torres, Gallagher et al. 2019). However, further characterisation is required to demonstrate the utility of these molecules for disease intervention. The lack of ATF6α crystal structure and mechanistic details of activation have hindered the identification of potential targets (Almanza, Carlesso et al. 2019).

1.2 Aims

The UPR is a major quality control program for maintaining ER proteostasis which can also determine cell fate by balancing pro-survival and pro-death mechanisms (Walter and Ron 2011). Apoptotic cell death has been identified as a key factor in the development and/or progression of several diseases. Pro-apoptotic signals which are engaged during chronic ER stress are frequently regulated through Ire1α and PERK, while ATF6α is more engaged in anti-apoptotic signalling (Sisinni, Pietrafesa et al. 2019). Increased understanding of the underlying molecular mechanisms of activation and regulation of UPR players expands the opportunities for characterising their roles in diseases and identifying novel targets for the development of therapeutic strategies. Currently, the roles of the three UPR sensors in diseases are not equally documented with the characterisation of ATF6α trailing PERK and Ire1α. This could be due to the later development of ATF6α pathway but is also representative of gaps in knowledge relating to mechanisms of activation and regulation. Thus, research into the activation and regulation of ATF6α pathway can improve fundamental understanding which can be utilised to exploit pro-survival responses in treatment of disease.

The work presented here focuses on the ATF6α arm of the UPR, investigating mechanisms and factors that contribute to retention and regulation of ER exit during activation in response to different chemical stressors. Firstly, we investigate how redox modulation contributes to the activation of ATF6α. To do this we isolated the lumenal domain, which is responsible for dimerisation, during ER stress to examine its redox status. Quantitative analyses of changes in the redox forms of ATF6α before and during ER stress led us to propose distinct roles for the monomer and one of two dimers in retention and trafficking, respectively. Given the reported interaction between ERp18 and ATF6α, and the ability of ERp18 to modulate the redox status of ATF6α (Oka, van Lith et al. 2019), we investigated how ERp18 impacts ATF6α activation and trafficking. This was done by quantifying stress dependent changes in redox forms of ATF6α, comparing these changes in cells expressing catalytically active or inactive mutants of ERp18 to cells deficient in ERp18. Our findings show that ERp18 reductase activity was responsible for regulating trafficking of the ATF6α dimer. We also present preliminary evidence for the involvement of a nucleotide

exchange inhibitor interacting with BiP in ER retention of ATF6α. Having ATF6α as a substrate of ERp18 presented the opportunity to interrogate ERp18 residues responsible for substrate binding. One residue within the putative binding peptide of ERp18, is identified, which contributes to its reductase activity *in vitro*. Finally, an experiment is proposed to identify the protease involved in non-canonical processing of ATF6α using a combination of biochemical, molecular and *in silico* techniques.

Chapter 2. Materials and methods

2.1 Assays

2.1.1 ATF6α ER-to Golgi trafficking

The ER-to-Golgi trafficking assay was carried out as previously described by Oka et. Al (2019). Briefly, cells were pre-treated with 30 μM S1P inhibitor [PF429242] for 1 h to prevent cleavage of ATF6α. Cells were then treated with either 1 mM DTT or 5 μM thapsigargin to induce trafficking. Inhibition of S1P leads to accumulation of ATF6α in the Golgi and hyper-glycosylation which is an indication of trafficking; this was visualised by immunoblotting with mouse anti ATF6α or V5 as described in section 2.4.5.

2.1.2 Insulin reduction assay

For the insulin disulfide reductase activity assay,0.17 mM human insulin (Sigma) was incubated with 3 μM purified protein made up to 100 μl with reaction buffer 50 mM Tris-HCl pH 7.4, 0.1 mM EDTA and 0.5 mM DTT at room temperature for 20 min. Precipitation of the ß chain was monitored as the change in OD_{600} measured for 80 min using SPECTROstar^{Nano} microplate reader (BMG Labtech).

2.1.3 Lumenal domain stabilisation assay

Cells were pre-treated with 20 mM NH_4Cl for 45 min, or with 100 nM Bafilomycin A_1, to inhibit lysosomal degradation before being treated with 10 mM DTT or 5 μM TG to induce the UPR. Cell lysis, immunoprecipitation and immunoblotting were executed as described in sections 2.4.52.4.6.

2.1.4 Redox shift assay

Cells were grown to confluence in 6 cm dishes and left untreated or treated with 1 μM or 5 μM TG for 1 h. Lysis was performed as described below. Lysates were separated under non-reducing conditions. The intensities of bands representing ATF6α redox forms were quantified using Odyssey Licor CLX imaging system.

2.1.5 Transcriptional activation of BiP

Cells were treated with 1 μM thapsigargin for 20 h or they were left untreated. Cells were then lysed according to the protocol described, resolved by SDS PAGE, and BiP identified by western blotting.

2.2 Cell culture and maintenance

2.2.1 Maintenance of cell lines

Working stocks of cells were grown in DMEM supplemented with 10% FBS and 100 units/ml penicillin and 100 µg/ml streptomycin at 37°C in a 5% CO_2 incubator. For long term storage, cells were resuspended in FBS containing 10 – 20% DMSO and kept at -150 ^{0}C.

2.2.2 Transfections

2.2.2.1 Transient transfections

Cells were transfected with plasmid DNA at 60 – 80% confluence with MegaTran (OriGene) transfection reagent according to the manufacturer's specification. For transient transfections, experiments were carried out 20 – 24 h post transfection or, when required, the pool of cells was kept under selection for 3 – 4 weeks or subjected to stable transfection as described in section 2.2.2.2.

2.2.2.2 Stable transfections

To generate stable cell lines, the transfected cells were placed on antibiotic selection for approximately 2–4 weeks until single colonies appeared. These were expanded and positive clones were identified by immunoblotting.

2.3 Cell lines

2.3.1 ERp18KO cell line

To establish HT1080/ERp18KO cells, CRISPR/Cas9 was used to knockout endogenous ERp18 from HT1080wt cells. Cells were co-transfected with plasmids containing guides and Cas9 DNA, and pPUR to confer puromycin resistance. They plated, at various dilutions, in DMEM containing 100 µg/ml puromycin. Puromycin resistant colonies were chosen, and the knockout verified by immunoblotting.

2.3.2 Cell lines expressing ATF6 and ERp18

HT1080/ERp18KO cells were stably transfected as described in section 2.2.2.2 with pCDNA3.1 hygromycin containing sequences for ATF6wt with an N-terminal

HA tag and a C-terminal V5 tag. These cells were then stably transfected as described in section 2.2.2.2 with pCDNA3.1 zeocin plasmid containing sequences for ERp18WT, ERp18CS, ERp18ΔC4, ERp18S136D and ERp18Y137T (see sections 2.4.1.1 & 2.4.1.3).

2.3.3 MANF

Previously characterised ATF6KO cells (Oka, Pierre et al. 2022) were stably transfected with pCDNA3.1 zeocin (+) plasmids containing the sequence for human MANF with a C-terminal Myc tag (MANF-Myc) flanked by NheI and NotI restriction sites.

2.4 Molecular and biochemical methods

2.4.1 DNA constructs

2.4.1.1 ERp18 constructs

Full length ERp18 wild type (ERp18wt) and EDEL deletion mutant (ERp18ΔC4) constructs containing a C terminal FLAG tag were ordered from Genscript in pUC57 vector. The sequences, flanked by EcoRI and BamH1 restriction sites (in lower case letters) were codon optimised for mammalian expression with a Kozak sequence (underlined) preceding the start codon (in bold). The double cysteine mutant ERp18CS was obtained by site directed mutagenesis of ERp18wt using the primer pair listed in table 2.

Table 2-1 DNA sequences of ERp18 constructs optimised for mammalian expression.

ERp18wt *gaattc*/GCCGCCACC **ATG**GAGACCA GGCCAAGACT GGGAGCAACA TGCCTGCTGG GCTTCTCCTT TCTGCTGCTG GTCATCAGCT CCGACGGCCA CAATGGCCTG GGCAAGGGCT TCGGCGACCA CATCCACTGG CGGACCCTGG AGGATGGCAA GAAGGAGGCA GCAGCAAGCG GACTGCCTCT GATGGTCATC ATCCACAAGT CCTGGTGCGG CGCCTGTAAG GCCCTGAAGC CAAAGTTCGC CGAGTCTACA GAGATCTCTG AGCTGAGCCA CAATTTTGTG ATGGTGAACC TGGAGGACGA GGAGGAGCCC AAGGACGAGG ACTTCTCTCC CGATGGCGGC TATATCCCTA GAATCCTGTT CCTGGACCCC AGCGGCAAGG TGCACCCAGA GATCATCAAC GAGAATGGCA ACCCTTCCTA CAAGTATTTC TACGTGTCTG CCGAGCAGGT GGTGCAGGGC ATGAAGGAGG CACAGGAGAG GCTGACCGGC GACGCCTTTC GCAAGAAGCA CCTGGATTAC AAGGACGATG ACGATAAGGA GGATGAGCTGTAA *ggatcc*
ERp18ΔC4: gaattc/ GCCGCCACC/ **ATG**GAGACCA GGCCAAGACT GGGAGCAACA TGCCTGCTGG GCTTCTCCTT TCTGCTGCTG GTCATCAGCT CCGACGGCCA CAATGGCCTG GGCAAGGGCT TCGGCGACCA CATCCACTGG CGGACCCTGG AGGATGGCAA GAAGGAGGCA GCAGCAAGCG GACTGCCTCT GATGGTCATC ATCCACAAGT CCTGGTGCGG CGCCTGTAAG GCCCTGAAGC CAAAGTTCGC CGAGTCTACA GAGATCTCTG AGCTGAGCCA CAATTTTGTG ATGGTGAACC TGGAGGACGA GGAGGAGCCC AAGCACGAGG ACTTCTCTCC CGATGGCGGC TATATCCCTA GAATCCTGTT CCTGGACCCC AGCGGCAAGG TGCACCCAGA GATCATCAAC GAGAATGGCA ACCCTTCCTA CAAGTATTTC TACGTGTCTG CCGAGCAGGT GGTGCAGGGC ATGAAGGAGG CACAGGAGAG GCTGACCGGC GACGCCTTTC GCAAGAAGCA CCTGGATTAC AAGGACGATG ACGATAAGTAA ggatcc
ERp18CS: gaattc/ GCCGCCACC/ **ATG**GAGACCA GGCCAAGACT GGGAGCAACA TGCCTGCTGG GCTTCTCCTT TCTGCTGCTG GTCATCAGCT CCGACGGCCA CAATGGCCTG GGCAAGGGCT TCGGCGACCA CATCCACTGG CGGACCCTGG AGGATGGCAA GAAGGAGGCA GCAGCAAGCG GACTGCCTCT GATGGTCATC ATCCACAAGT CCTGGAGCGG CGCCTCCAAG GCCCTGAAGC CAAAGTTCGC CGAGTCTACA GAGATCTCTG AGCTGAGCCA CAATTTTGTG ATGGTGAACC TGGAGGACGA GGAGGAGCCC AAGGACGAGG ACTTCTCTCCC GATGGCGGCT ATATCCCTAG AATCCTGTTC CTGGACCCCA GCGGCAAGGT GCACCCAGAG ATCATCAACG AGAATGGCAA CCCTTCCTAC AAGTATTTCT ACGTGTCTGC CGAGCAGGTG GTGCAGGGCA TGAAGGAGGC ACAGGAGAGG CTGACCGGCG ACGCCTTTCG CAAGAAGCAC CTGGATTACA AGGACGATGA CGATAAGGAG GATGAGCTGTAA ggatcc

Table 2-2 Primer sequences used for site directed mutagenesis of ERp18 double cysteine mutant.

Primer Name	Primer Sequence (5' to 3')
ERp18CS_Fwd	5'-cacaagtcctggagcggcgcctccaaggccctgaag-3'
ERp18CS_Rev	5'-cttcagggccttggaggcgccgctccaggacttgtg-3'

2.4.1.2 Sub-cloning into pCDNA 3.1 Zeocin (+)

Full length ERp18 sequences were amplified by PCR using primers containing a 5' NheI restriction site and a 3' XbaI site to facilitate subcloning into pCDNA 3.1 Zeo (+) for mammalian expression. Ligation reactions containing restriction-digested amplicons and vector were set up in a ratio of 1 vector :3 insert and incubated overnight at 16 °C. DNA isolated from ampicillin-resistant colonies of XL1- Blue *E. coli* transformed with the ligation reaction was sequenced to verify successful cloning.

2.4.1.3 Mutagenesis

The following primer pairs were used for site directed mutagenesis of ERp18wt to give $ERp18^{S136D}$ and $ERp18^{Y137T}$.

Table 2-3 Primer sequences used for mutagenesis of ERp18.

ERp18 S136D Rev	5'-gacacgtagaaatacttgtagtcagggttgccattctcgttgat-3'
ERp18 S136D_FWD	5'-atcaacgagaatggcaaccctgactacaagtatttctacgtgtc-3'
ERp18_Y136T-Fwd	5'-c gag aat ggc aac cct tcc acc aag tat ttc tac gtg tct-3'
ERp18_Y136T-Rev	5'-aga cac gta gaa ata ctt ggt gga agg gtt gcc att ctc g-3'

2.4.2 Cell lysis

2.4.2.1 Detergent-based cell lysis

Media were removed from cells, and they were incubated with PBS supplemented with 25 mM N-Ethylmaleimide for 5 min at room temperature. Cells were collected by scraping and centrifugation at 1,000 × g for 5 min and then washed twice with ice-cold PBS. The cells were then resuspended in lysis buffer [1% (v/v) Triton X-100, 50 mM Tris–HCl (pH 7.4), 150 mM NaCl, 2 mM ethylenediaminetetraacetic acid (EDTA), and 0.5 mM phenylmethyl sulfonyl fluoride (PMSF)], incubated on ice for 10 min, followed by centrifugation at 15,000 × g for 10 min to obtain the post-nuclear supernatant.

2.4.2.2 Cell fractionation

Cells were washed twice using ice cold PBS supplemented with EDTA free protease inhibitor, collected using a cell scraper and centrifuged at 3000 xg for 7 min at 4 ºC. Cells were then resuspended in 1 ml buffer A (10 mM HEPES pH 7.4, 250 mM sucrose, 10 mM KCl, 1.5 mM MgCl2, 1 mM EDTA, and 1 mM EGTA) and incubated on ice for 30 min. They were lysed by 30 passages through a 23-gauge needle or by sonication as described below. Cells were centrifuged at 1000 xg for 7 min which separated the membrane and soluble components (supernatant), from the nuclear material (pellet). The pellet was washed in Buffer A and centrifuged 1000 xg for 7 min. The nuclear extract was obtained by resuspending the pellet in buffer B (10 mM HEPES (pH 7.6), 2.5% glycerol, 420 mM NaCl, 1.5 mM MgCl2, 1 mM EDTA, and 1 mM EGTA) with incubation at 4 ºC for 60 min, followed by centrifugation at 100 000 xg for 30 min.

2.4.2.3 Sonication

Prior to sonication, cells were incubated in buffer A at 4 ºC for 30 min. They were lysed using a program of 10s on/20s off, for 6 cycles, at 70% amplitude using a FB-120 Sonic dismembrator (Fisher Scientific).

2.4.3 Cross-linking

Cells were grown to 90 % confluence in 15 cm dishes. Media were removed and cells were washed with 10 ml PBS or PBS supplemented with 0.1 mM $CaCl_2$ and 1

mM $MgCl_2$. Cells in each dish were incubated with 10 ml crosslinking solution containing 0.5 mM DSP in PBS for 30 min at room temperature. The cross-linking solution was removed, and excess DSP was quenched with 50 mM Tris pH 7.5 in PBS. Cells were collected by scraping and centrifugation at 1500 rpm for 5 min.

2.4.4 SDS-PAGE

2.4.4.1 1D gel electrophoresis

Lysates prepared were mixed with SDS loading buffer to 1X concentration with or without 100 mM DTT for reducing and non-reducing conditions respectively. Gels were run at 20 mA and 300 V for approximately 2 h.

2.4.4.2 2D gel electrophoresis

Gels 1 mm thick were run in the first dimension under non-reducing conditions. Lanes for analysis in the second dimension were excised with a scalpel and incubated with 100 mM DTT in PBS for 10 min to reduce proteins. The excised gel was placed laterally atop a 1.5 mm resolving gel and sealed with 1 % agarose. The gel was then run 20 mA and 300 V for approximately 2 h.

2.4.5 Immunoblotting

For Western blotting, proteins were transferred to nitrocellulose membrane (Li-Cor Biosciences), which were blocked in 5% (w/v) non-fat dried skimmed milk in TBST (Tris-buffered saline with Tween-20: 10 mM Tris, 150 mM NaCl (pH 7.5), and 0.1% (v/v) Tween-20) for 60 min. Primary antibodies were diluted in TBST, and incubations were carried out for 1 – 4 h, at room temperature or for 16 h at 4 °C. IRDye fluorescent secondary antibodies were used for detection, typically at 1:10,000 dilutions. Blots were scanned using an Odyssey CLX imaging system (Li-Cor Biosciences).

2.4.6 Immunoprecipitation

Prior to immunoprecipitation, the post-nuclear supernatant was precleared by incubating with protein A Sepharose beads (Generon) for 10 – 30 min at 4°C. The mixture was then precleared by centrifugation at 14,000 × g for 1 min and the supernatant incubated with protein A Sepharose beads and the appropriate

antibody. Immunoprecipitated material was washed twice in lysis buffer. Proteins were eluted by boiling at 95°C for 5 min in SDS–PAGE sample buffer [200 mM Tris–Cl (pH 6.8), 3% SDS, 10% glycerol, 1 mM EDTA, and 0.004% bromophenol blue] prior to SDS–PAGE under either reducing (treated with 50 mM DTT) or non-reducing conditions.

2.4.7 Protein expression and purification

2.4.7.1 Subcloning into pET28a

Mature human ERp18 sequences (residues 24 – 172) was amplified by PCR using primers containing a 5' BamH1 restriction site and a 3' Xho1 site to facilitate subcloning into pET28a vector containing an in frame, N-terminal His tag, and a kanamycin resistance gene. Ligation reactions containing restriction-digested amplicons and vector were set up in a ratio of 1 vector :3 insert and incubated overnight at 16 °C. DNA isolated from kanamycin-resistant colonies of DH5α transformed with the ligation reaction was sequenced to verify successful cloning.

2.4.7.2 Expression and lysis

Protein production was carried out in E. coli strain BL21 (DE3). Strains were grown at 37 °C shaking at 200 rpm in LB medium containing 25 µg/ml Kanamycin. Expression was induced at an OD_{600} of 0.5 for 4 h with 0.5 mm isopropyl ß-d-thiogalactoside (IPTG). Cells were pelleted by centrifugation at 15 000 rpm for 10 min. The pellet was resuspended in 20 ml TBS lysis buffer (50 mM Tris pH 8.0, 150 mM NaCl and 1% (v/v) Triton X-100) supplemented with 10 µg/ml DNase (Roche Applied Science), 100 µg/ml lysozyme and 1 EDTA-free protease inhibitor tablet and incubated on ice for 30 min. Cells were lysed by sonication as described in section 2.4.2.3 and debris was removed by centrifugation (15 000 rpm for 20 min).

2.4.7.3 Purification

Lysates were filtered through a 0.45 µM filter and loaded onto an immobilized metal affinity chromatography (IMAC) column (Cytiva His GraviTrap) precharged with Ni^{2+} and equilibrated in binding buffer (20 mM Sodium Phosphate, 300 mM

NaCl and 20 mM imidazole pH 7.4). The column was washed with 10 ml binding buffer and proteins were eluted using 20 mM Sodium Phosphate, 300 mM NaCl and 500 mM imidazole pH 7.4. Proteins were dialysed into 1x TBS buffer (50 mM Tris pH 8.0, 150 mM NaCl) and stored at -80 °C in 50 µl aliquots.

2.5 Reagents

2.5.1 Antibodies

All antibodies used are listed in (Table 2-4).

Table 2-4 Antibodies used in study

Antibody	SOURCE
Primary Antibodies	
Rabbit polyclonal anti-alpha Tubulin	Abcam
Rabbit monoclonal anti-ERp18	Abcam [EPR9025]
Rabbit anti-ERp57	Bulleid Lab
Rabbit monoclonal anti-HDAC2	Abcam [Y461]
Mouse monoclonal anti-ATF6	Abcam
Mouse monoclonal anti-GAPDH	ThermoFisher Scientific
Mouse monoclonal anti-V5	Invitrogen
Mouse monoclonal anti-Myc - clone 4A6	Merck
Mouse monoclonal anti-HA	Sigma
Rabbit anti-HA	Sigma
Mouse monoclonal anti-BiP/GRp78	BD Biosciences
Rabbit monoclonal Recombinant anti-ARMET/MANF	Abcam [EPR22538-206]
Mouse anti-FLAG	Sigma
Rabbit anti FLAG	Cell signalling
Rabbit anti V5	Stephen High
Secondary Antibodies	
Goat anti-Mouse IRDye 800	Fisher Scientific
Goat anti-Mouse IRDye 680	Fisher Scientific
Goat anti-Rabbit IRDye 800	Fisher Scientific
Goat anti-Rabbit IRDye 680	Fisher Scientific

2.5.2 General Reagents

Chemicals and other routinely used reagents were sourced from ThermoFisher, Invitrogen or Generon.

Chapter 3. Redox changes to ATF6α during the UPR and the consequences on ER to Golgi trafficking

3.1 Introduction

3.1.1 The mechanism of ATF6α activation

The ATF6α response to ER stress can be roughly divided into 3 phases which consists of (1) stress detection and release from retention factors in the ER, (2) packaging and transport to the Golgi and (3) cleavage and transactivation.

3.1.1.1 Stress detection

Sensing ER stress involves interplay between BiP, and other unknown regulatory factors, and the lumenal cysteines. The ER chaperone BiP, the main inhibitory regulator of ATF6α, stably interacts with ATF6α and maintains it in an inactive state in the absence of ER stress possibly by blocking its Golgi localisation signals (Shen, Snapp et al. 2005). During ER stress, release from BiP exposes the GLSs resulting in ATF6α being packaged into COP II vesicles for trafficking to the Golgi (Shen, Chen et al. 2002). However, the mechanism of BiP release is unclear. The canonical interaction between BiP and ATF6α supports the model of unfolded proteins outcompeting ATF6α. But there is also evidence for active regulation that may involve factors that modulate BiP binding affinity in varying conditions (Wang and Sevier 2016, Yan, Rato et al. 2019, Preissler, Rato et al. 2020).

Although studies have implied the involvement of the ATF6α lumenal cysteines, their role in stress detection remains unclear. Interestingly, both cysteines fall within BiP binding sequences and cysteine 467 is adjacent to GLS1. Furthermore, these cysteines are thought to be reduced during ER stress (Chen, Shen et al. 2002, Nadanaka, Okada et al. 2007). It is possible that BiP release allows access to reduce the cysteines or that reduction of the cysteines lead to release of BiP; however, the sequence of these events is yet to be experimentally determined.

3.1.1.2 Packaging and transport to the Golgi

BiP release and reduction of lumenal cysteines is followed by packaging into COPII vesicles which transport the reduced monomer to the Golgi. While reduction is important in the formation of a transport-competent species, it is

not exclusively responsible for activation and both are necessary for successful transport (Chen, Shen et al. 2002, Schindler and Schekman 2009, Sato, Nadanaka et al. 2011).

Two small PDI-like proteins, endoplasmic reticulum protein 18 (ERp18) and protein disulfide isomerase A5 (PDIA5), have been shown to modulate ATF6α redox state and regulate ATF6α transport to the Golgi. ERp18 was identified as an interacting partner to ATF6α during ER stress and can reduce ATF6α cysteines. In its absence, there is increased trafficking between the ER and the Golgi while overexpressing it attenuates ATF6α stress response (Oka, van Lith et al. 2019). PDIA5 (also known as PDIR) is also able to modulate ATF6α redox status and is important in ER-Golgi transport. SiRNA knockdown of ATF6α leads to impaired transport of ATF6α (Higa, Taouji et al. 2014).

3.1.1.3 Cleavage and transactivation

Intramembrane proteolysis represents the final regulatory step of ATF6α activation that directly controls the release of the transcription factor which will translocate to the Nucleus to modulate protein expression. Site-1-protease (S1P) recognises and cleaves at the sequence RRHLL contained within the lumenal domain adjacent to the transmembrane domain. The sequence is positioned to allow access by S1P which is also membrane anchored with its catalytic domain oriented toward the lumen (Espenshade, Cheng et al. 1999). Most of the lumenal domain is removed during S1P cleavage which prepares ATF6α for cleavage by S2P. But it is unclear what happens to it and whether it plays any further role in ATF6α response. Preventing S1P cleavage by chemical inhibitors or mutating the RRHLL sequence also blocks S2P cleavage and activation demonstrating S2P dependence on S1P cleavage (Chen, Shen et al. 2002, Oka, van Lith et al. 2019). S2P cleavage releases the N-terminal fragment which contains the DNA binding bZIP domain and the transactivation factor that relocates to the Nucleus to upregulate target genes.

3.1.2 Redox changes in the ER during the UPR

Protein folding occurs within an oxidative environment that is maintained by mechanisms involving enzymes such as Ero1α, peroxiredoxin IV, and maintaining

equilibrium between levels of oxidised (GSSG) and reduced glutathione (GSH) (Appenzeller-Herzog, Riemer et al. 2008, Baker, Chakravarthi et al. 2008). Fluctuations from steady state have previously been interpreted by observing changes in the GSH:GSSG ratio or detected using redox responsive fluorescent proteins (Appenzeller-Herzog, Riemer et al. 2008, Appenzeller-Herzog, Riemer et al. 2010, Tavender and Bulleid 2010). Chemo-toxic stress induced via calcium depletion, puromycin mediated blocking of protein synthesis or inhibition of proteasomal degradation all make the ER more reducing (Lohman and Remington 2008, Bulleid and van Lith 2014). However, proteasome inhibition causes a small increase in oxidation prior to reduction by increasing levels of lumenal GSH (Oku, Kariya et al. 2021). Overexpression of a misfolding-prone protein was shown to increase production of reactive oxygen species (ROS) making the ER more oxidised (Malhotra, Miao et al. 2008).

Redox changes in the UPR sensors reported during ER stress do not necessarily correlate with the perturbation observed during the UPR and are not uniform. For example, in response to calcium depletion, ATF6α reportedly shifts toward the monomeric state while PERK and IRE1 shift toward their oligomeric state (Liu, Schröder et al. 2000, Nadanaka, Okada et al. 2007, Carrara, Prischi et al. 2015). These findings not only suggest different mechanisms of activation but also implicate redox changes in the schema of activation.

3.1.3 Aims

Several layers of regulation are integrated into the activation mechanism of ATF6α. The role of the monomer (formed through reduction of lumenal cysteines) and BiP binding are well documented. Yet, questions remain concerning the mechanism of BiP release, redox modulation and the role of ATF6α dimers.

This chapter aims to interrogate the role of redox and oligomeric status in the regulation and trafficking of ATF6α. This is done by isolating the lumenal domain after S1P cleavage to examine its redox status in response to various stressors. We also investigate the redox changes of full length ATF6α by using an assay to follow ER-to-Golgi trafficking of ATF6α in response to different ER stressors.

3.2 Results

3.2.1 ATF6α redox changes in trafficking

3.2.1.1 Alterations in the redox status of endogenous ATF6α in response to UPR activation.

Activation of the ATF6 branch of the UPR is thought to occur via reduction to monomeric ATF6α. Cellular fractionation studies have indicated that reduced monomeric ATF6α is localised to the Golgi when ER stress was generated using chemical stressors or physiological conditions such as glucose starvation (Nadanaka, Yoshida et al. 2006, Nadanaka, Okada et al. 2007). Chemicals such as DTT affect the redox balance of the ER while others, such as thapsigargin, do not. To examine the trafficking of ATF6α under different redox conditions we utilised a hypergylcosylation assay. Inducing the UPR while site-1-protease (S1P) is inhibited, prevents cleavage and causes accumulation of ATF6α in the Golgi where it becomes hyperglycosylated by the addition of O-glycans to the lumenal domain. This hyperglycosylated form, which displays slower electrophoretic mobility, is indicative of trafficking from the ER to the Golgi in response to UPR activation (Oka, van Lith et al. 2019).

When HT1080wt cells were treated with 10 mM DTT in the presence of S1P inhibitor ($S1P_i$) (Hay, Abrams et al. 2007), which prevents cleavage and leads to the accumulation of hyperglycosylated ATF6α, we obtained results reflecting findings by Oka et. al (2019) (Figure 3-1A). In cells that were not treated, immunoblotting with mouse anti ATF6 antibody detected three redox forms of endogenous ATF6α i.e., the monomer (designated M), and two interchain disulfide bonded dimers designated 467D and 618D (lane 1). Two bands were detected in cells treated with DTT only: the monomer and the cleaved form of ATF6α, ATF6-N (lane 2). Cells that were treated with DTT and $S1P_i$ contained two additional bands (M*) identified as hyperglycosylated monomer (lane 3). The second was identified as a potential dimer of ATF6 and will be addressed in the discussion. This finding was consistent with the trafficking of monomeric ATF6 as previously described (Chen, Shen et al. 2002, Nadanaka, Okada et al. 2007).

To capture any redox changes that may occur during trafficking of ATF6α, we induced the UPR by calcium depletion which does not directly reduce proteins. Untransfected HT1080 cells were treated with 5 μM thapsigargin (TG) in the presence of $S1P_i$ to prevent ATF6α cleavage. As a control, cells were either untreated or treated with TG only. To preserve the redox status of the proteins, cells were treated with 25 mM NEM before lysis and lysates were resolved under non-reducing conditions (Figure 3-1B). Lysates of untreated cells contained three bands representing the three redox forms of ATF6α with the monomer (M) being the major form and roughly equivalent amounts of the dimers 467D and 618D (Figure 3-1B lane 1). Treatment with TG led to a change in the relative quantities of the various forms of ATF6α; we observed a reduction in the amount of monomer and a corresponding increase in dimer 467D while dimer 618D remained largely unchanged (lane 2). When S1P was inhibited, TG treatment resulted in a similar change in redox forms with the appearance of two additional bands. The first, ATF6-P, represented an alternatively processed form of ATF6α produced by cleavage by another protease (see chapter 5) when S1P is inhibited (Oka, van Lith et al. 2019). The second (467D*) displayed slower electrophoretic mobility than the other forms of ATF6α (lane 3). We reasoned that this is likely to be the hyperglycosylated form of dimer 467D based on a similar change in electrophoretic mobility seen with hyperglycosylated monomeric ATF6α (Figure 3-1A and (Oka, van Lith et al. 2019)).

To investigate whether these redox changes can occur when the UPR is activated via reduction, we induced the UPR with a concentration of DTT that was 10-fold lower than used in the first experiment (1 mM) and examined lysates under non-reducing and reducing conditions (Figure 3-1C & D). Lysates from untreated cells, resolved under non-reducing conditions, displayed three forms of ATF6α as expected (Figure 3-1C lane 1). When cells were treated with DTT, the monomer and the 467D were present but 618D was not visible (lane 2). We reasoned that the absence of dimer 618D was due to the fact that it may have been reduced. This reduction would also account for an apparent decrease of dimer 467D and less significant decrease of the monomer when cells are treated with DTT (Figure 3-1C lane 2) compared to TG treatment (Figure 3-1B lane 2). During the inhibition of S1P, DTT treatment led to the appearance of 467D*, the putative

hyperglycosylated form of dimer 467D which is indicative of trafficking of dimeric ATF6α.

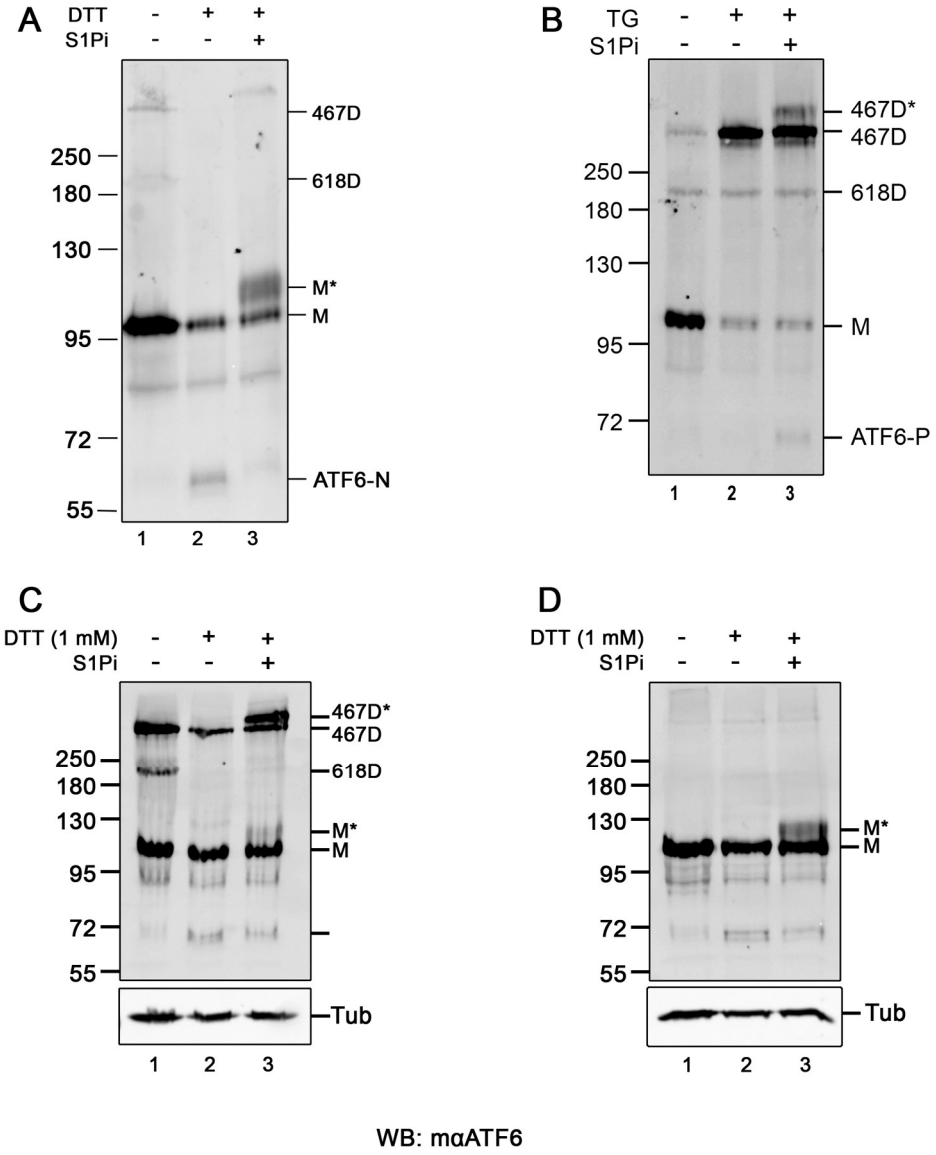

Figure 3-1 ER stress promotes redox shift and trafficking of ATF6.
(A) HT1080wt cells were untreated or treated with 10 mM DTT for 30 min in the presence of S1P inhibitor (PF 429242). Lysates were resolved under non-reducing conditions and proteins were identified by immunoblotting with mouse anti ATF6 antibody. (B) HT1080wt cells were treated with 5 μM thapsigargin (TG) for 1 h in the presence of S1P inhibitor (PF429242). As a control, cells were left untreated or treated with TG only. Lysates were resolved under non-reducing conditions and proteins were identified by immunoblotting with mouse anti ATF6 antibody. (C) HT1080wt cells were untreated or treated with 1 mM DTT for 30 min in the presence of S1P inhibitor (PF 429242). Lysates were resolved under non-reducing conditions and proteins were identified by immunoblotting with mouse anti ATF6 antibody. (D) HT1080wt cells were untreated or treated with 1 mM DTT for 30 min in the presence of S1P inhibitor (PF 429242). Lysates were resolved under reducing conditions and proteins were identified by immunoblotting with mouse anti ATF6 antibody.

A small quantity of hyperglycosylated monomer was detected, but it is unclear whether this is from [direct] hyper-glycosylation of the monomer or reduction of hyperglycosylated dimer (lane 3). Furthermore, lysates from HT1080wt cells treated with DTT in combination with S1P inhibition revealed two prominent bands that were recognised by the antibody when resolved under reducing conditions (Figure 3-1D lane 3) compared to a single band when untreated (lane 1) or treated with DTT only (lane 2). DTT reduces the disulfide bonds in all forms thereby converting them to the monomer. The upper band represented Golgi-localised, hyperglycosylated monomeric ATF6α (M*) which was likely formed by reduction of the disulfide bonds present in hyperglycosylated dimeric ATF6α while the lower band, also visible in untreated (lane 1) and DTT-treated cells (lane 2), represents unmodified ATF6α.

These results indicated that ER stress leads to a shift in the redox forms of ATF6α: a decrease in monomeric ATF6α and an increase in 467D. In addition, the appearance of the slower migrating, hyperglycosylated dimer when S1P is inhibited is indicative of trafficking of this species from the ER to the Golgi; the site of O-glycosylation.

3.2.1.2 Alterations in the redox status of exogenous ATF6 in response to UPR activation.

3.2.1.3 Establishing a cell line expressing HA-ATF6wt-V5

Research into ATF6 activation and function has traditionally been done by overexpressing exogenous ATF6α in cells that already contain endogenous ATF6α. While these experiments have been invaluable, there are limitations to how accurately they reflect normal physiological processes. For example, overall levels of ATF6α in these cell lines exceed normal physiological levels which can lead to additional effects such as trafficking of ATF6α in the absence of ER stress. Additionally, there is no way to determine how the endogenous protein affects the processing and trafficking of the exogenous protein and vice versa. We sought to circumvent these limitations during our investigation of the ATF6α redox shift and trafficking phenotype by creating a cell line that expresses exogenous ATF6α with an HA tag on the N terminus and a V5 tag on the C terminus which also allows us to follow the fate of the lumenal domain.

ATF6KO cells, created and characterised in our lab (Oka, Pierre et al. 2022), were transfected with ATF6wt DNA and grown under hygromycin selection as described in the materials and methods. Seven hygromycin resistant clones were selected, and expression of the protein was determined by immunoblotting with mouse anti V5 antibody (Figure 3-2). Further characterisation was necessary to decide which of the clones 3,4,6 or 7 were suitable for further use.

ATF6α is a transcription factor that upregulates BiP expression in response to ER stress. There is a significant reduction in BiP induction in cells deficient of ATF6α when compared to cells expressing wild type ATF6α (Oka, Pierre et al. 2022). In order to determine whether this phenotype was recovered by exogenous expression, the activation of BiP expression in revertant clones ATF6RV3 and ATF6RV6 was compared to that of endogenous ATF6α in HT1080wt cells. Immunoblotting of lysates of unstressed cells showed that the highest level of ATF6α was produced in untransfected HT1080wt cells followed by ATF6RV3 then ATF6RV6 with clear distinction between endogenous and exogenous ATF6α as the tagged protein migrated slower than the endogenous protein (Figure 3-3A). We hypothesised that the induction of BiP would correlate with the expression of ATF6α, however, there were some additional bands (indicated by black arrows) produced in clone ATF6RV3 which suggested possible problems with expression which may affect function. ATF6KO, HT1080wt, ATF6RV3 and ATF6RV6 cells were either untreated or treated with 1 μM TG for 20 h.

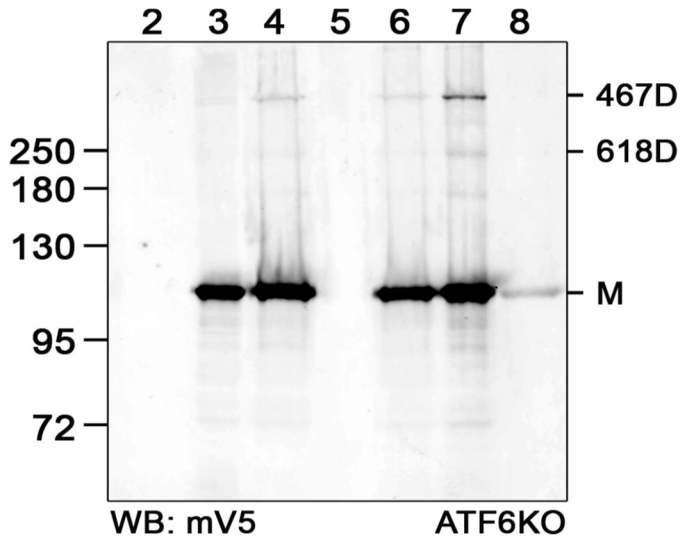

Figure 3-2 Stable expression of ATF6α in ATF6KO cells.
Several clones of ATF6KO cells stably transfected with HA-ATF6wt-V5 DNA were picked after two weeks of growth under hygromycin selection and tested for expression of ATF6α by immunoblotting using mouse anti v5 antibody.

Lysates were then subjected to immunoblotting to detect BiP and tubulin (as a loading control). In all cells, BiP was upregulated by treatment with TG with HT1080wt showing the greatest upregulation (Figure 3-3B). There was some upregulation of BiP in the ATF6KO cells in response to TG treatment although this was significantly lower than HT1080wt. This indicated that while ATF6α is largely responsible for regulating BiP expression during ER stress, there are also other mechanisms involved in BiP regulation following a UPR. Initially, it appeared as if ATF6RV3 showed greater upregulation of BiP than ATF6RV6, however; quantification (Figure 3-3C) showed that upregulation in ATF6RV6 was greater even though the expression of ATF6α was lower. Due to the higher induction of BiP expression and the absence of additional bands in ATF6RV6, it was chosen for comparison with two other clones.

Comparing the expression of ATF6α among clones ATF6RV4, ATF6RV6, and ATF6RV7 revealed that ATF6RV4 had the highest expression, producing similar levels of protein to HT1080wt, followed by ATF6RV7 then ATF6RV6 (Figure 3-4A). As before, we investigated whether we were able to restore the induction of BiP in the revertant cell lines. Cells were either untreated or treated with 1 μM TG for 20 h and ATF6KO cells were utilised as a negative control. As previously seen, there was an increase in BiP expression in all cells relative to the KO cells when treated with thapsigargin and it was found that ATF6RV4 was able to induce BiP expression at levels comparable to HT1080wt (Figure 3-4B and 4C).

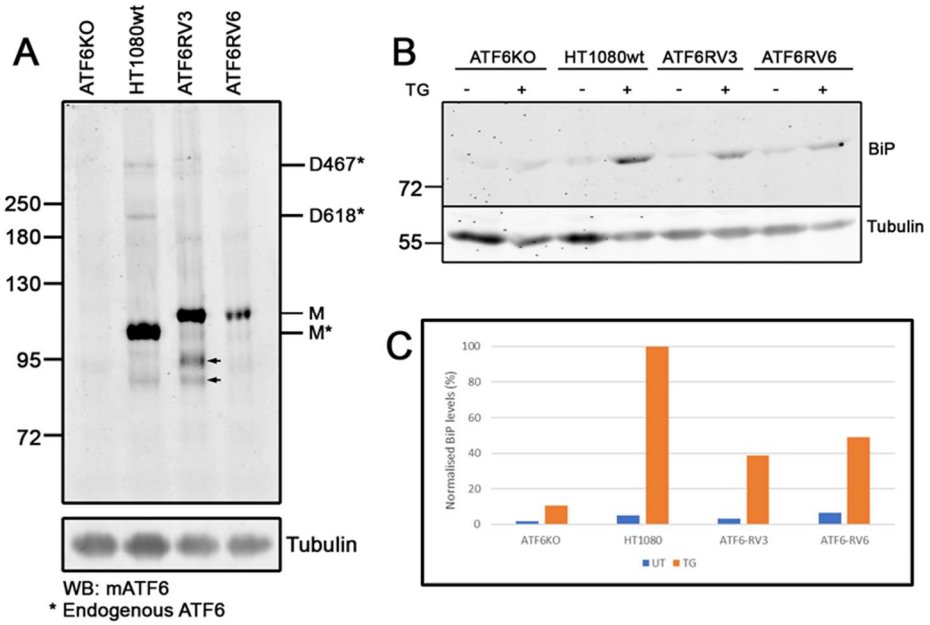

Figure 3-3 Investigating the expression and function of exogenous ATF6α in revertant clones ATF6RV3 and ATF6RV6.
(A) Lysates of ATF6KO, HT1080wt, ATF6RV3 and ATF6RV6 cells were subject to immunoblotting with mouse anti ATF6 to compare the expression of endogenous and exogenous ATF6. The asterisk represents endogenous ATF6. (B) ATF6KO, HT1080wt, ATF6RV3 and ATF6RV6 cells were treated or not with 1μM TG for 16 h. Proteins were separated by SDS PAGE and BiP expression was detected by immunoblotting with mouse anti BiP. (C) quantification (n=1) of BiP expression relative to tubulin (loading control) was determined using ImageJ.

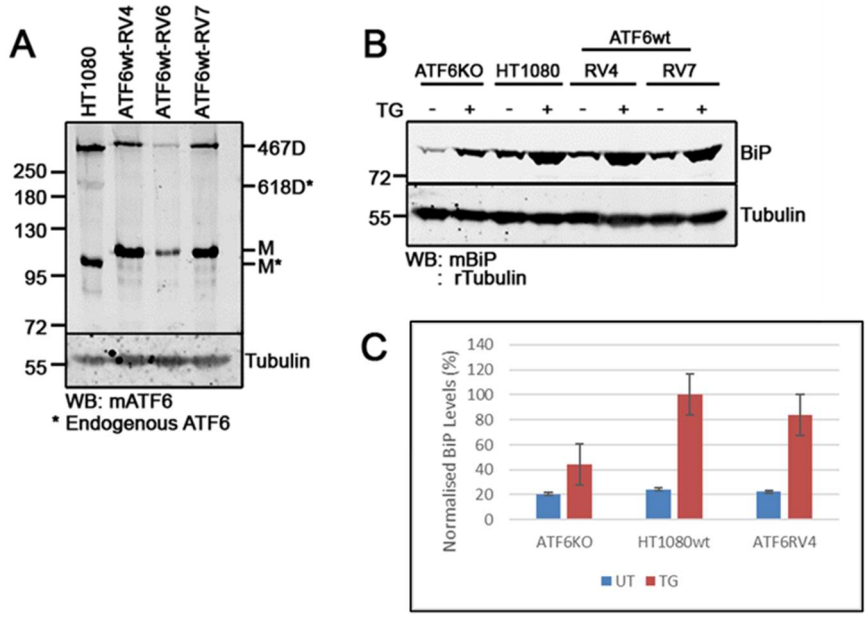

Figure 3-4 Comparison of the expression and function of exogenous ATF6α.
(A) The expression of tagged ATF6α in clones RV4, RV6 and RV7 was compared to the expression of endogenous ATF6α in wildtype HT1080 cells. Proteins were identified by immunoblotting with mouse anti ATF6. Tubulin is used as a loading control. (B) ATF6KO, HT1080wt, ATF6wt-RV4 and -RV7 were left untreated or treated with 1μM thapsigargin for 20 h to determine and compare their ability to induce BiP expression. BiP levels were determined by western blotting with mouse anti BiP. Tubulin was used as a loading control. (C) BiP levels, relative to tubulin, were quantified by densitometry using the program ImageJ. Results presented as the mean of three independent experiments with error bars representing +/- S.D.

3.2.1.4 Trafficking of exogenous ATF6

Given that the ATF6WT-RV4 cells exhibited the ATF6wt phenotype with respect to BiP induction, we induced the UPR with TG to assess whether the redox shift from monomer to 467D is maintained and inhibited S1P cleavage to assess hyperglycosylation and determine whether 467D is trafficked. ATF6WT-RV4 cells were untreated or treated with 5 μM TG in the presence or absence of $S1P_i$ (Figure 3-5A). In untreated cells, immunoblotting with mouse anti V5 detected ATF6α monomer and dimer 467D but not dimer 618D (lane 1). This may have been due to low levels of protein as this dimer was detected in all other samples. Treatment with TG led to an increase in dimer 467D (lane 2) and the appearance of the putative hyperglycosylated form of the 467D in the presence of $S1P_i$ (lane 3).

Trafficking of exogenous ATF6α was also investigated using a time course to determine how quickly activation occurs in cells stably expressing ATF6WT. ATF6WT-RV4 cells were untreated, treated with thapsigargin only (for 20 min), or pre-treated with S1P inhibitor before treatment with thapsigargin for 10, 20 and 30 min (Figure 3-5B). Compared to the untreated cells (lane 1) there was a decrease in monomeric ATF6α and an increase in 467D in cells treated with TG only for 20 min (lane 2). For cells treated with $S1P_i$ and TG, the hyperglycosylated form of dimer 467D appeared after 20 min of treatment (lanes 3 – 5). These results indicated that the UPR is rapidly induced leading to a decrease in the amount of monomeric ATF6α and an increase in 467D which putatively traffics to give a slower migrating hyperglycosylated dimer in the presence of $S1P_i$. This hyperglycosylated species confirms the trafficking of ATF6α to the Golgi.

Given that the lumenal cysteines are responsible for the dimerisation of ATF6, we hypothesised that any interchain disulfides that form during activation should be preserved in the cleaved ATF6 lumenal domain (ATF6-LD) and can be used to determine the redox status of the redox form of ATF6α that was cleaved by S1P.

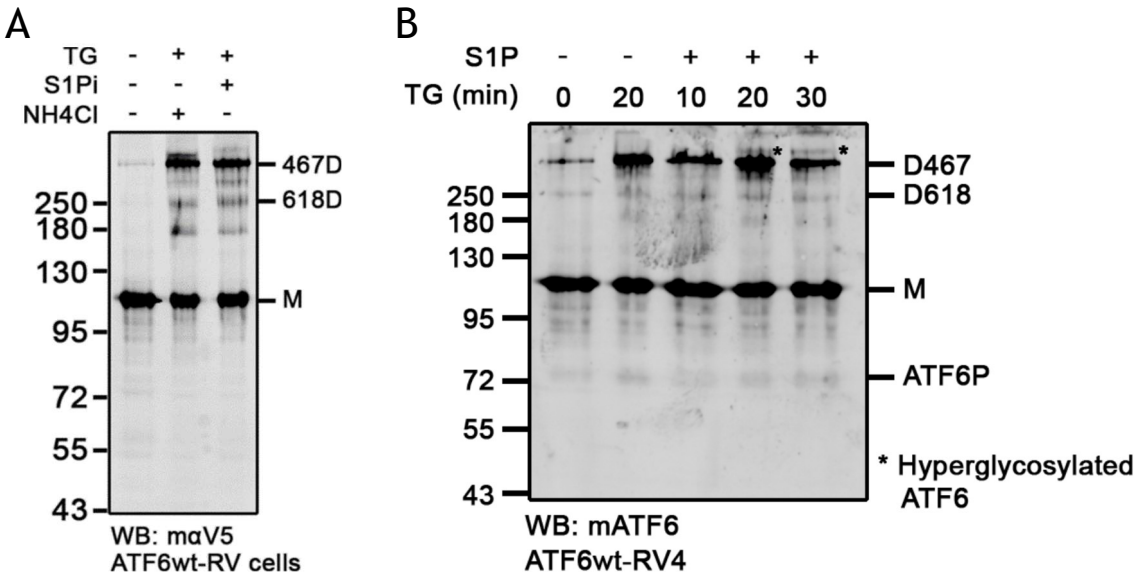

Figure 3-5 Trafficking of Exogenous ATF6
(A) ATF6KO cells stably expressing HA-ATF6Wt-V5 were left untreated or treated with 5 μM thapsigargin for 1 h in the presence or absence of S_1P inhibitor. Proteins were resolved under non reducing conditions and identified by western blotting with mouse anti V5. (B) ATF6KO cells stably expressing ATF6WT were treated with S1P inhibitor followed by thapsigargin for the indicated times. As a control, cells were treated with thapsigargin only or left untreated. Proteins were resolved under non-reducing conditions and identified by immunoblotting with mouse anti ATF6.

3.2.2 Investigating the fate and redox status of the lumenal domain

3.2.2.1 The lumenal domain of ATF6α is stabilised by inhibiting lysosomal degradation

Intra-membrane proteolysis of ATF6α by S1P and S2P separates the cytoplasmic and lumenal domains, designated ATF6-N and ATF6-LD respectively. It is known that ATF6-N migrates to the nucleus where it regulates transcription; however, what happens to ATF6-LD remains unknown. ATF6-LD contains binding sites for regulators such as BiP (Shen, Chen et al. 2002, Shen, Snapp et al. 2005) and the cysteines that are involved disulfide formation during activation. Thus, understanding the fate of ATF6-LD can provide valuable insight into regulation. Given that the lumenal cysteines are responsible for stabilising ATF6α dimers, we hypothesised that redox changes that occur during activation should be preserved in the cleaved ATF6 lumenal domain (ATF6-LD) and can be used to determine the redox status of the form of ATF6α that was processed by S1P or S2P. In regard to its fate, it was hypothesized that ATF6-LD would either be secreted - in which case it could be isolated from the medium – or it would be degraded and could be isolated from cell lysates. Furthermore, if it is indeed degraded, this will be accomplished via the lysosomes or the proteasome.

To determine whether the lumenal domain is secreted or degraded, its post-cleavage localisation, i.e., intracellular or extracellular, was investigated by determining whether it can be isolated from the lysates or media of cells treated with DTT to induce ATF6α cleavage. Being a strong reducing agent, DTT produces rapid activation of ATF6α which allowed accumulation and detection of a cleavage product within 30 min of treatment. The ATF6α construct used has a C-terminal V5 tag which facilitates immunoprecipitation, and identification, of ATF6-LD and full length ATF6α with anti V5 antibody.

Cells were untreated or treated with DTT (10 mM) for 15 and 30 min. Lysates and media from cells were subject to immunoprecipitation with mouse anti V5 and proteins resolved under reducing conditions were detected by immunoblotting (Figure 3-6A). After 15 min of treatment with DTT, a V5-reactive band was visible at approximately 43 kDa which is the expected size of the lumenal domain (lanes 2 & 3). The band was noticeably absent in untreated

cells (lanes 1 & 4) and was immunoprecipitated from the lysates of cells treated with DTT (lanes 5 & 6) but not the media (lanes 8 & 9). From this result it was determined that this band - likely to be the lumenal domain - represents a protein that was not secreted, but subject to degradation.

To determine the degradation pathway, cells were untreated or treated with 20 mM NH_4Cl for 45 min (to inhibit the lysosomal hydrolases) and/or 20 μM MG132 for 1 h (to inhibit the proteasome) before being treated with 10 mM DTT for 1h. Proteins were immunoprecipitated, eluates resolved under non-reducing SDS/PAGE conditions and proteins were identified by immunoblotting with mouse anti V5. Lysates of cells not treated with DTT contained clear bands representing monomeric ATF6α and the antibody chains (Figure 3-6B lanes 1 – 3). In samples that were treated with DTT, bands of similar size to those seen in the initial experiment were present and stabilised in samples that were pre-treated with NH_4Cl compared to samples pre-treated with MG132 (Figure 3-6B lanes 4 - 7). This showed that stabilisation of this 43 kDa band was achieved when lysosomal hydrolases were inhibited indicating that the degradation of ATF6-LD is via the lysosome, and not the proteasome.

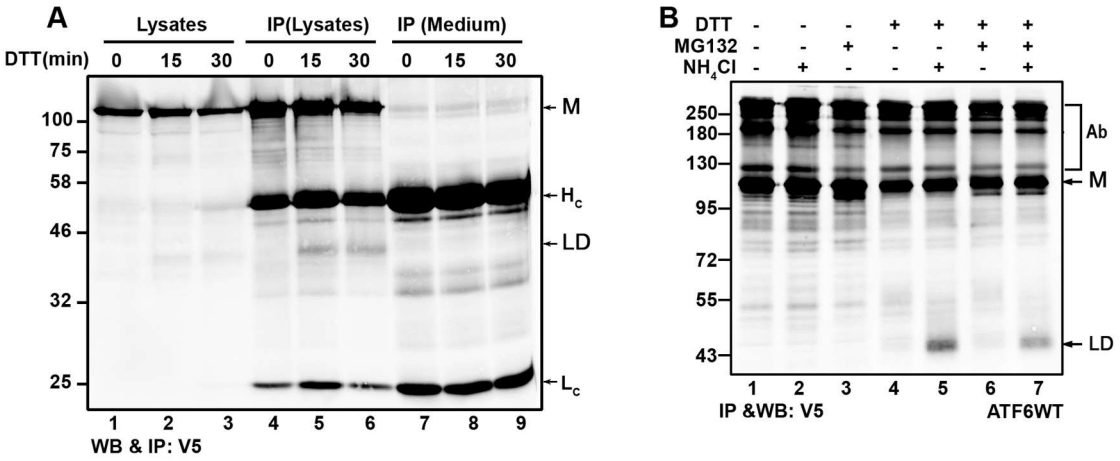

Figure 3-6 Inhibiting lysosomal degradation stabilises the lumenal domain of ATF6 (ATF6-LD).
(A) Reduced lysates and mediums from ATF6WT cells which were untreated or treated with 10 mM DTT for the indicated times were immunoprecipitated and immunoblotted with mouse anti V5 antibody. Bands corresponding to the expected size of the lumenal domain are observed only in lysates of DTT treated cells. H_c and L_c represent the heavy and light antibody chains respectively. (B) Cells were treated, or untreated, with 10 mM DTT for 1 h after being treated with 20 mM NH_4Cl for 45 min or MG132 for 1 h or both. Lysates were resolved under non-reducing conditions and subjected to immunoprecipitation and immunoblotting with mouse anti V5 antibody. Ab represents antibody chains.

The production of ATF6-LD is a direct consequence of S1P cleavage. To confirm that the detected band was indeed the lumenal domain, we investigated whether its formation is prevented when S1P is inhibited. When cells pre-treated with S1Pi were treated with DTT, the bands indicative of the lumenal domain were not seen (Figure 3-7A lanes 4 & 8) similar to cells that were untreated (lanes 1 & 5). However, these bands were visible in the absence of S1P inhibition (lanes 2 & 5) and were more prominent in the presence of NH_4Cl (lanes 3 & 7). These results demonstrated that the observed ~43 kDa band is the lumenal domain of ATF6α formed by S1P cleavage and degraded via the lysosomes. The sizes of these bands were unchanged when analysed under reducing or non-reducing conditions (Figure 3-7A lanes 3 &7). This is consistent with the fact that activation of ATF6α by DTT occurs via direct reduction and the dogma that monomeric ATF6α is trafficked and processed (Nadanaka, Okada et al. 2007).

Proteins that pass through the Golgi are subject to modification of glycan side chains during which some residues may be removed by endoglycosidase H (Endo H) allowing the addition of various other glycan residues. These changes confer resistance to Endo H which can then be indicative of passage through the Golgi (Stanley 2011). These proteins however remain sensitive to Peptide -N-Glycosidase F (PNGase). To determine whether ATF6-LD was formed by cleavage of protein that entered the Golgi, samples from Figure 3-7A were treated with either Endo H or PNGase. As a control, samples were left untreated (Figure 3-7B). Considering full-length ATF6α, samples treated with Endo H (lane 2) showed a clear shift in mobility compared to the untreated samples (lane 1). This was expected and indicated that the full-length protein is ER localised and therefore is sensitive to Endo H cleavage. The mobility-shift created by PNGase digestion was equivalent to that of Endo H indicating comparable deglycosylation (lane 3). Considering ATF6-LD, PNGase treatment led to a large shift in mobility consistent with the removal of glycan residues. Digestion with Endo H led to a mobility shift for a fraction of the protein which suggested partial resistance to EndoH likely gained from trafficking to the Golgi where the glycans undergo modification to confer resistance. This result is not surprising because not all proteins passing through the Golgi are subject to modification.

Treatment of cells with high concentrations of DTT led to the activation and trafficking of monomeric ATF6α. Pre-treatment with NH_4Cl allowed the preservation of monomeric lumenal domain which reflected the redox status of the trafficked species thus supporting our hypothesis that the redox status of the lumenal domain would reflect that of the redox form that has been cleaved. Furthermore, the fact that S1Pi prevented the formation of the lumenal domain and resistance of the lumenal domain to EndoH digestion suggested that it was formed in the Golgi.

These results agreed with previous findings of the activation of monomeric ATF6 but were not consistent with the shift in redox status of ATF6α seen when activation occurs with thapsigargin and lower concentrations of DTT nor the trafficking of 467D.

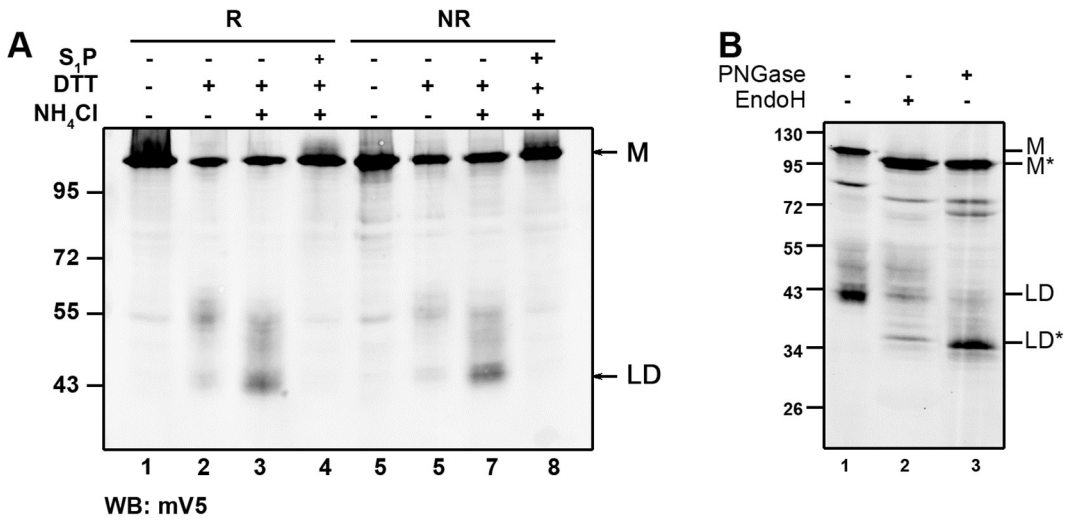

Figure 3-7 S1P-dependent production and glycosylation status of the lumenal domain. (A) ATF6WT cells were treated with 20 mM NH_4Cl for 45 min before being treated with 10 mM DTT for 45 min. As a control for cleavage cells were pre-treated S1Pi for 1 h. (B) Samples from (A) were digested, or not, with PNGase or Endo H to determine the glycosylation status. Proteins were resolved under reducing and non-reducing conditions and identified by western blotting with Mouse anti V5 antibody. Asterisks represent de-glycosylated proteins.

3.2.2.2 Redox status of the lumenal domain

The formation of ATF6-LD was investigated under non-reducing conditions using thapsigargin which induces the UPR by depleting ER calcium levels (Hay, Abrams et al. 2007). HEK293 cells overexpressing wild-type ATF6α (HEK-ATF6WT) were pre-treated with NH_4Cl followed by thapsigargin treatment for 1 h. Proteins from lysates were resolved under reducing and non-reducing conditions and identified by immunoblotting with mouse anti V5 (Figure 3-8A). Under reducing conditions ATF6LD was visible as a monomer in treated cells (lanes 2 & 3) and absent in lysates of untreated cells (lane 1), or cells treated with S1Pi (lane 4). When lysates were analysed under non-reducing conditions there was surprisingly no band representing the monomer in treated cells; instead, a band at roughly 2 times the expected size of ATF6-LD was visible (lanes 6 & 7). Interestingly pre-treatment with S1Pi abolished the formation of this band (lane 8). This led us to conclude that ATF6-LD dimer, (reactive with V5 antibody) was formed by S1P cleavage.

Given that previous reports have shown that only monomeric ATF6α traffics to the Golgi, and this form is preferentially cleaved by S1P (Nadanaka, Okada et al. 2007), it was necessary to exclude the possibility of dimerisation of ATF6-LD occurring after the cleavage of monomeric ATF6α. If this were the case, the appearance of monomeric ATF6-LD would precede that of the dimer. To investigate this, cells were treated with thapsigargin at 30 min intervals up to a maximum of 2 h after pre-treatment with NH_4Cl or left untreated (Figure 3-8B). In order to preserve the redox status of proteins, cells were treated with N-Ethylmaleimide (NEM) before lysis and examined under non-reducing conditions. As expected, cells that were untreated or treated with NH_4Cl only did not contain bands representing ATF6-LD (lanes 1 & 2). In cells that were treated with thapsigargin in the presence of NH_4Cl, the amount of ATF6-LD dimer accumulated with time (lanes 3 – 6). Notably, monomeric ATF6-LD was not detected throughout the course of this experiment. As a further control, a time-course of treatment with thapsigargin in the absence of NH_4Cl was carried out (Figure 3-8C). Similar results were obtained with dimeric ATF6-LD accumulating over time (although this was not as substantial). Again, no monomeric ATF6-LD was detected throughout the experiment.

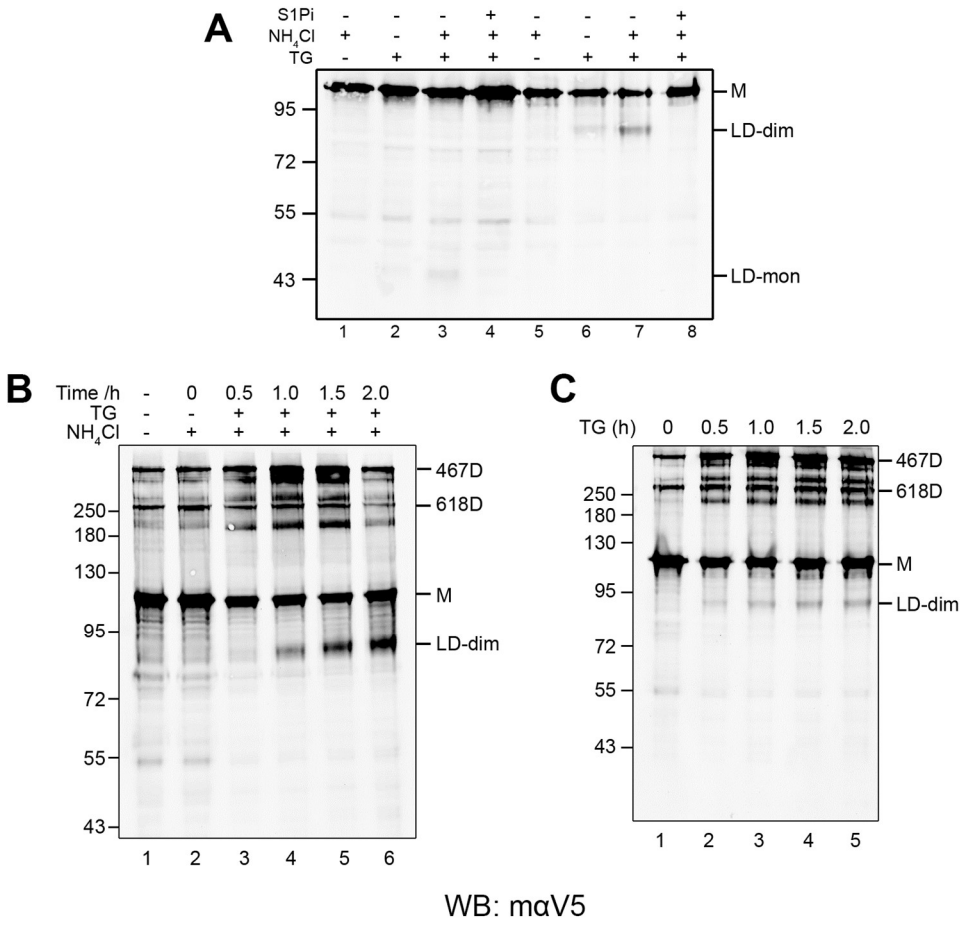

Figure 3-8 ATF6-LD exists as a dimer when the UPR is induced by calcium depletion.
(A) ATF6WT cells were pre-treated with 20 mM NH4Cl for 45 min and S1P inhibitor (lanes 4 & 8 only) for 1 h followed by treatment with 5 μM thapsigargin for 1 h. Lysates were subjected to SDS PAGE under reducing (Lanes 1 – 4) and non-reducing (lanes 5 – 8) conditions. Proteins were identified by immunoblotting with mouse anti V5 antibody. (B) ATF6WT cells were pre-treated with NH_4Cl for 45 mins followed by treatment with 5 μM thapsigargin for the times indicated. (C) As a control, cells were treated with thapsigargin without pre-treatment with NH_4Cl. Lysates were resolved under non-reducing conditions and proteins were identified by immunoblotting with mouse anti V5 antibody.

3.2.2.3 Lumenal domain dimer is stabilised by Bafilomycin A

Ammonium chloride is a potent and broad-spectrum base that rapidly affects the pH of the entire cell. To circumvent any pleiotropic effects of NH_4Cl, we utilised a more specific inhibitor of the lysosomal hydrolases, Bafilomycin A_1 (Baf A_1), which blocks vacuolar H^+-ATPase and prevents acidification of the lysosomes (Dröse and Altendorf 1997). In order to optimise treatment, we titrated Baf A_1 into the medium of cells with concentrations ranging from 0 – 250 nm for 1 h before treatment with 5 μM thapsigargin for 1 h (Figure 3-9A).

Untreated cells displayed all three redox forms of ATF6α (lane 1) while dimeric lumenal domain was seen in cells treated with thapsigargin only (lane 2). The intensity of ATF6-LD increased when cells were treated with thapsigargin in the presence of 100 nm BafA_1 which further supported our findings that ATF6-LD is degraded by the lysosomes (lane 3). Concentrations beyond 100 nm caused no significant increase in the intensity of band representing ATF6-LD (lanes 4 – 6) leading to the conclusion that 100nM Baf A_1 was optimal. We then investigated whether Baf A_1 had a similar effect to NH_4Cl over time. HEK-ATF6WT cells were treated with 5 μM thapsigargin for up to 2 h after treatment with Baf A_1 for 1 h. As a control, cells were left untreated or treated with thapsigargin or Baf A_1 (Figure 3-9B). In order to preserve the redox status of proteins, cells were treated with 25 mM NEM before lysis and examined under non-reducing conditions. The relative quantities of all redox forms of ATF6α were consistent in cells that were untreated or treated with Baf A_1 (lanes 1 and 2). This indicated that Baf A_1 did not affect ATF6 dimerisation. In cells treated with thapsigargin only for 1.5 h (lane 7), there was an increase in the 467D and formation of ATF6-LD that was comparable to the amount produced after 0.5 h of treatment in the presence of Baf A_1 (lane 3).

In the presence of Baf A_1, there was a marked increase in the amount of ATF6-LD formed from 0.5 h to 1 h and this level remained consistent throughout the duration of the time-course (lanes 4 to 6). The results with Baf A_1 were consistent with those obtained with NH_4Cl supporting the conclusion that the lumenal domain is degraded by lysosomal hydrolases. In both experiments, however, there were some additional bands (identified by arrowheads on Fig 9B and X, Y and Z in Fig 10A) that were consistently present. In order to determine

whether these bands contained ATF6, we carried out 2D electrophoresis on samples and immunoblotted with an alternative antibody, rabbit HA, that recognises full length ATF6 and ATF6-N (Figure 3-10A). The strip containing bands X, Y and Z along with the recognised forms of ATF6 (all reactive to the V5 antibody) was excised and treated with 50 mM DTT before being electrophoresed in the second dimension (left panel, Figure 3-10A). In dimension 2, immunoblotting with mouse anti v5 confirmed the expected size of the monomeric lumenal domain and that the other bands migrated to the size expected for monomeric ATF6 except for band Y, which was no longer detected (Figure 3-10A, top right panel). Immunoblotting with rabbit anti HA antibody did not detect any of the bands X, Y and Z but detected bands corresponding to monomeric ATF6α and dimer 467D. Interestingly, dimer 618D was detected with anti V5 but not anti HA antibody. We reasoned that this may have been due to the better binding efficiency of the V5 antibody compared to HA and the low levels of protein present.

To investigate this further we repeated the lumenal domain stabilisation assay using Baf A_1 and identified proteins by immunoblotting with rabbit anti HA antibody (Figure 3-10B). Monomeric ATF6α and dimers 467D & 618D were all detected as expected along with band X. This suggested that band X contains full length ATF6α and could possibly be a dimer composed of exogenous and endogenous ATF6α. The other bands Y and Z were only reactive to V5 and are likely to be due to non-specific cross reactivity. Considered together these results show that the lumenal domain, which is formed by direct S1P cleavage, exists as a dimer suggesting that dimeric ATF6α is trafficked to the Golgi.

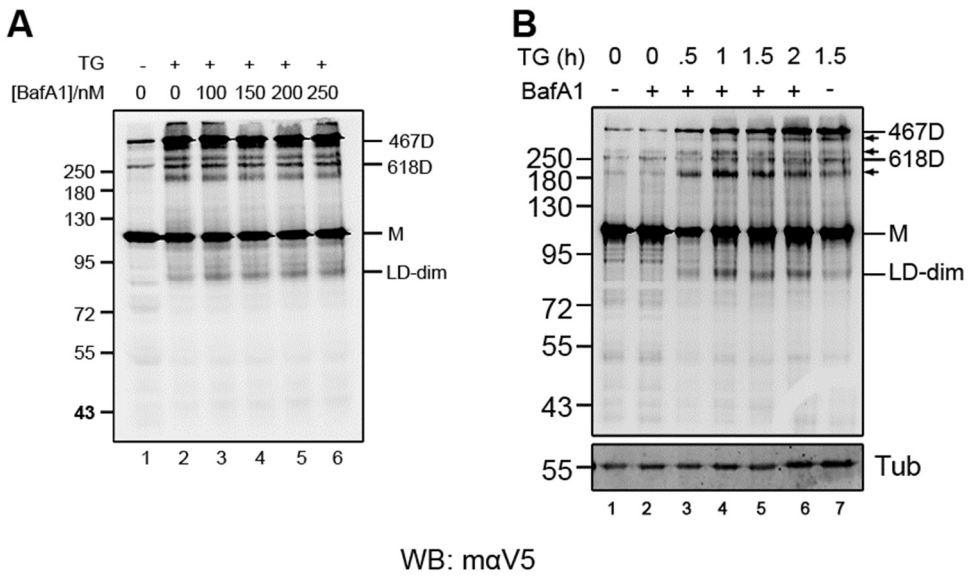

Figure 3-9 Dimeric ATF6-LD is stabilised with Bafilomycin A_1.
(A) ATF6WT cells were pre-treated with increasing concentrations of BafA1 for 1 h followed by treatment with 5 μM thapsigargin for 1 h. As a control, cells were untreated or treated with TG only as indicated. Lysates were resolved under non reducing conditions and proteins identified by western blotting with mouse anti V5 antibody. (B) ATF6WT cells were pre-treated with 100 nm $BafA_1$ for 1 h followed by treatment with 5 μM thapsigargin for the times indicated. As a control, cells were either untreated, treated with $BafA_1$ only or TG only as indicated. Lysates were resolved under non reducing conditions and proteins identified by western blotting with mouse anti V5 antibody.

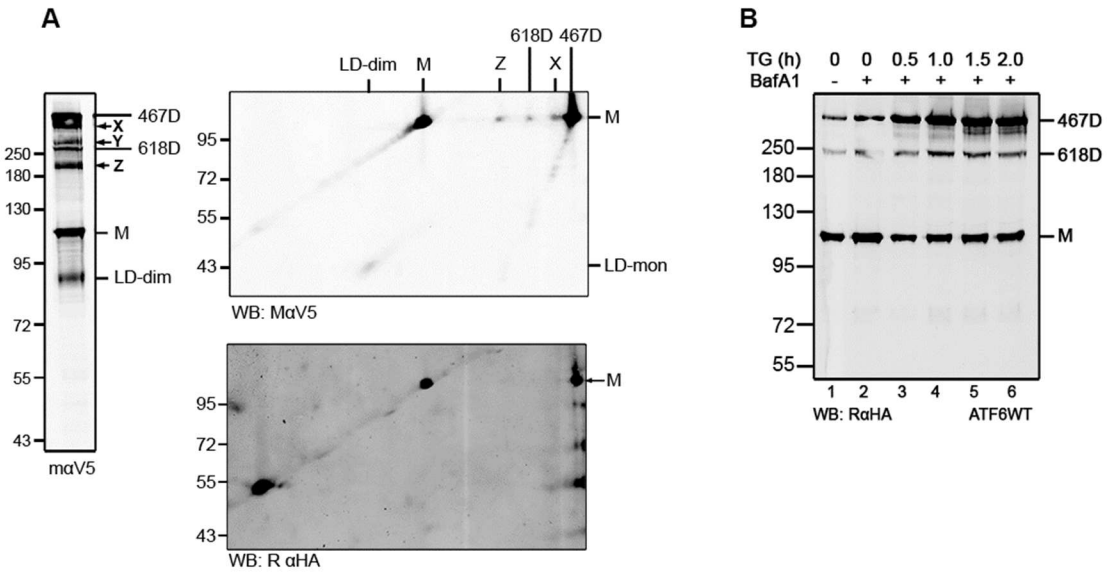

Figure 3-10 ATF6 composition of additional v5 reactive bands.
(A)Two-dimensional gel electrophoresis was carried out on samples treated with TG in the presence of NH_4Cl. Proteins were separated based on their electrophoretic mobility in SDS PAGE in both dimensions. Immunoblotting was done with mouse V5 in both dimensions and rabbit anti HA in dimension 2 only. X, Y and Z represent V5- reactive bands that do not correspond to any recognised form of ATF6. (B) ATF6WT cells were pre-treated with 100 nm $BafA_1$ for 1 h followed by treatment with 5 μM thapsigargin for the times indicated. As a control, cells were either untreated, treated with $BafA_1$ only or TG only as indicated. Lysates were resolved under non reducing conditions and proteins identified by western blotting with rabbit anti HA antibody.

3.2.2.4 Trafficking and processing of redox forms of ATF6α

To better understand the roles of the ATF6 dimers in activation and trafficking, we examined, and compared, trafficking and the redox status of the lumenal domain formed from ATF6WT and C467A and C618A mutants. ATF6KO cells transiently transfected with ATF6wt, ATF6C467A or ATF6C618A DNA were untreated or treated with 1 mM DTT in the presence of $S1P_i$. Lysates were resolved under non-reducing SDS/PAGE conditions and proteins were identified by immunoblotting with mouse anti ATF6 antibody (Figure 3-11A). In untreated cells expressing ATF6WT, ATF6α monomer and dimer 467D were detected (lane 1). The absence of dimer 618D was often seen with transient transfections into this cell line (data not shown). In unstressed cells expressing mutants C467A and C618A, the 618D and 467D were detected respectively in addition to the monomer (lanes 3 and 5). In treated cells expressing wild type ATF6α, hyperglycosylated 467D was detected (lane 2). This species was also detected in treated cells expressing C618A, which can only form dimer 467D, but not in cells expressing C467A. This suggests the specific trafficking of the 467D with no trafficking of the 618D during ER stress.

Given this outcome we reasoned that ATF6-LD would be formed from the processing of dimer 467D. HEK293 cells overexpressing ATF6WT and C467A and C618A mutants were untreated or treated with 5 μM TG in the presence of NH_4Cl (Figure 3-11B). ATF6WT cells treated with NH_4Cl, and TG (lane 2) produced a band just below 95 kDa that was absent from the untreated cells (lane 1). This was previously identified as the dimeric form of the lumenal domain. Treated cells expressing ATF6-C618A produced a band of the same mobility as the treated ATF6WT expressing cells (lane 4); which was not present in untreated cells (lane 3). This band was notably absent in the treated or untreated samples of cells expressing ATF6-C467A (lanes 5 & 6). However, there was some monomeric lumenal domain present in these cells, indicating trafficking of the monomer (lane 6). These data confirmed the processing of dimer 467D to produce dimeric ATF6-LD under conditions of ER stress and the processing of monomer in the absence of 467D.

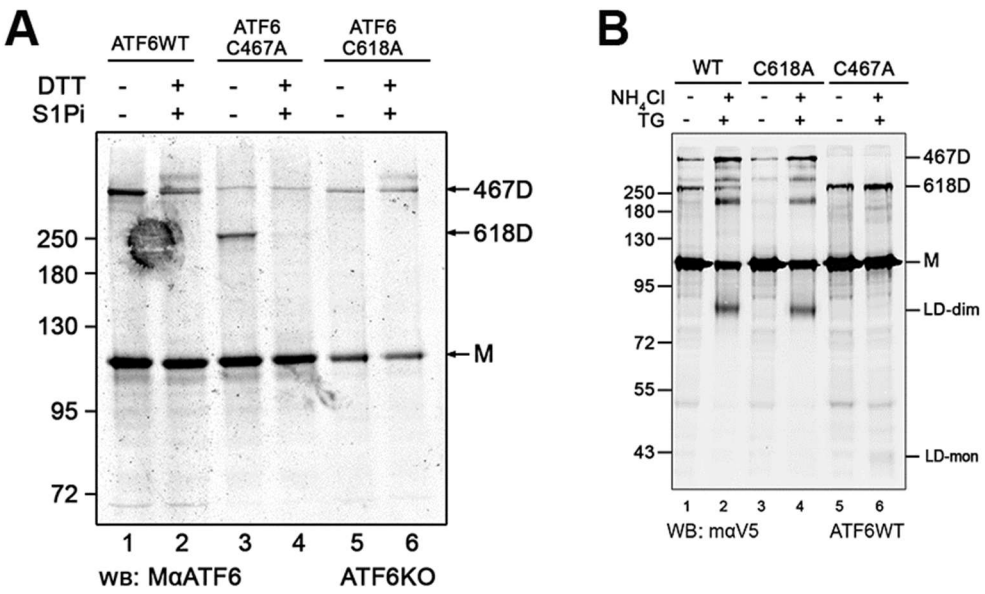

Figure 3-11 Dimeric ATF6LD production from dimer 467D.
(A)ATF6KO cells transiently transfected with ATF6wt, c467a and c618a DNA were left untreated or were treated with 30 μM S1P inhibitor and 1 mM DTT. Proteins were separated by SDS PAGE under non-reducing conditions and identified by immunoblotting with mouse anti ATF6. (B) Cells stably expressing ATF6WT, C618A and C467A mutants were treated with NH_4Cl followed by TG. Proteins were resolved on by SDS PAGE under non reducing conditions and ATF6 and its lumenal domain were identified by immunoblotting with mouse anti v5 antibody.

3.3 Discussion

3.3.1 ATF6α activation

The mechanism of activation of ATF6α is not yet fully understood. The early stages involve release from retention factors such as BiP, followed by rearrangement of lumenal cysteines which facilitates packaging into COPII vesicles for transport to the Golgi. There, S1P and S2P cleave ATF6α to release the soluble transcription factor that travels to the nucleus to activate transcription of its target genes. In this experiment we identified a previously unreported redox shift from monomer to a specific cysteine-dependent dimer, 467D, during the early stages of activation triggered by reductive and non-reductive ER stress. This redox shift is sustained through the latter stages of activation evidenced by Golgi-specific modification of 467D and recovery of cleaved dimeric lumenal domain. Importantly, activation of monomeric ATF6α occurred when the formation of 467D was prevented by a C467A mutation.

Reductive and non-reductive stressors disrupt protein folding and variably trigger the UPR by targeting specific post-translational modifications and interactions that lead to misfolding. The reducing agent DTT challenges the formation of disulfide bonds, tunicamycin causes misfolding by preventing N-glycosylation (Kozutsumi, Segal et al. 1988) while calcium depletion accelerates BiP ADP release and ATP binding causing release of its substrates (Li, Alexandre et al. 1993, Preissler, Rato et al. 2020). Nevertheless, reduction of inter- and intra-molecular disulfides was identified as an important universal step in activation (Nadanaka, Okada et al. 2007).

3.3.2 ATF6α trafficking in response to reductive stress

Usually, the appearance of the transcription factor ATF6-N is used as a marker for the activation of ATF6α. However, Golgi processing also produces the lumenal domain which can also serve as a marker. Strong reductive stress led to the rapid activation of ATF6α with the cleaved (monomeric) lumenal domain appearing within 15 min (Figure 3-6) and resistance to EndoH confirmed that it entered the Golgi as part of ATF6α monomer (Figure 3-7). In the presence of S1P inhibitor which prevents S1P cleavage of ATF6α, strong reductive stress led

to the appearance of the hyperglycosylated monomer which is also indicative of ER-Golgi trafficking (Figure 3-1). These results are congruent with previous findings (Higa, Taouji et al. 2014, Oka, van Lith et al. 2019) and confirmed the role of reduction in creating a transport competent monomer. However, milder (10x lower concentration) reductive stress, in the presence of S1P inhibitor, generated hyperglycosylated 467D which suggested trafficking of 467D. Some hyperglycosylated monomer was also observed; however, the larger quantity of 467D suggested that the dimer was more readily trafficked than the monomer. The accumulation and hyperglycosylation of 467D in the presence of S1P inhibitor was previously seen however, it could not be reconciled within the paradigm that existed (Nadanaka, Okada et al. 2007). And while this model suggested that reduced monomer was the preferred substrate of S1P, it utilised the double cysteine mutant – a species that is unlikely to exist and thus has limited physiological relevance (Nadanaka, Okada et al. 2007). Additionally, recent work by Oka et al (2022) has demonstrated S1P cleavage of the physiologically relevant 467D. Exclusive trafficking of monomer ATF6α has been reported when Chinese hamster ovary cells were treated with 1 mM DTT (Nadanaka, Okada et al. 2007). But this likely suggests variable sensitivities of different cell lines to reductive ER stress. Similarly, ATF6α transported within COPII vesicles (Schindler and Schekman 2009) could be more accessible to DTT and reduction of any disulfides leading to identification of the reduced monomer.

3.3.3 ATF6α trafficking in response to non-reductive stress

Activation of ATF6α during non-reductive stress (initiated by calcium depletion) was also relatively rapid with evidence of activation appearing within 20 min (Figure 3-5). In the presence of S1P inhibitor, ER stress caused hyper-glycosylation of the 467D (Figure 3-1 & 5) but not the monomer. Moreover, increasing levels of 467D and decreasing levels of monomer correlated with treatment, and pointed toward a redox shift from monomer to 467D during the early stages of activation of endogenous ATF6α (Figure 3-1B). The levels of 618D were relatively constant. Correspondingly, cleaved lumenal domain, isolated within 30 min, was dimeric. The absence of the lumenal domain when S1P was inhibited confirmed its origin and its accumulation in the presence of known inhibitors of lysosomal hydrolases suggested degradation as its fate (Figure 3-8).

Combined with the absence of monomeric ATF6-LD at the earliest timepoints, this confirmed the trafficking and processing of dimeric ATF6α while excluding the possibility of post-cleavage disulfide formation in the Golgi. These results added another dimension to ATF6α activation but are congruent with some recent findings which showed that 467D colocalised with Golgi markers under conditions of proteotoxic or chemo-toxic stress and that S1P was able to cleave 467D (Oka, Pierre et al. 2022).

3.3.4Trafficking and processing of 467D during ER stress

The 467D was previously thought to be a higher order oligomer of ATF6α with an unidentified protein based on slower electrophoretic mobility displayed during non-reducing SDS/PAGE (Nadanaka, Okada et al. 2007). However, mass spectrometric analysis confirmed that it exclusively contained ATF6α (Oka, van Lith et al. 2019), while a later study proposed the underlying structural basis of the difference in mobility (Koba, Jin et al. 2020). Thus, it was possible that O-glycosylation of 618D could alter its structure and reduce its mobility making it appear larger than N-glycosylated 467D. To address this, we examined the effect of ER stress on single cysteine mutants of ATF6α with respect to O-glycosylation and processing by S1P.

During mild reductive stress in the presence of S1P inhibitor, the phenotype displayed by ATF6-C618A, which exclusively forms the 467D, reflected that of ATF6WT i.e., there was a band which migrated just above 467D. Importantly, this phenotype was not seen in cells expressing ATF6-C618A which is incapable of forming 467D. Correspondingly, non-reductive stress induced cleavage by S1P produced dimeric lumenal domains in cells overexpressing wild type ATF6α and C618A mutant but not the C467A mutant. Interestingly, a small amount of monomeric lumenal domain was recovered from cells expressing ATF6-C467A which confirms the trafficking of monomeric ATF6α; but the larger quantity of dimeric lumenal produced confirms that 467D is more readily trafficked. A similar result was obtained using DTT, but with robust reduction and limited resistance to DTT observed throughout our experiments, it was difficult to distinguish whether hyperglycosylated monomer observed (Figure 3-1C, lane 3) originated from trafficked monomer or breaking of disulfide bonds in trafficked 467D.

Redox signalling is an important feature of the UPR. Redox shifts, from monomer to dimer, have been reported during the activation of both PERK and IRE1α (Shamu and Walter 1996, Bertolotti, Zhang et al. 2000). On the other hand, a dimer-to-monomer shift was proposed for ATF6α. The current ATF6-activation model, in which the monomer is trafficked upon reduction, establishes the importance of reduction but acknowledges the existence of additional regulatory elements on the basis that reduction does not exclusively lead to activation (Higa, Taouji et al. 2014). Non-reductive stress in a relatively oxidising environment such as the ER, does not lead to direct reduction of proteins. Hence, the initial reduction of the intra-chain disulfide in monomeric ATF6α is likely to be catalysed by a reductase such as ERp18 or PDIR which can reduce ATF6α (Higa, Taouji et al. 2014, Oka, van Lith et al. 2019). Similarly, formation of C467-C467 disulfide is likely to involve an oxidase given that it can form even in the reductive environment that exists during ER stress where one would expect cystines to be reduced.

Our findings that ATF6α undergoes a similar shift to PERK and IREα during activation supports a model in which reduction of the lumenal cysteines of monomeric ATF6α facilitates the formation of the C467-C467 disulfide, through release from BiP, which allows a non-covalent interaction that brings 467 cysteines in proximity (Koba, Jin et al. 2020). This reshuffling of the disulfides may both arise from, and lead to, conformational changes within the lumenal domain that facilitate the engagement of other factors involved in preparing ATF6α for trafficking. Thus, disulfide rearrangement, the enzymes responsible for catalysis along with other factors may partially or wholly represent an additional level of regulation for ATF6α. Future research would be aimed towards identifying potential candidates and characterising their role in ATF6α regulation.

Chapter 4. The role of ERp18 in ATF6α Regulation

4.1 Introduction

The revealed role of redox-dependent dimerisation of ATF6α prompted the examination of factors believed to be directly or indirectly involved in ATF6α regulation during the UPR. These include candidates that interact directly with ATF6α, such as BiP, or partners that may modulate the binding of a direct interacting partner. It was imperative to consider oxidoreductases, such as ERp18, as they are likely to be involved in modulating ATF6α redox status during the UPR.

4.1.1 BiP regulation in the UPR

BiP functions as a master regulator in the unfolded protein response in several ways. It binds exposed hydrophobic regions in nascent chains to allow them to achieve native conformation. It also binds proteins defective in folding preventing their exit and directing them towards the degradation pathway. Additionally, it maintains ATF6α, and other UPR transducers, in an inactive state and releases them during ER stress thus restoring proteostasis.

BiP-substrate engagement is regulated by an ATPase cycle which often requires nucleotide exchange enhancers and/or inhibitors that can modulate BiP-client binding affinity. Mesencephalic astrocyte-derived neurotrophic factor (MANF) is a nucleotide exchange inhibitor known to increase BiP affinity for substrates by inhibiting ADP release as well as ATP binding (Yan, Rato et al. 2019). Therefore, BiP binding, and stress-dependent release, of ATF6α might be regulated by changes in the MANF-BiP association.

4.1.2 ERp18 involvement during ER stress

The small PDI-like protein ERp18 is known to engage ATF6α during ER stress and regulates the critical step of ATF6α trafficking from the ER to Golgi (Oka, Pierre et al. 2022). The absence of ERp18 from cells leads to aberrant processing of ATF6α which can promote ER stress dependent apoptosis (Jeong, Lee et al. 2008, Oka, van Lith et al. 2019). In contrast, overexpression of ERp18 can prevent apoptosis induced by ER stress, a function that requires the active site cysteines (Jeong, Lee et al. 2008). Given that ERp18 can reduce ATF6α disulfides, its ability to regulate ATF6 trafficking is likely based on its reductase activity.

However, the stability of the reduced form and the redox potential of ERp18 suggest that it can also act as an oxidase (Alanen, Williamson et al. 2003) and may also be involved in ATF6α dimerisation during ER stress. This is also supported by the apparent preference of ERp18 to engage cysteine 467 which forms the disulfide in the trafficking competent dimer 467D (Oka, van Lith et al. 2019).

Structural comparison between ERp18 and other thioredoxin-like proteins revealed that ERp18 has an additional loop that contains residues that are important for substrate binding (Rowe, Ruddock et al. 2009). Having ATF6α as a substrate of ERp18 created the opportunity to interrogate the role of ERp18 in ATF6α regulation as well as identify residues in the ERp18 loop that are involved in the interaction.

4.1.3 Aims and objectives

The aim of this chapter is to identify factors involved in the ATF6α ternary complex that may contribute to regulating ATF6α activation. Additionally, the role of ERp18 in regulation ATF6α trafficking is interrogated. Finally, site directed mutagenesis is used to assess the contribution of putative binding residues in the ERp18-ATF6α interaction.

4.2 Results

4.2.1 ER proteins associated with ATF6α

4.2.1.1 Assessing the contribution of MANF to ATF6α ternary complex

4.2.1.1.1 Assessing the interaction between BiP and MANF

BiP recognises, and binds to ATF6α, as a canonical substrate in unstressed cells and releases it during stress. Several cofactors are known to regulate BiP binding including the nucleotide exchange inhibitor (NEI) MANF which has been shown stabilise some BiP-substrate complexes (Glembotski, Thuerauf et al. 2012, Yan, Rato et al. 2019). In order to investigate MANF contribution to aspects of ATF6α regulation while overcoming the low expression of endogenous MANF in HT1080/ATF6KO cells, we stably transfected cells with pcDNA 3.1 zeocin encoding MANF with a C terminal Myc tag (MANF-Myc). Immunoblotting with rabbit anti Myc identified two clones expressing MANF-Myc. The expression of exogenous MANF exceeded that of the endogenous protein. Clone A1 was used for experiments (Figure 4-1A).

To investigate whether MANF interacts with BiP, we immunoprecipitated MANF-Myc and immunoblotted to identify BiP having stabilised the interaction using *in vivo* crosslinking as previously described (Yan, Rato et al. 2019). Untransfected cells were used as a control (Figure 4-1B). Immunoblotting detected the presence of BiP in lysates of both transfected and untransfected cells, and MANF-Myc in transfected lysates only (lanes 3 & 4). BiP was recovered with MANF from lysates of transfected cells (lane 1), but not from untransfected cells (lane 2). This result demonstrated that there was no interaction between MANF-Myc and the agarose beads used and confirmed that BiP and MANF interacted in unstressed cells.

To determine whether MANF is associated with BiP as a functional part of the ATF6α ternary complex, we investigated whether MANF and BiP co-immunoprecipitated with ATF6α in stressed and unstressed conditions. Given the sensitivity of some co-factors to detergents in the lysis buffer, DSP crosslinking was used to stabilize the interaction (Shen, Snapp et al. 2005, Glembotski, Thuerauf et al. 2012).

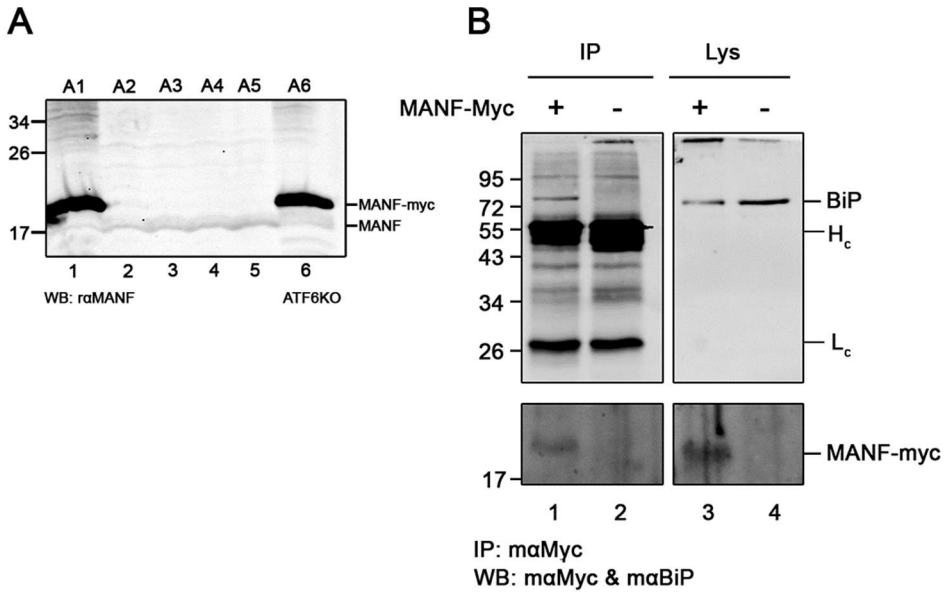

Figure 4-1 MANF associates with BiP.
(A) HT1080/ATF6KO cells transfected with MANF cloned pCDNA3.1 Zeocin were placed under zeocin selection until single colonies emerged. Six clones were selected expression was determined by western blotting with rabbit anti Myc. (B) ATF6KO cells overexpressing MANF-Myc were treated with DSP to stabilise the interaction. Cells not expressing MANF-Myc were used as a control. Lysates were subjected to immunoprecipitation with mαMyc, and complexes were dissociated with DTT before SDS PAGE. Proteins were identified by immunoblotting with mαBiP and rαMANF. L_C and H_C refer to the light and heavy antibody chains respectively.

HEK293 cells overexpressing ATF6WT were treated with or without thapsigargin. It was shown that the complex dissociates in response to ER stress (Shen, Chen et al. 2002, Shen, Snapp et al. 2005) hence, it was hypothesised that the complex could only be isolated in the absence of ER stress. As a control, cells were not subjected to crosslinking with DSP. ATF6α was immunoprecipitated using mouse αV5, DTT was used to dissociate the crosslinked complexes and MANF and ATF6α were identified by immunoblotting with rαMANF and mαV5 antibody respectively.

Immunoblotting with rabbit αMANF revealed the presence of MANF in lysates of all samples (Figure 4-2A, lanes 1 – 4). The slower migration of MANF in lanes 2 & 4 compared to lanes 1 & 3 was possibly the result of modification of residues by DSP causing changes in the hydrodynamic volume. However, MANF was not recovered with ATF6α (lanes 5-8). Though this may have suggested that MANF is not a part of the complex, analysis of the lysates immunoblotted with mouse αV5 showed significantly lower quantities of ATF6 in lysates treated with DSP compared to the controls (Figure 4-2B, compare lanes 1&3 to 2&4).

This difference was also reflected in the immunoprecipitated samples (compare lanes 5&7 to 6&8). This suggested that the loss of ATF6α was related to the crosslinking. It is possible that crosslinking stabilised the interaction among membrane components thereby reducing the efficiency of solubilisation, and release of ATF6α, during lysis.

To circumvent this problem, we transiently expressed MANF with a C-terminal Myc tag (MANF-Myc) along with soluble V5 tagged ATF6α lumenal domain (ATF6LD) in ATF6α knockout cells. Cells were transfected with MANF-Myc and/or ATF6LD. To prevent dissociation of the complex in the absence of crosslinking, cells were lysed by sonication in Buffer A (10 mM HEPES (pH 7.4), 250 mM sucrose, 10 mM KCl, 1.5 mM MgCl2, 1 mM EDTA, and 1 mM EGTA) which does not contain detergents that might cause complexes to dissociate. Mouse αV5 was used to immunoprecipitate ATF6α as the bait for its complex. Immunoblotting with mouse αV5 and rabbit αMANF showed that the transfections were successful since proteins were detected in the lysates from transfected cells only (Figure 4-2C lanes 2 – 4 compared to lane 1). The transfection efficiency of MANF-Myc was greater in cells that were transfected with both MANF-Myc and ATF6LD individually transfected cells. Immunoblot analysis of the immunoprecipitated proteins showed that ATF6α and MANF co-immunoprecipitated (Figure 4-2C, lane 8) but the identification of MANF in the sample without ATF6LD (lane 7) suggested possible non-specific interaction with the agarose beads used. Although the signal in the double-transfected cells were greater, it was unclear whether this was due to the higher expression of MANF. Furthermore, BiP, a known interacting partner of both MANF and ATF6α, did not co-immunoprecipitated as revealed by immunoblot analysis (Figure 4-2C). Given that non-specific interaction between the beads and endogenous MANF was not observed, we sought to optimise the lysis of cells treated with DSP.

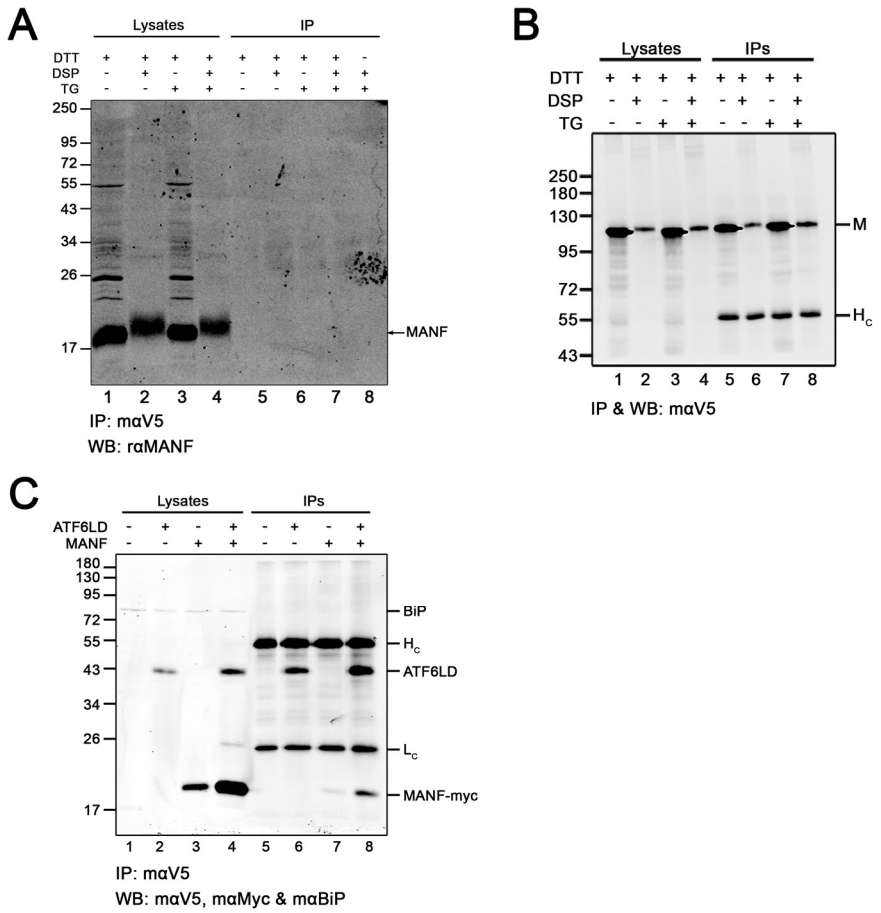

Figure 4-2 Investigating the contribution of MANF to the ATF6 ternary complex.
HEK293 cells overexpressing ATF6 were either treated or not with thapsigargin to activate the UPR. DSP crosslinking was used to trap ATF6α interacting partners before complexes were isolated by immunoprecipitation with mouse anti V5. Complexes were dissociated with DTT before being resolved by SDS PAGE and proteins identified by immunoblotting with rabbit anti MANF (A) and mouse anti V5 antibodies (B). (C) Lysates of ATF6KO cells transiently transfected with MANF-Myc and/or ATF6 lumenal domain were subject to immunoprecipitation with mouse V5 to isolate ATF6 ternary complexes. Lysates and eluates were electrophoresed under reducing conditions and membranes probed with the appropriate antibodies of proteins expected to be complexed.

4.2.1.1.2 Optimisation of lysis of cross-linked cells

In order to increase the efficiency of membrane solubilisation and ATF6α extraction during crosslinking, we sought to optimise the lysis process. We compared extraction of ATF6α when HEK/ATF6WT cells treated with 1 mM DSP were lysed under three conditions: D - incubation with detergent-based lysis buffer, N – lysis using a 23-gauge needle in buffer A (without detergents) and S – lysis by sonication after incubating in buffer A (Figure 4-3A). To compare the levels of ATF6α and as an indicator of ER membrane rupture, we immunoblotted for PDI, a soluble ER protein. The quantity of ATF6α recovered was greatest when cells were lysed by sonication (lane 3), followed by detergent-based lysis (lanes 1) and least in cells lysed with the 23-gauge needle (lane 2). The level of PDI were consistent in each sample. This result confirmed the effectiveness of sonication in ER membrane solubilisation during lysis without crosslinking. Next, we investigated whether including a sonication step during lysis with detergent can improve the yield of ATF6α after in-cell crosslinking.

HT1080 wild-type cells were treated or not with 1 mM DSP and lysed with or without sonication. As a control for membrane solubilisation cells were not treated with DSP and lysed using detergent without sonication (Figure 4-3 Sonication improves membrane solubilisation. Immunoblot analysis of lysates indicated that ATF6α extraction was reduced in DSP treated cells that were lysed without sonication, compared to the control (lane 6 compared to lane 5). The quantity of ATF6α detected in lysates of cells treated with DSP and lysed by sonication were comparable to the control (lanes 7). The variation in quantities of ATF6α recovered by immunoprecipitation reflected that seen in the lysates (lanes 1-3 compared to lanes 6 – 8). Successful crosslinking was confirmed by the appearance of high molecular weight species present in the sample of immunoprecipitated proteins analysed under non-reducing conditions (lane 4). These results demonstrated the utility of sonication in improving ER membrane solubilisation during lysis of cells following DSP crosslinking.

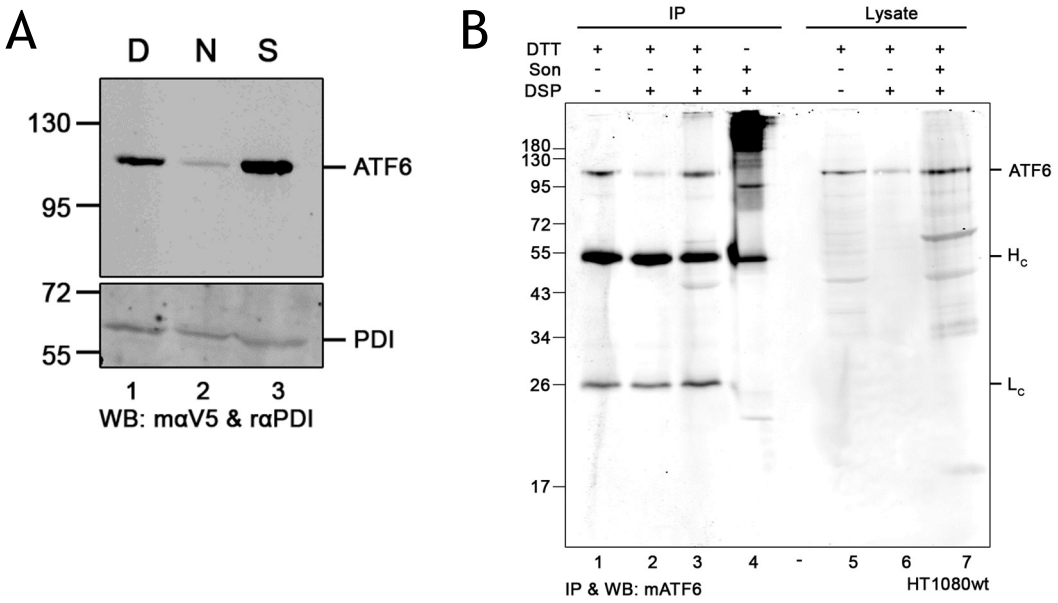

Figure 4-3 Sonication improves membrane solubilisation.
(A) Cells overexpressing ATF6WT were treated with DSP and lysed for 10 min with lysis buffer (50 mM Tris pH 7.5, 150 mM NaCl and 1% (v/v) Triton X-100), by resuspending in buffer A (10 mM HEPES (pH 7.4), 250 mM sucrose, 10 mM KCl, 1.5 mM MgCl2, 1 mM EDTA, and 1 mM EGTA) and passing through a 23 gauge needle or by sonication after incubation in buffer A. Lysates were resolved under reducing conditions and proteins were identified by immunoblotting with mαATF6 and rαPDI. (B) Cells overexpressing ATF6WT were treated with DSP to trap interacting partners. Cells were lysed for 10 min with lysis buffer with or without sonication to assess membrane solubilisation. As a control, cells not treated with DSP were lysed without sonication. ATF6α was recovered by immunoprecipitation with mαATF6. Complexes were dissociated with DTT before being resolved by SDS PAGE and proteins identified by immunoblotting with same antibody.

4.2.2 ERp18

4.2.2.1 ERp18 binds to endogenous ATF6α

The interactome of ATF6α changes in response to ER stress. ERp18 has been shown to be associated with ATF6α particularly during ER stress acting as a reductase (Oka, van Lith et al. 2019). In order to confirm the interaction between ATF6α and ERp18, endogenous ERp18 was immuno-isolated from HT1080 wild-type cells treated with or without TG, and ATF6α was identified by immunoblotting. To investigate non-specific interaction with the beads, immunoprecipitation was also carried out using rabbit anti FLAG antibodies (Figure 4-4). As expected, ERp18 and ATF6α were detected in all lysates (lanes 1 & 2). Immunoprecipitated material from αFLAG did not contain either protein thereby confirming that there was no interaction between the beads and ATF6α or ERp18 (lanes 5 & 6). ATF6α was isolated from immunoprecipitates from αERp18 in both treated and untreated cells confirming that ERp18 interacts with ATF6α in the absence and presence of stress.

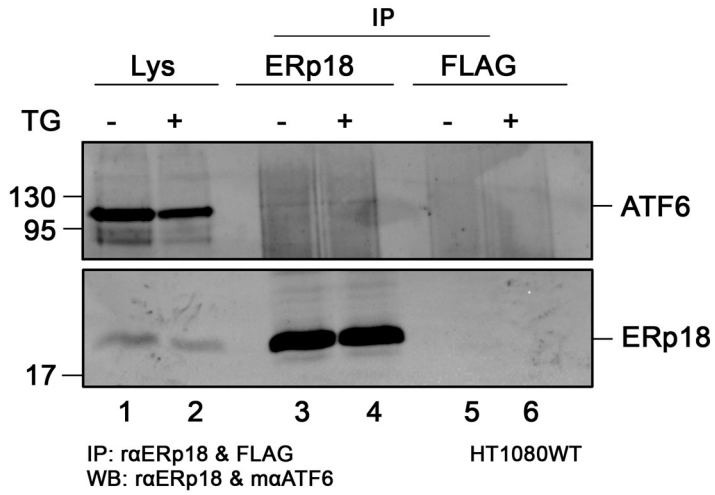

Figure 4-4 Interaction between endogenous ATF6α and ERp18.
HT1080 wild type cells were treated or not with 5 μM TG for 1 h. Lysates were subjected to immunoprecipitation with rαERp18 or FLAG (as a control), and complexes were dissociated with DTT before SDS PAGE. Proteins were identified by immunoblotting with mαATF6 and rαERp18.

4.2.2.2 Creating a cell line expressing ERp18-FLAG and HA-ATF6WT-V5

In order to characterise the ERp18-ATF6α interaction we created a cell line in which ATF6α and ERp18 were exogenously expressed. To remove interference, endogenous ERp18 was knocked out using CRISPR/Cas9, then tagged ATF6WT was introduced into the cell line followed by various mutants of ERp18 to create the resulting cell lines.

4.2.2.2.1 CRISPR/Cas9 Knockout of endogenous ERp18

In order to knockout endogenous ERp18, HT1080 wild-type cells were transfected with plasmids containing guide sequences and Cas9 DNA, previously published (Oka, van Lith et al. 2019), and pPUR, a plasmid to confer resistance to puromycin. Cells were maintained under puromycin selection until single colonies emerged. Successful knockout of ERp18 was determined by immunoblotting with rαERp18 (Figure 4-5). ERp18 was successfully knocked out in all but two clones: A1 (lane 1) and C2 (lane 7).

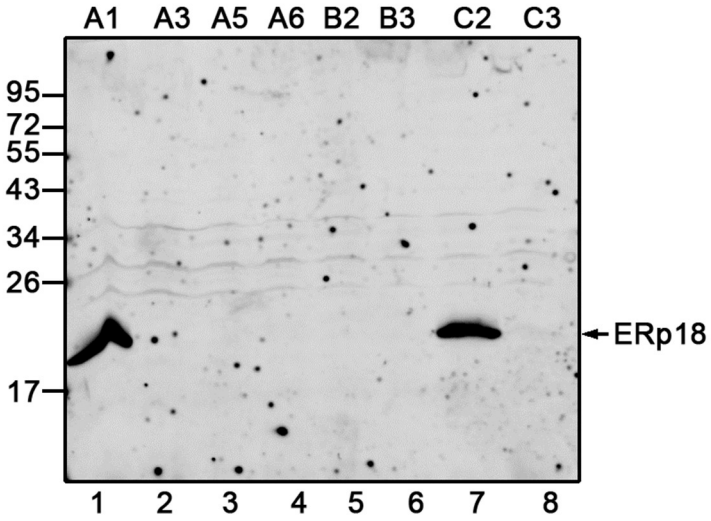

Figure 4-5 Identifying ERp18KO clones.
HT1080WT cells, co-transfected with CRISPR/Cas9 guides and a puromycin selective marker, were placed under puromycin selection until single colonies emerged. Eight (8) clones were expanded, and phenotypes were checked by western blotting with rαERP18.

4.2.2.2.2 Stable transfection of HA-ATF6wt-V5

Cells from HT1080/ERp18KO clone A3 (Figure 4-5 lane 2) were transfected with pcDNA 3.1 hygromycin vector containing ATF6wt DNA. They were grown under hygromycin selection until single hygromycin-resistant colonies emerged. Expression of ATF6WT was determined by immunoblot analysis of reduced and non-reduced lysates with mαV5 (Figure 4-6). Similar, acceptable levels of expression were observed in clones A3 (lanes 1 & 5) and B3 (lanes 2 & 6). Therefore, clone B3 was used for further experiments.

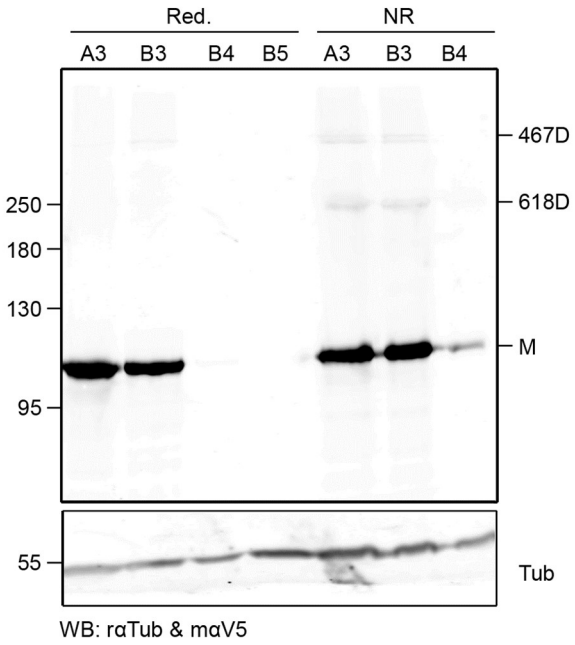

Figure 4-6 Identifying clones expressing HA-ATF6WT-V5
HT1080/ERp18KO cells were transfected with ATF6wt DNA cloned into pCDNA3.1 containing a Hygromycin selective marker and placed under selection until single colonies were visible. Three (3) clones were expanded, and phenotypes were checked by western blotting with mαV5.

4.2.2.2.3 Stable transfection of ERp18 constructs

In order to interrogate the requirement of the active site cysteines in the interaction between ATF6α and ERp18, we designed human ERp18 wild-type (ERp18WT) and double cysteine mutant (ERp18CS) constructs to contain a C-terminal FLAG (DYKDDDDK) sequence immediately before the EDEL sequence. To determine the involvement of EDEL in ER retention we designed a deletion mutant missing the EDEL sequence; ERp18ΔC4 (Figure 4-7A). HT1080/ERp18KO cells expressing ATF6WT were transfected with ERp18-wt, -CS and -ΔC4 DNA cloned into pCDNA 3.1 zeocin (+). Cells were cultured under zeocin selection and single colonies were chosen to determine expression via immunoblotting (Figure 4-7B).

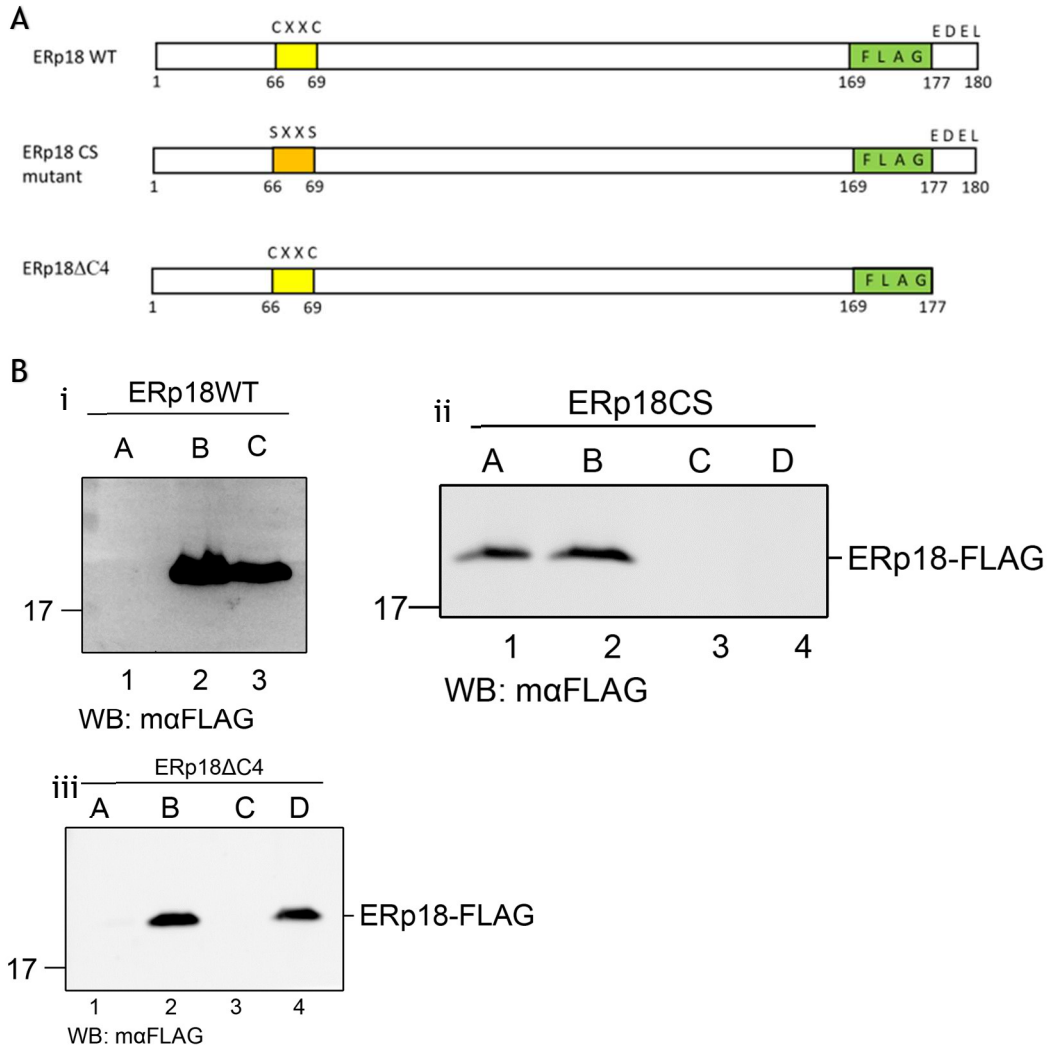

Figure 4-7 Stable transfection of ERp18-FLAG.
(A) ERp18 wild-type, double cysteine and C4 deletion mutants designed to contain a C-terminal FLAG tag. (B)HT1080/ERp18KO cells were transfected with (i) ERp18WT, (ii) ERp18CS and (iii) ERp18ΔC4 DNA cloned in pCDNA 3.1 Zeocin (+) and placed under zeocin selection. Single colonies were selected and expanded, and expression was verified by immunoblotting with mαFLAG antibody.

4.2.2.2.4 Localisation of ERp18WT-FLAG

In order to confirm the subcellular localisation of ERp18-FLAG, immunofluorescence was used to visualise the protein in cells stably expressing ERp18WT-FLAG using untransfected (ERp18KO) cells as a control (Figure 4-8A(i)). Microscopic examination detected fluorescence in cells expressing ERp18WT only, and the pattern of fluorescence was characteristic of the reticular network indicating ER localisation (8A (ii)). No fluorescence was detected in ERp18KO cells.

To determine whether the EDEL sequence is involved in ER retention, we transfected cells with DNA encoding ERp18WT or ERp18ΔC4 lacking the ER retention motif. The pTet-One vector used allowed the regulation of expression with the presence of doxycycline in the medium. It was hypothesised that if the EDEL sequence functionally engages the KDEL receptor, its deletion would lead to secretion of the protein which could then be isolated from the medium, while the wild-type protein would be retained and isolated from the lysates. As a control, cells were grown in the absence of doxycycline (Figure 4-8B **- Dox**). Immunoblotting with mαFLAG detected ERp18 in lysates of cells grown with media containing doxycycline. Additionally, ERp18 was immunoprecipitated from lysates of ERp18WT as well as ERp18ΔC4 (**+Dox** lanes 5 &6). ERp18ΔC4 was immunoprecipitated from both the medium and lysates while ERp18WT was precipitated from the lysates only. Considered together these data indicate that ERp18-FLAG is localised to the ER and that the EDEL sequence is involved in ER retrieval.

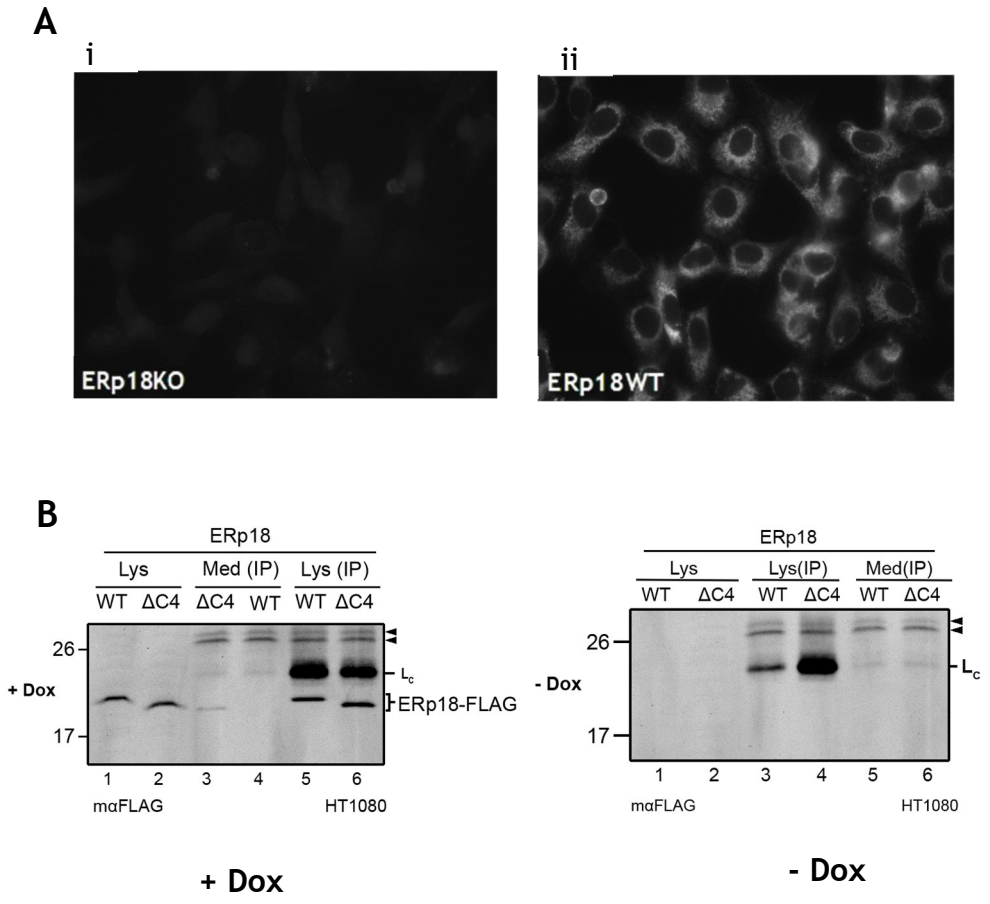

Figure 4-8 ER localisation of ERp18-FLAG
(A) HT1080/ERp18KO cells (i), or cells stably expressing ERp18WT-FLAG (ii) were fixed on cover slips with methanol. Immunostaining was conducted with mαFLAG, and fluorescence of Alexa Fluor 488 secondary antibody was detected using the 40X objective. (B) HT1080 cells expressing ERp18-WT, or ΔC4 in the doxycycline-inducible pTETOne plasmid were cultured in the presence (i) or absence (ii) of doxycycline. Lysates and media were subjected to immunoprecipitation with mαFLAG. Proteins were resolved under reducing SDS PAGE conditions and identified by immunoblotting with mαFLAG. Arrowheads point to non-specific immunoreactive bands.

4.2.2.3 Investigating the ATF6α-ERp18 interaction

Having confirmed the expression and localisation of ERp18-FLAG, we sought to validate the interaction between exogenous ERp18 and ATF6α. To do this, we carried out co-immunoprecipitation using cells stably expressing ATF6α and ERp18WT-FLAG. ERp18WT was immuno-isolated using mouse anti FLAG antibodies and ATF6α was detected by immunoblotting with rabbit anti V5. As a control, the assay was carried out in cells lacking ERp18. To determine whether the active site cysteines contribute to binding we utilised cells expressing the double cysteine mutant ERp18CS-FLAG (Figure 4-9). ATF6α was identified in lysates of all cells (lanes 4 – 6) while ERp18 was detected in cells expressing ERp18, as expected (lane 4 compared to lanes 5 & 6). No ATF6α was detected in the immunoprecipitates from ERp18KO, indicating there was no interaction between ATF6α and the agarose beads used (lane 1). Despite varying amounts of ERp18 in the lysates (lanes 5 & 6), comparable amounts of ERp18 were isolated, and ATF6α was recovered with ERp18WT but not ERp18CS (lane 2 vs 3). This suggested the requirement of cysteines in substrate binding.

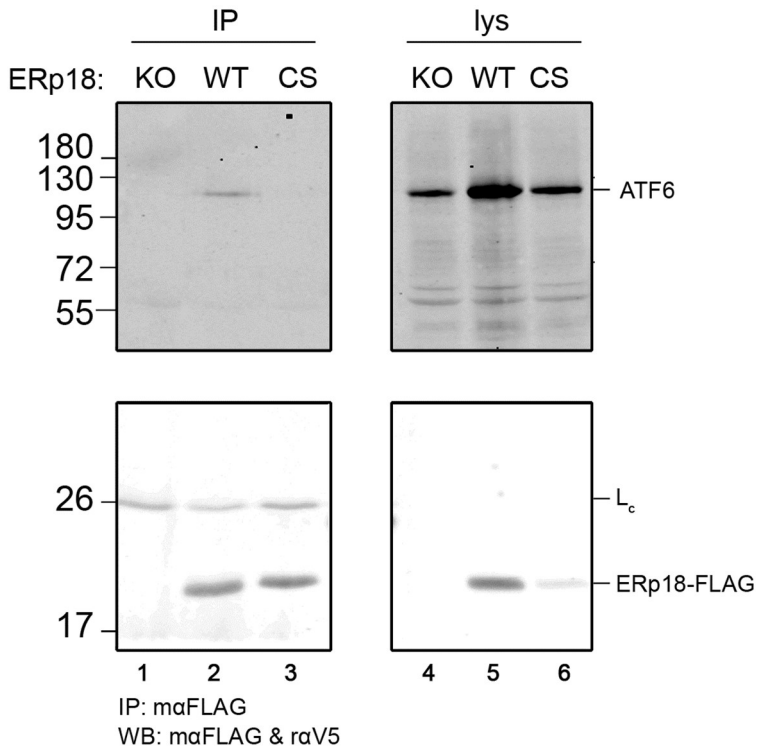

Figure 4-9 Interactions between HA-ATF6WT-V5 and ERp18-FLAG.
HT1080/ERp18KO cells or cells expressing ERp18WT-FLAG or ERp18CS-FLAG, also expressing HA-ATF6WT-V5, were treated with 0.5 mM DSP to stabilise protein-protein interactions. ERp18 was immunoprecipitated from lysates with mαFLAG and ATF6α was identified by immunoblotting with rαV5. Proteins were resolved under reducing conditions.

4.2.2.4 ERp18 regulates ATF6α redox transition during ER stress

In order to interrogate the functional significance of ERp18 interaction with ATF6α, we examined ER stress-dependent phenotypes generated when ERp18 is knocked out. Reported phenotypes include aberrant cleavage of ATF6α to produce ATF6-P, an increase in trafficking kinetics and a redox shift from monomer to 467D (Oka, van Lith et al. 2019, Oka, Pierre et al. 2022). While ATF6-P was not detected in this cell line (data not shown), the M to 467D redox shift was observed and therefore utilised.

ERp18KO and ERp18WT cells were left untreated or treated with 1 μM or 5 μM TG for one hour to induce ER stress. Lysates were resolved under non-reducing conditions and proteins were identified by immunoblotting. The relative amounts of the three redox forms of ATF6α were quantified and compared between ERp18KO and ERp18WT. At steady state, ERp18KO cells contained all three forms of ATF6α with the monomer accounting for 82%, and 618D & 467D accounting for 10% and 7% of total ATF6α respectively. Treatment with 1 μM TG resulted in a decrease in the monomer to 32% and an increase in 467D to 55%. 618D increased slightly to 12%. ER stress induced with 5 μM TG led to similar changes compared to the untreated cells; the monomer decreased to 25%, 467D increased to 60% and 618D remained at 12% (Figure 4-10A & D).

At steady state, the amounts of the redox forms of ATF6α in ERp18WT cells were similar to the knockout cells (85% M and 7% 618D and 467D). The addition of 1 μM TG led to the monomer decreasing to 48% and 467D increasing to 39%, while 618D increased to 13%. In the presence of 5 μM, compared to the untreated cells, the monomer decreased to 46%, 467D increased to 41% and 618D to 13% (Figure 4-10B and E). Untreated ERp18KO cells contained less monomer and more 467D than untreated ERp18WT cells. Similarly, TG treated ERp18WT cells contained more monomer and less 467D compared to ERp18KO cells. These results suggested that ERp18 antagonised the shift from monomer to 467D that occurs during ER stress.

To determine whether the cysteine residues were involved, we quantified redox forms of ATF6α in cells expressing a cysteine-less mutant ERp18CS. When untreated, M, 618D and 467D accounted for 92%, 5% and 3% of total ATF6α

respectively. After treatment with 1 μM TG, the monomer decreased to 33%, 618D increased to 12% and 467D increased to 56%. Similar changes were observed in the presence of 5 μM TG; the monomer decreased to 29%, 618D increased to 16% and 467D increased to 57%. These changes reflected changes observed with ERp18KO and indicated the requirement of the cysteine residues for ERp18 function in relation to ATF6α.

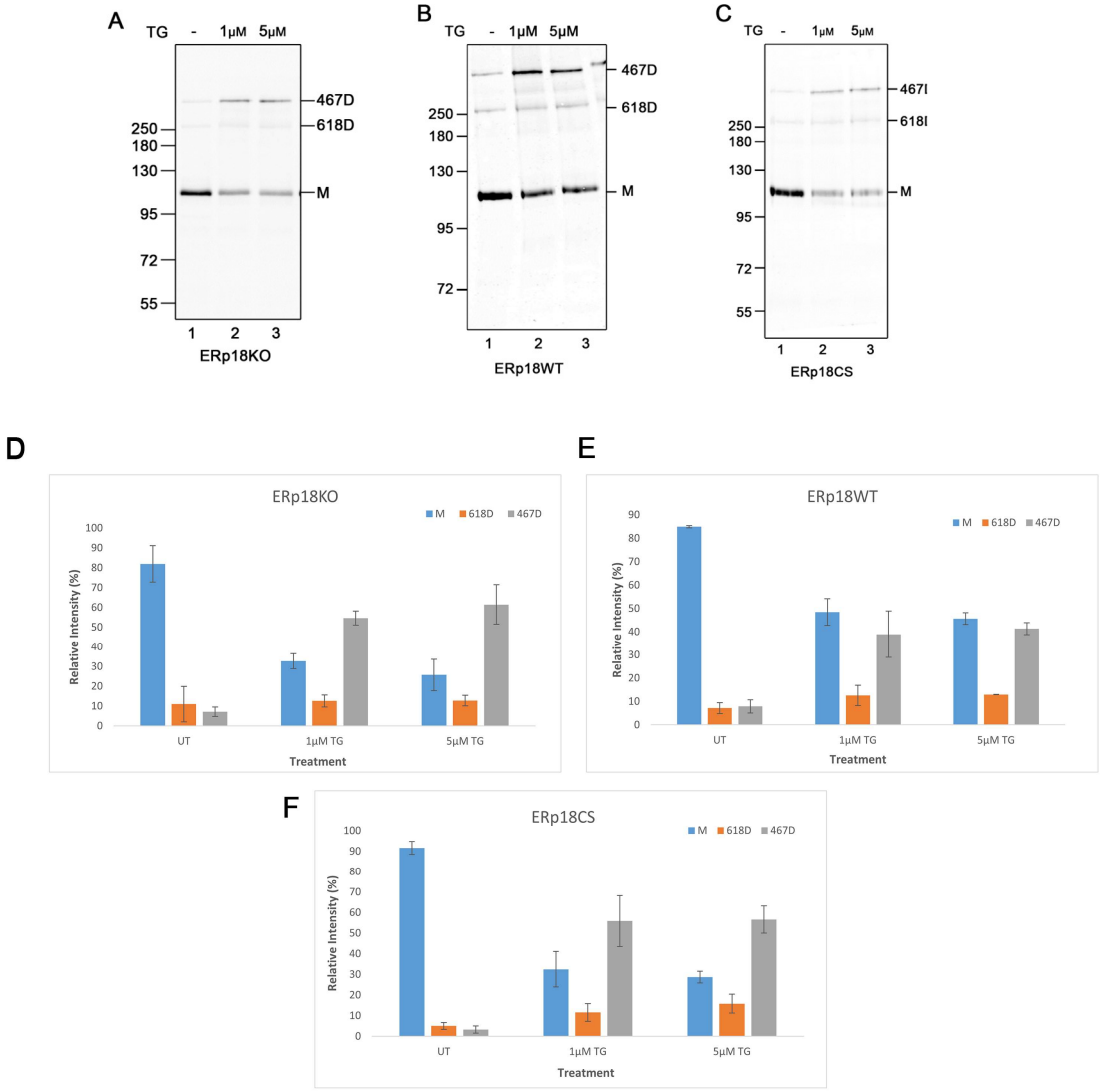

Figure 4-10 ERp18 regulates ATF6α 467D redox transition.
HT1080/ATF6WT lacking ERp18 (A) or expressing ERp18WT (B) or ERp18CS (C) were untreated or treated with 1 μM or 5 μM TG for 1 h to induce ER stress. Lysates were resolved under non-reducing SDS-PAGE conditions and immunoblotted with mouse anti V5 to detect ATF6α. (D, E, F) The relative intensity of redox forms (467D, 618D and M) of ATF6α was quantified by densitometry and presented with error bars representing standard deviation of 3 independent experiments (D & F) or 2 independent experiments (E).

4.2.2.5 Redox status of ERp18-FLAG

Biochemical analysis indicated that ERp18 can function as an oxidase or reductase (Jeong, Lee et al. 2008, Rowe, Ruddock et al. 2009, Oka, van Lith et al. 2019). An indicator of protein function, *in vivo,* is the change in redox status after catalysis; oxidases are likely to be oxidised in the resting cell and reduced after catalysis, and vice versa for reductases. To determine the change in redox status of ERp18 in response to stress, we utilised an AMS (4-acetamido-4′-maleimidylstilbene-2,2′-disulfonic acid) shift assay. The addition of AMS to free thiols increases the molecular weight by 0.5kDa. Thus, oxidised and reduced forms of the same protein would display different electrophoretic mobilities. Cells were either untreated or treated with thapsigargin for 1 h. They were incubated with NEM prior to lysis to alkylate (and prevent AMS labelling of) existing free thiols. Samples were then treated with the reducing agent TCEP to reduce disulfides which generated [new] thiols which were then labelled with AMS. Therefore, an increase in molecular weight would indicate an oxidised protein. As controls, cells were treated with DTT, to completely reduce proteins, or diamide to completely oxidise proteins. Lysates were resolved under reducing conditions and proteins were identified by immunoblotting (Figure 4-11). In unstressed cells, the mobility of ERp18 matched the mobility of ERp18 from cells treated with DTT in which the proteins are reduced (compare lanes 1 & 3). On the other hand, in cells treated with TG, the mobility matched that of cells treated with diamide (compare lanes 2 & 4). This result indicated that ERp18 is reduced in resting state and becomes oxidised during ER stress suggesting that it functioned as a reductase. Examination of the redox status of ERp57, a known reductase, showed that both oxidised and reduced forms are present in resting and stressed cells (Figure 4-11B). However, during stress, there was a decrease in the reduced protein and increase in the oxidised form. This is also indicative of ERp57 acting as a reductase during ER stress. Considered together these findings indicate that ERp18 reduces 467D to monomer and thus antagonises the stress induce shift from M to 467D.

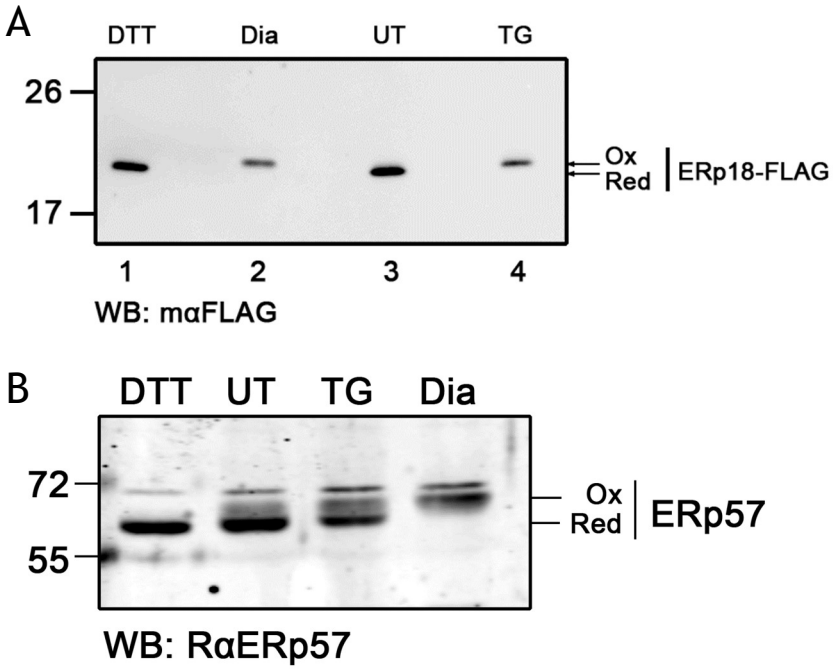

Figure 4-11 AMS shift assay of ERp18WT.
HT1080 cells expressing ERp18WT-FLAG were left untreated or treated with DTT, to reduce ER proteins, diamide to oxidise proteins, or TG to induce ER stress. Free thiols were alkylated with 25 mM NEM and lysates were reduced with TCEP prior to AMS alkylation of newly formed thiols. Lysates were resolved by SDS PAGE, and proteins identified by immunoblotting with mαFLAG (A). rαERp57 (B) and mαV5 (C).

4.2.3 Functional analysis of putative ERp18 binding mutants

4.2.3.1 *In cellulo* analysis of ERp18 mutants

4.2.3.1.1 Creating a cell line expressing putative ERp18 binding mutants.

4.2.3.1.1.1 ERp18 mutagenesis and stable transfection of ERp18^{S136D} & ERp18^{Y137T}.

In order to assess the contribution of specific residues to ERp18 function, site directed mutagenesis was used to mutate Serine-136 to aspartic acid and Tyrosine-137 to threonine to give ERp18^{S136D}, ERp18^{Y137T} respectively. Both residues are found within a loop believed to be involved in substrate binding and are located on the surface in the 3D structure in close proximity to the active site (Figure 4-12A). We hypothesised that the change, from polar uncharged to charged (Serine → Aspartate) or hydrophobic to polar uncharged (Tyrosine → Threonine), would sufficiently diminish the interaction thereby diminishing ERp18 activity. ERp18KO cells were transfected with pcDNA3.1 zeocin (+) plasmid containing the mutant sequences. Zeocin resistant colonies were chosen after selection and a positive clone, for each mutant, was identified by western blotting (Figure 4-12B).

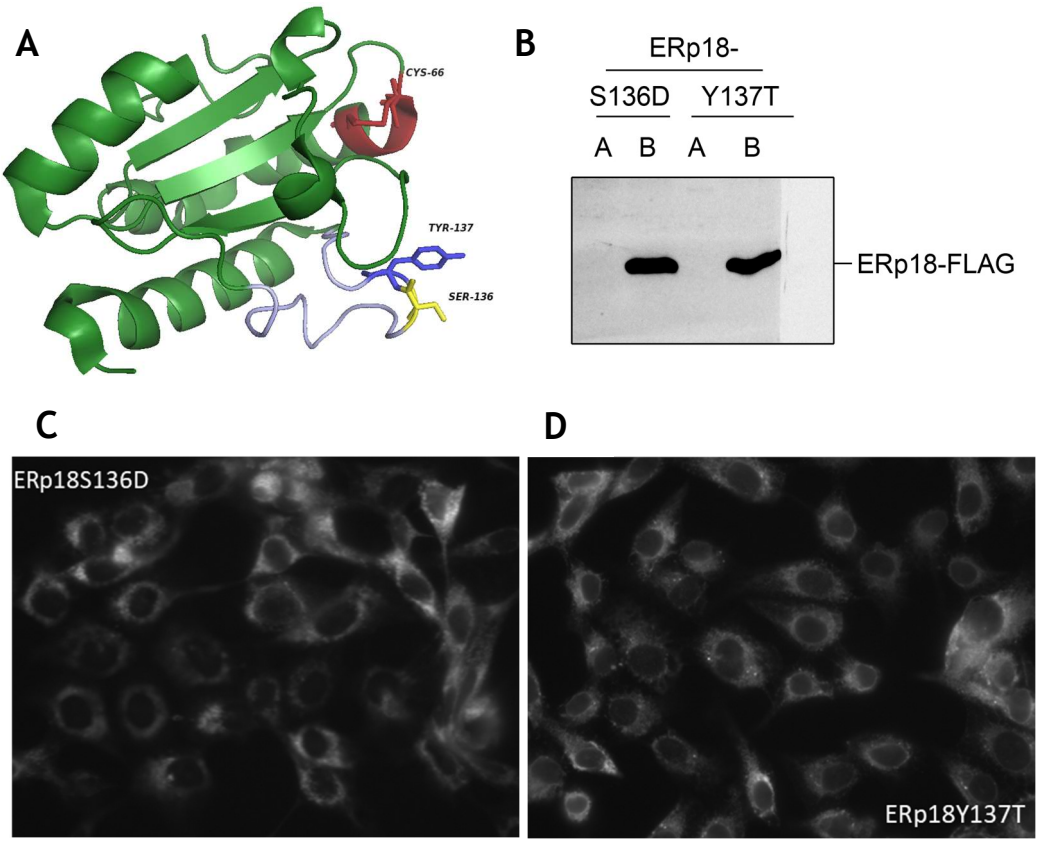

Figure 4-12 Expression and ER localisation of ERp18 mutants.
(A) PyMOL generated image of oxidised ERp18 (1SEN) showing the main thioredoxin fold in green and active site in red. A loop inserted into the thioredoxin fold and putatively involved in substrate binding is shown in grey with two key residues S136 and Y137 in yellow and blue respectively. (B) HT1080/ERp18KO cells were transfected with ERp18^{S136D} & ERp18^{Y137T} DNA cloned in pCDNA 3.1 Zeocin (+) and placed under zeocin selection. Single colonies were selected and expanded, and expression was verified by immunoblotting with mαFLAG antibody. HT1080/ERp18KO cells stably expressing ERp18S136D (C) and ERp18Y137T (D) were fixed on cover slips with methanol. Immunostaining was conducted with mαFLAG, and fluorescence of Alexa Fluor 488 secondary antibody was detected using the 40X objective.

4.2.3.1.1.2 ERp18S136D and ERp18Y137T are localised to the ER.

In section 4.2.2.2.4 it was shown that ERp18WT-FLAG was localised to the ER as a consequence of the C-terminal EDEL retention sequence. ERp18S136D and Y137T both contained this sequence and should therefore be targeted to the ER. In order to confirm their ER localisation, immunofluorescence was used to visualise the stably expressed protein. Microscopic examination revealed a pattern of fluorescence which was characteristic of the reticular network indicating ER localisation (Figure 4-12 C & D). Having confirmed the localisation of these mutants, we investigated whether they had any effect on trafficking of ATF6α.

4.2.3.1.2 Effect of mutations on regulation of ATF6α redox switch.

The effect of the mutations was assessed by the ability of the mutants to antagonise the formation of 467D during stress. Cells stably expressing ERp18S136D or ERp18Y137T were left untreated or treated with 1 μM and 5 μM TG to induce ER stress. Relative quantities of ATF6α were determined and presented as the mean of three (3) independent experiments (Figure 4-13). In the absence of ER stress, the relative quantities of M, 618D and 467D were similar at 89%, 6% and 5%, for ERp18S136D, and 90%, 6% and 4 % for ERp18Y137T. For ERp18S136D expressing cells in the presence of 1 μM TG, M decreased to from 89 to 63%, 618D increased from 6% to 11% and 467D increased from 4% to 26%. In the presence of 5 μM TG, the changes were similar at 61%, 12% and 28% for M, 618D and 467D respectively (Figure 4-13A). For cells expressing ERp18Y137T in the presence of 1 μM TG, M decreased from 90% to 60%, 618D increased from 6% to 11% and 467D increased from 4% to 29%. In the presence of 5 μM TG, M decreased to 61%, 618D increased to 10% and 467D increased to 29%. Compared to the findings presented in section 4.2.2.4 the quantity of M in both mutants, during TG-induced stress, was greater than both ERp18KO and ERp18WT cells. Likewise, the quantity of 467D was less in the mutants which mirrored wild type effect with a possible difference in efficiency of binding and/or catalysis.

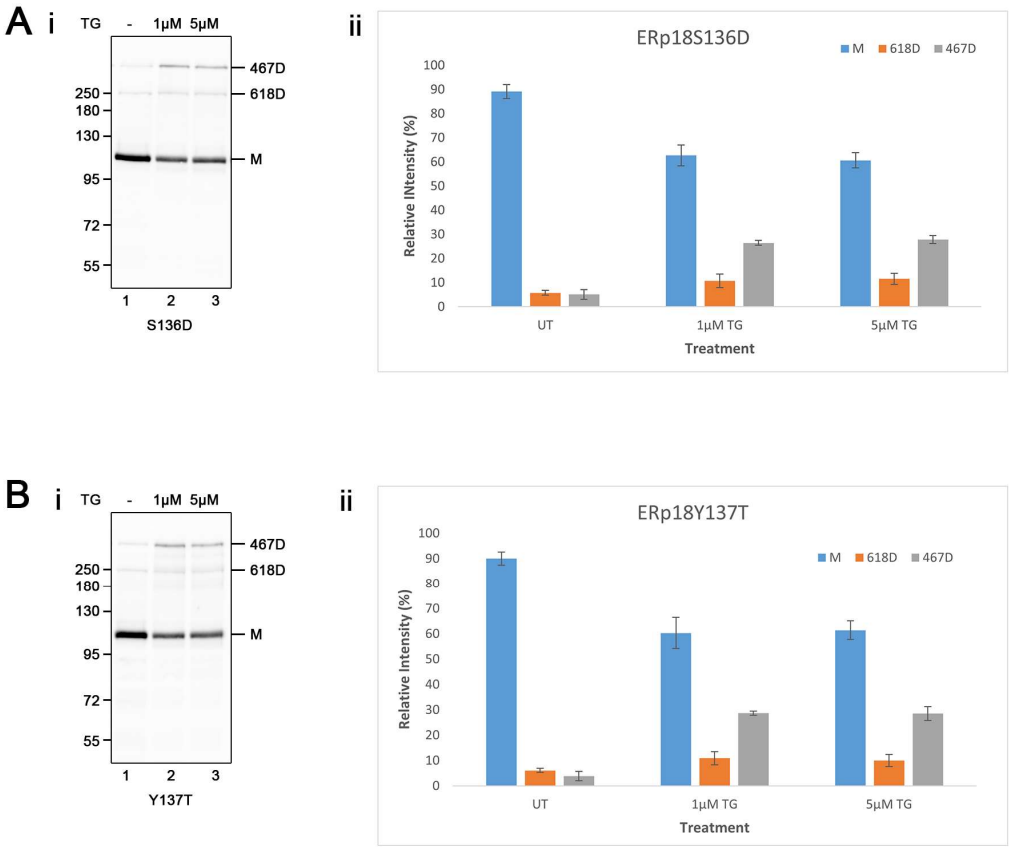

Figure 4-13 ERp18 binding mutants regulate ATF6α redox switch.
HT1080/ATF6WT expressing ERp18S136D (A (i)) or ERp18Y137T (B (i)) were untreated or treated with 1 μM or 5 μM TG for 1 h to induce ER stress. Lysates were resolved under non-reducing SDS-PAGE conditions and immunoblotted with mouse anti V5 to detect ATF6α. The relative intensity of redox forms (467D, 618D and M) of ATF6α was quantified by densitometry and presented with error bars representing standard deviation of 3 independent experiments (A & B (ii)).

4.2.3.1.3 Investigating association of ERp18 mutants with ATF6α.

In order to investigate the binding of ERp18 to ATF6α, a pull-down assay was used to isolate ERp18 and examine ATF6α bound in the absence or presence of ER stress. Cells expressing ERp18WT, ERp18S136D or ERp18Y137T were left untreated or treated with 1 & 5 μM TG for 1 h. ERp18KO cells were used as a control. ERp18 was immunoprecipitated using FLAG M2 affinity beads (sigma). ERp18-ATF6α complexes were eluted with 1X SDS loading buffer and resolved under reducing conditions and ERp18 and ATF6α were identified by immunoblotting. ATF6α was detected in all lysates but ERp18 was detected only in lysates containing ERp18 (Figure 4-14B). Despite different levels of expression (Figure 4-14C), ATF6α was recovered with ERp18WT as well as the mutants in both untreated and treated conditions (Figure 4-14A lanes 2 – 7) but was not recovered in the absence of ERp18 indicating that it did not interact with the agarose beads (lane 1). For ERp18WT and S136D, similar amounts of ATF6α were

recovered with ERp18 isolated from the lysates of untreated and treated cells. For ERp18Y137T cells, less ATF6α was recovered from treated cells compared to untreated cells. Importantly, the mutations did not prevent binding to ATF6α.

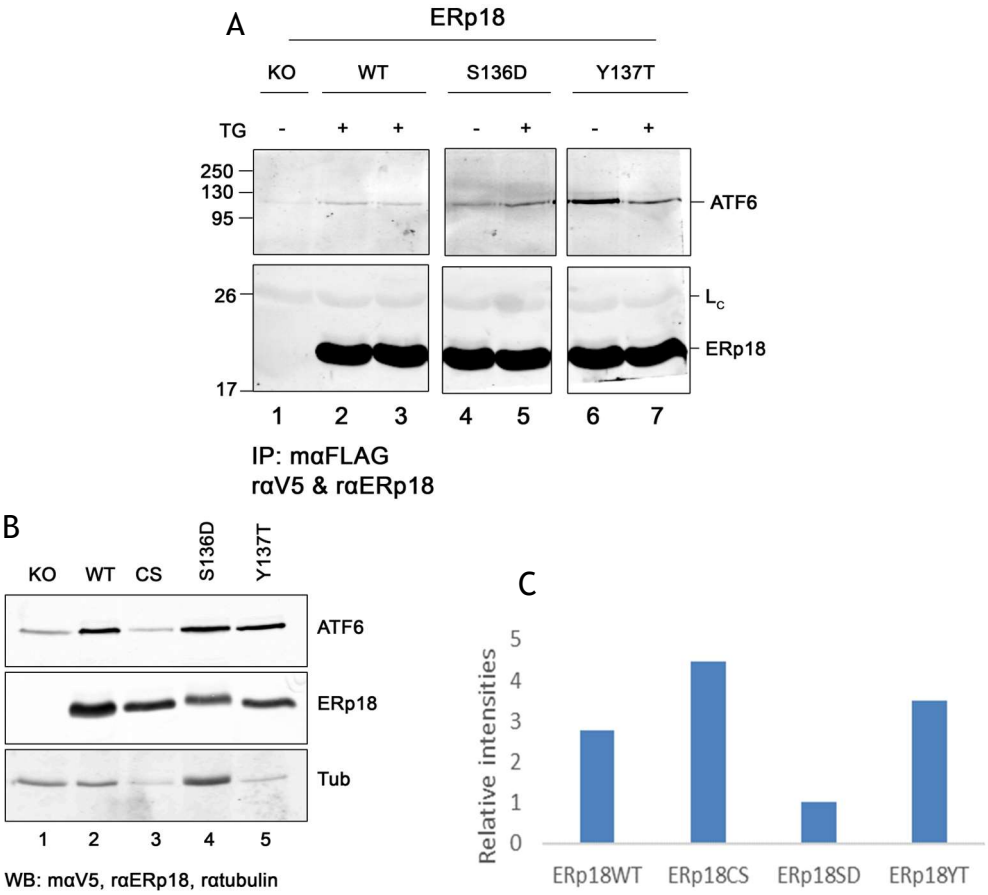

Figure 4-14 ERp18 mutants interact with ATF6α
(A) Cells expressing indicated ERp18-FLAG were left untreated or treated with 5 μM TG for 1 h. Cells were lysed and ERp18 was immunoprecipitated using FLAG M2 affinity beads. Lysates were resolved under reducing conditions and ATF6α and ERp18 were identified by immunoblotting with rabbit anti V5 and ERp18 antibodies, respectively. (B) Immunoblot of lysates showing the expression of ERp18 and ATF6α. (C) Quantification of ERp18 expression (n = 1).

4.2.3.2 *In vitro* analysis of ERp18 reductase activity

4.2.3.2.1 Expression and purification of ERp18

In order to assess any changes in ERp18 activity *in vitro*, ERp18WT, -CS, S136D & Y137T were expressed and purified from *E. coli*. Sequences encoding mature ERp18-FLAG (residues Ser^{24} – Leu^{172}) with an N-terminal His tag were cloned into the bacterial expression vector pET28a. Proteins were expressed as soluble proteins in the cytoplasm of BL21 (DE3) *E. coli* and purified using immobilised metal affinity chromatography with elution into 1X TBS with 1 mM EDTA.

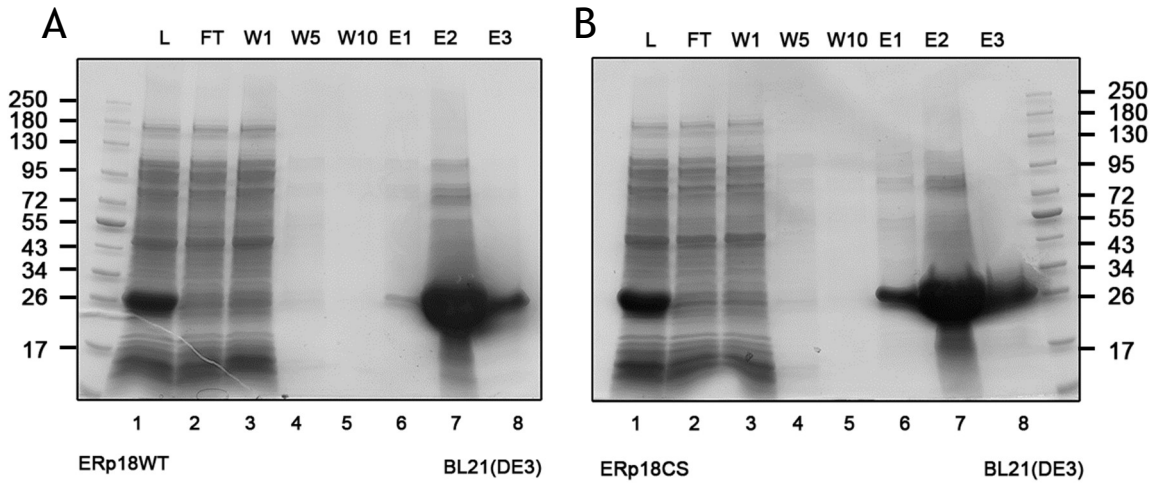

Figure 4-15 ERp18 is expressed and purified as a soluble protein.
Representative gels of ERp18WT (A) and CS (B) expressed in *E. coli* and purified by immobilised metal affinity chromatography.

4.2.3.2.2 Insulin reduction assay

To assess the effect of the mutations on ERp18 activity, we examined their ability to reduce insulin *in vitro*, compared to the ERp18WT using Thioredoxin (Trx1) as a positive control. To ensure proteins were reduced before the addition of insulin, 3 μM of each protein was incubated for 30 min in 1X TBS containing 0.5 mM DTT before the addition of insulin to a final concentration 0.17 mM. The change in OD at 650 nm, caused by the precipitation of insulin upon reduction, was then followed for 60 min. As a negative control, insulin was incubated with 1X TBS and DTT without enzyme (Figure 4-16Figure 4-16 *In vitro* reductase activity of ERp18.. As expected thioredoxin exhibited the highest reductase activity. There was a gradual increase in OD from 0 to 25 min followed by a rapid increase up to 60 min. ERp18WT exhibited lower reductase activity than Trx1; the increase in OD over time was more gradual towards a

lower maximum at 60 min. The activity of ERp18S136D was comparable to that of ERp18WT while ERp18Y137T demonstrated lower reductase activity. This suggested that the Y137T, but not the S136D, mutation affected the reductase activity of ERp18. There was no difference in change in OD between ERp18CS and the negative control with no significant reduction of insulin. These results indicated that the reductase activity of ERp18 was reliant on the presence of a protein containing active site cysteines and that Tyr-137 contributed toward the binding or mechanism of ERp18 reduction.

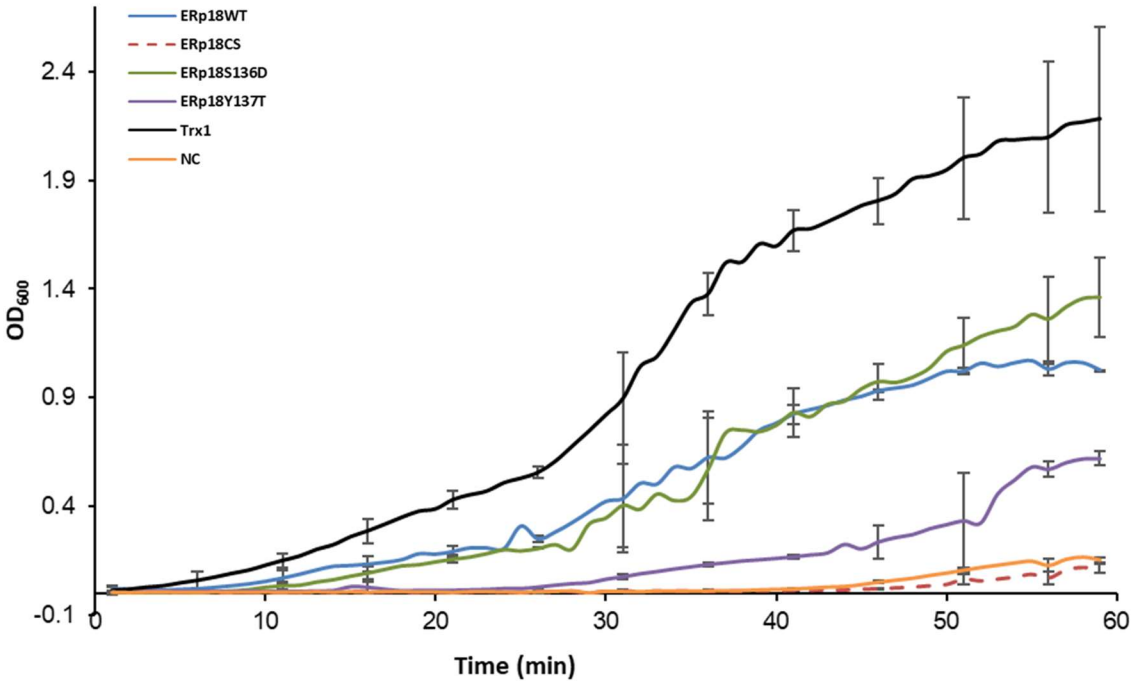

Figure 4-16 ***In vitro*** **reductase activity of ERp18.**
ERp18WT, CS, S136D or Y137T, to a final concentration of 3 μM, was incubated with 0.17 mM insulin in reaction buffer (50 mM Tris pH 7.5 containing 0.5 mM DTT). The reduction of insulin was monitored as an increase in turbidity which affects the OD 650 nm. Trx1 was used as a positive control and insulin was incubated with the reaction buffer and DTT for a negative control.

4.3 Discussion

In this chapter, direct and indirect interacting partners involved in ATF6α regulation were examined. MANF, a nucleotide exchange inhibitor, was shown to interact with BiP and was recovered with ATF6LD at steady state. ERp18WT was shown to antagonise the formation of dimer 467D during ER stress by reducing the C467-C467 disulfide bond. Point mutations to produce putative binding mutants ERp18S136D & Y137T did not affect ERp18 activity in cells but the latter diminished the reductase activity *in vitro*.

4.3.1 MANF in the ATF6α regulatory complex

The involvement of MANF in the ATF6α arm of the UPR is proposed based on its ability to modulate BiP binding and the fact that its overexpression reduces apoptosis caused by ER stress (Apostolou, Shen et al. 2008, Hellman, Arumäe et al. 2011, Yan, Rato et al. 2019). In agreement with previous work, MANF was recovered with BiP in unstressed cells (Yan, Rato et al. 2019). It was also recovered, when co-expressed, with ATF6LD. This provided some indication that MANF may be part of the ATF6α ternary regulatory complex. However, this could not be confirmed for full length ATF6α due to inefficient extraction of ATF6α following crosslinking (Figure 4-2). Including sonication in the lysis process improved the solubilisation of the ER membrane and extraction of ATF6α thus establishing a lysis protocol which could be used to interrogate functional interaction between MANF and full length ATF6α (Figure 4-3). However, time became a limiting factor and future directions for this experiment would be included in the discussion.

4.3.2 ERp18 antagonises ATFα redox shift

ERp18 engages ATF6α during ER stress and regulates trafficking by antagonising the redox shift from monomer to dimer 467D. Overexpression of ERp18 diminished the amount of 467D relative to the monomer (Oka, Pierre et al. 2022) & (Figure 4-10). In the absence of ERp18, this redox shift (from monomer to 467D) was more pronounced (Figure 4-10). Considering that dimer 467D is trafficked (chapter 3), this result is congruent with increased trafficking of ATF6α in ERp18 knockout cells (Oka, van Lith et al. 2019) and supports the idea

that monomeric ATF6α is involved in ER retention (Oka, Pierre et al. 2022). In the absence of ERp18, the formation of 467D is unregulated leading to increased ATF6α, in the form of 467D, leaving the ER while less ATF6α monomer remains in the ER. Conversely, when ERp18 is overexpressed less 467D is produced and more monomer is retained.

Functional ERp18-ATF6α interaction requires the reductase activity of active site cysteines supported by a more pronounced redox shift in cells expressing the cysteine-less mutant. Additionally, the redox status of ERp18WT, determined by the AMS shift assay, changes from reduced (in steady state) to oxidised (during stress). A similar shift is also seen in ERp57, a known reductase (Figure 4-11). These data support a model in which ERp18 regulates ATF6α trafficking by reducing the intermolecular C467 disulfide.

ERp18 residues S136 and Y137 were implicated in substrate binding. However, mutating these amino acids to aspartic acid and threonine, respectively, did not diminish the reduction of ATF6α as anticipated. They were recovered with ATF6α in stressed and unstressed cells and displayed similar activity to ERp18WT (Figure 4-14). This suggests that the residues are not involved in binding ATF6α or do not sufficiently alter the binding to impact reductase activity. However, the Y137T mutation diminished reductase activity *in vitro* (Figure 4-16).

4.3.3 Analysis of ERp18 binding peptide

The position of peptide binding loop in ERp18 was determined using structure-based alignment with other thioredoxin-like proteins without considering other AGR family members (Rowe, Ruddock et al. 2009). Recent studies with AGR2 have identified alternative peptide binding sites for intra- and extracellular clients (Mohtar, Hernychova et al. 2018, Maurel, Obacz et al. 2019). Comparison among members of the AGR family shows 40% homology between ERp18 and AGR2/AGR3, 80% homology among alternative binding sites for Reptin (a) and EpCAM (b) and only 20% homology within the ERp18 binding loop (Figure 4-17). This might suggest that binding peptide a or b contribute more to ERp18-client interaction. However, mapping the Reptin binding site onto ERp18 structure shows that the residues are buried and likely to be involved in packing rather than substrate interactions. On the other hand, part of the EpCAM binding

peptide and ERp18 binding loop map onto the surface and therefore can be involved in substrate interactions (Figure 4-14B). Moreover, a point mutation in the suggested ERp18 binding loop affects *in vitro*, but not *in vivo*, reductase activity.

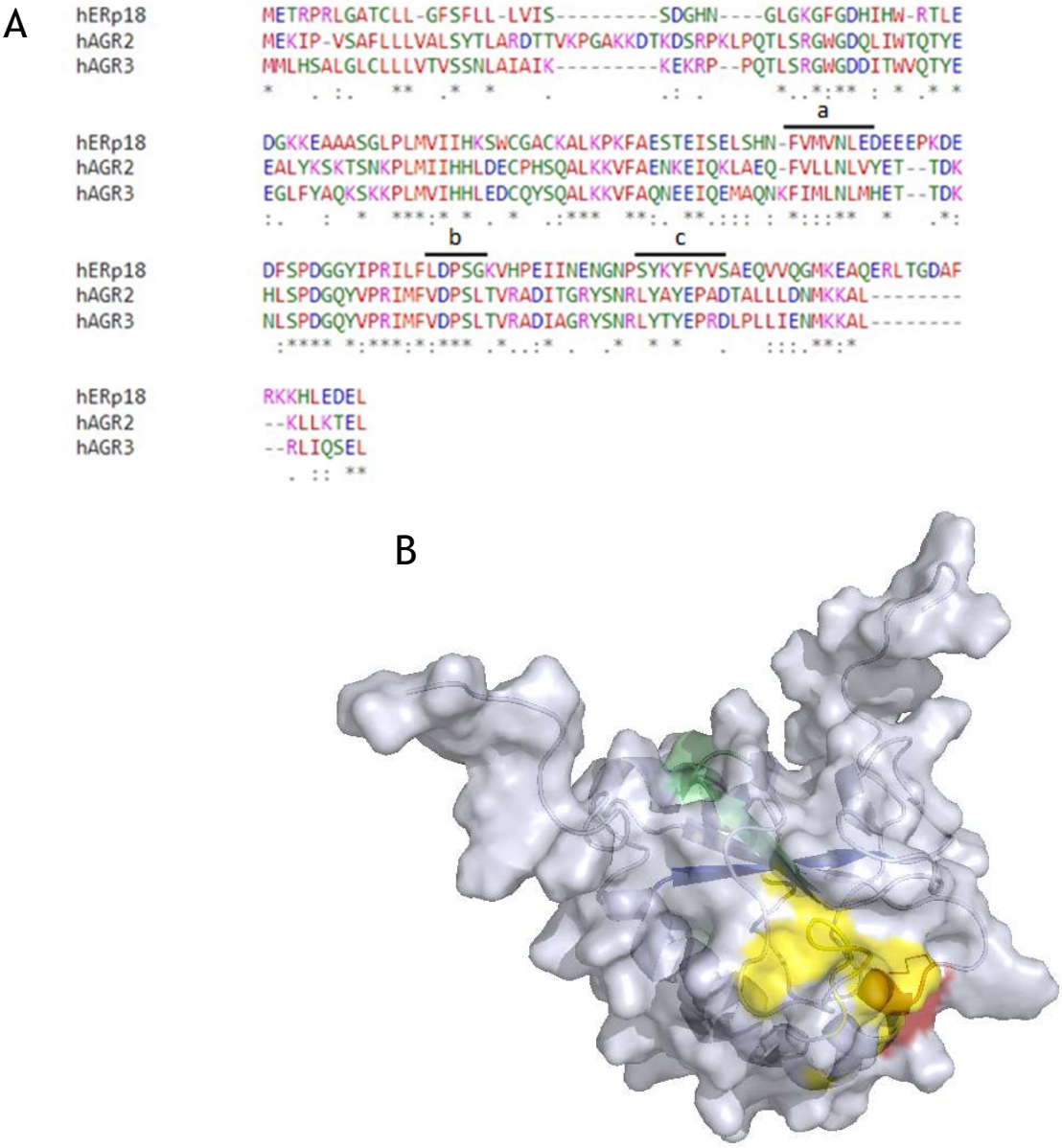

Figure 4-17 Substrate binding peptides in AGR proteins.
(A) Sequence alignment of the AGR proteins showing conservation of amino acid residues in peptide binding sequences. Binding site a and b are involved in AGR2 interaction with Reptin and EpCAM respectively. Binding site c has been proposed based on structural analysis of ERp18. (B) PyMOL generated surface and cartoon overlay of oxidised ERp18 (PDB 2k8v) showing the active site in red, Reptin binding equivalents in blue, EpCAM binding equivalents in green and ERp18 peptide binding loop in yellow.

Considering the larger size of ATF6α (75 kDa), it may require a larger surface to stabilise its interactions compared to insulin which is 5x smaller. This might suggest that additional residues, such as the EpCAM binding site, may contribute to ATF6α interaction.

Hydrophobic residues that are important in thioredoxin-substrate interactions display large differences in chemical shifts between the reduced and oxidised states (Qin, Clore et al. 1995). For ERp18, the chemical shift differences in the ERp18 binding loop are higher than the region that corresponds to the EpCAM binding site. Thus, the effect of the Y137T mutation on ERp18 activity is reasonable and mutations of other hydrophobic residues within the loop (e.g., Y139, F140 & Y141) might further diminish its activity. Simultaneously, mutations within the binding sites EpCAM can be explored to determine their involvement in the ERp18-ATF6α interaction.

Chapter 5. Identifying Protease Q

5.1 Preface

This chapter presents, in the form of a grant proposal, several experiments that are designed to investigate non-canonical proteolytic processing of ATF6α. It was written during the first wave of Covid 19 related lockdowns in the UK. It served to mitigate against time lost during the months in which data collection was not possible.

5.2 Summary and research questions

Activating transcription factor 6α (ATF6α), an important mediator and effector during the unfolded protein response, is regulated by intramembrane proteolysis. Canonical processing of ATF6α by site-1 and site-2 proteases releases a transcription factor that upregulates genes that help the cell to survive ER stress. When S1P is blocked, ATF6α is aberrantly processed to produce ATF6-P by an unknown protease designated 'protease Q'. ATF6-P can also be formed when ATF6α bypasses ERp18 quality control in cells containing functional S1P. This may represent an additional level of ATF6α regulation in the Golgi. The aim of this project is to identify this unknown protease. Doing so would provide insight into alternate processing and/or trafficking mechanisms of ATF6α. To do this, the following questions will be investigated:

Where is protease Q located?
What are the cleavage and recognition sites?
Is the oligomeric status of the substrate important?
What inhibitors affect protease Q?

5.3 BACKGROUND

5.3.1.1 The unfolded protein response

The unfolded protein response (UPR) refers to the collective processes that the cell engages to mitigate the imbalance between the amount of unfolded and misfolded proteins in the endoplasmic reticulum (ER) lumen and its folding capacity termed ER stress (Walter and Ron 2011). In an effort to restore ER homeostasis and to escape apoptosis, the transcriptome is altered by (1) upregulating the expression of chaperones and other enzymes involved in protein

folding to increase folding capacity; (2) upregulating the expression of proteins involved in ER-associated degradation (ERAD) to remove proteins that fail to be folded; and (3) downregulating the expression of other proteins (Schroder and Kaufman 2005). These transcriptional and translational programs are mediated by three UPR regulators: inositol requiring enzyme 1 (IRE1), PKR-like ER kinase (PERK), and activating transcription factor 6α (ATF6α).

5.3.1.2 Structure and function of ATF6α

The ER stress response protein ATF6α, resides as a 90 kDa type II transmembrane transcription factor that spans the endoplasmic reticulum (ER) and cytoplasm. The transmembrane domain, which contains a cleavage sequence for site-2 protease, anchors the protein in the ER membrane with the N-terminal section protruding into the cytoplasm and the C terminal section into the ER lumen. The cytoplasmic domain consists of a transactivation domain (TAD) and a basic leucine zipper (bZIP) domain which allows it to upregulate transcription of target genes. The lumenal domain contains an S1P cleavage site, two Golgi localisation sequences which overlap with sequences that bind with the HSP70 chaperone BiP, and two cysteine residues (C467 & C618) which are important in the detection and response to ER stress (Sato, Nadanaka et al. 2011). ATF6α occurs as a monomer or as dimers of different apparent sizes formed by the lumenal domain cysteines (Oka, van Lith et al. 2019, Koba, Jin et al. 2020).

As an effector of the UPR, ATF6α upregulates the transcription of several genes including GRP78 which encodes the molecular chaperone BiP that attaches itself to unfolded proteins to retain them in the ER. ATF6α is activated by regulated intramembrane proteolysis (Rip) which involves site-1 and site-2 protases (S1P and S2P respectively) located in the Golgi (Ye, Rawson et al. 2000). In unstressed conditions ATF6α is kept in the ER by its interaction with BiP which blocks its Golgi localisation signals (GLSs). During ER stress BiP is released, exposing the GLSs resulting in ATF6α being packaged into COPII vesicles and sent to the Golgi (Shen, Chen et al. 2002). Before being transported to the Golgi, ATF6α interacts with the PDI-like protein ERp18 which functions as a quality control checkpoint possibly based on redox status (Oka, van Lith et al. 2019). At the Golgi, most of the lumenal domain of ATF6α is removed by S1P cleavage near the transmembrane domain. This prepares ATF6α for cleavage by S2P

within the transmembrane domain to release the soluble transcription factor (ATF6-N) which moves to the nucleus. There it binds to the consensus sequence of the cis-acting ER stress response elements ERSE (CCAAT – N9 – CCACG) along with the nuclear transcription factor NF-Y to induce transcription of UPR related genes (Yoshida, Okada et al. 2000).

Canonical processing of ATF6α, which is dependent on S1P and S2P, during ER stress produces a 50 kDa (N terminal) fragment designated ATF6-N (Ye, Rawson et al. 2000) and an intermediate membrane-associated fragment lacking only the lumenal domain which is removed by S1P (Adachi, Yamamoto et al. 2008). The ~43 kDa lumenal domain also produced by S1P cleavage is known to be degraded by the lysosomes (Chapter 3). Inhibition of S1P during ER stress produces a fragment that is larger than both ATF6-N and membrane-associated ATF6α (Ye, Rawson et al. 2000). This fragment, called ATF6-P, is also formed in unstressed cells lacking the small PDI-like protein ERp18 (Oka, van Lith et al. 2019). ERp18 acts as a quality control checkpoint for trafficking and processing of ATF6α as [ERp18] deficient cells with functional S1P produces ATF6-P. Interestingly, ATF6-P is also produced in ERp18WT containing competent S1P that over express ATF6α (Oka, van Lith et al. 2019). It follows that ATF6-P can be formed when the ER quality control checkpoint is bypassed (Figure 5-1). This may suggest the existence of another trafficking mechanism for ATF6α that escapes ER quality control. However, the formation ATF6-P when S1P is inhibited during ER stress suggests that the route to S1P is the same and that another quality control mechanism at the Golgi may determine the fate of ATF6α based on the ability of S1P to cleave.

The fact that ATF6-P is formed by cleavage by another protease raises a few questions. The core question is; what is the identity of this protease Q? ATF6α is a transmembrane protein, therefore the protease may be of the intramembrane protease family. But the larger size of ATF6-P compared to the S1P intermediate may suggest that cleavage occurs at a point further away from the transmembrane domain which can be accessible to a soluble protease.

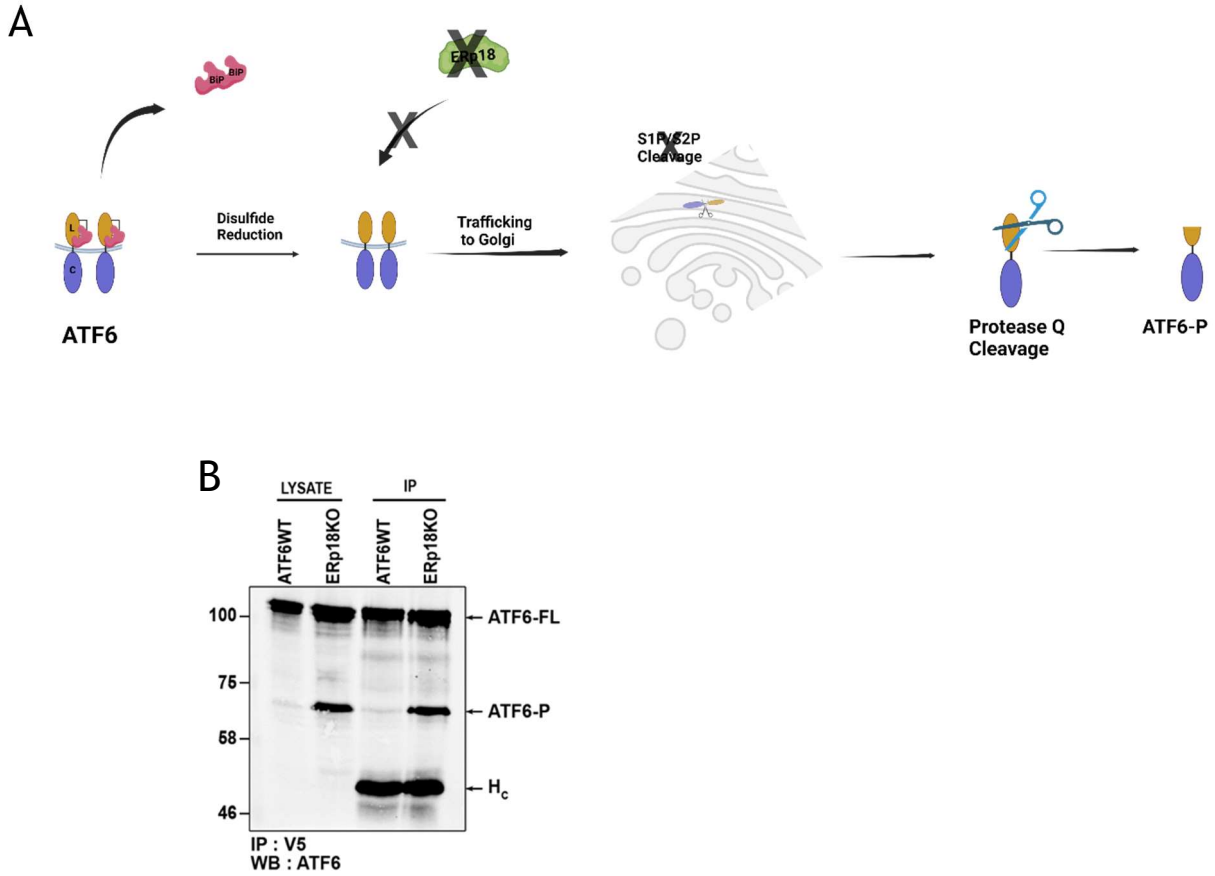

Figure 5-1 Non-canonical processing of ATF6α in ERp18KO cells.
(A) In the absence of ERp18, ATF6α escapes BiP binding and is likely trafficked to the Golgi where S1P cleavage is bypassed. This allows ATF6α to be processed by an unidentified protease (Protease Q) to produce ATF6-P (Created with Biorender.com) (B) Western blot of Immunoprecipitates from cells overexpressing ATF6α with (lanes 1 & 3) or without (lanes 2 & 4) ERp18. ATF6-P is clearly seen in ERp18KO cells. H_c represents the antibody heavy chain.

To identify protease Q several dimensions of the non-canonical ATF6α would be investigated. An important aspect of the cleavage to address is the location of the protease; is the protease located within the same compartment as S1P? ATF6α must be trafficked to the Golgi to be cleaved by S1P. At face value this can be interpreted as non-canonical cleavage also occurring in the Golgi, but other possible outcomes should be considered when S1P is inhibited. There are three possible scenarios (1) cleavage may happen within the same compartment as S1P, (2) ATF6α can be moved further along the secretory pathway where it is cleaved or (3) ATF6α can be returned to the ER where it is cleaved. However, unpublished data from the lab excludes the possibility of scenario (3) occurring. Given the abundance of proteases that are located throughout the secretory pathway, defining where the cleavage happens is important in reducing the number of possibilities and identifying the protease responsible.

Another important aspect is to identify the required elements for cleavage such as the enzyme's recognition site as well as the oligomeric status of the substrate. Research has clearly demonstrated the involvement of proteases in the regulation of critical processes in the cell governed mainly by complementarity between protease and substrate (Neurath and Walsh 1976). The caspases, for example, precisely regulate the cascade of reactions leading to apoptotic cell death. The specificity with which each enzyme cleaves its substrate ensures precise activation of the process. Precise regulation of the activation of ATF6α depends on the recognition of specific sequences by S1P and S2P. Site-1 protease recognises and cleaves at the RRHLL sequence in lumenal domain of ATF6α while site-2 protease recognises and cleaves at the NYGP sequence located within the transmembrane domain (Ye, Rawson et al. 2000). Thus, mapping potential recognition sites in the lumenal domain can help identify candidate proteases.

The importance of the oligomeric status of the substrate of intramembrane proteases has been previously demonstrated. While reduced monomer ATF6α, for example, is more efficiently cleaved by S1P Nadanaka, Okada et al. (2007), recent findings indicate that disulfide bonded ATF6α can be cleaved by S1P (Oka, Pierre et al. 2022). ERp18 interacts with ATF6α during ER stress, possibly changing the redox and folding status of ATF6α in preparation for S1P

processing. It is possible that in the absence of ERp18 and ER stress this S1P-compliant conformation is not obtained thereby making ATF6α resistant to S1P and susceptible to protease Q.

5.4 Experimental system

Several ATF6α constructs and cell lines, used and characterised by Oka et al (2019), are readily available for this project. The ATF6α constructs contain an N-terminal HA tag and a C-terminal V5 tag which will allow the detection and/or isolation of the cytoplasmic and lumenal domains after any cleavage event with the appropriate antibodies. ATF6-P is preferentially formed when ATF6α cannot be cleaved by S1P. This can be achieved by chemically inhibiting S1P, expressing a mutant of ATF6α that is resistant to S1P cleavage, knocking out ERp18 or overexpressing ATF6α.

Primarily, experiments will be carried out in HEK293 cells that overexpress various forms of ATF6α (WT, C467A, C618A and ATF6-S1P) in which ERp18 has been knocked out. Other cell lines which are useful are ERp18KO (not expressing ATF6α) and wild type HEK293.

5.5 Identifying the cleavage site of Protease Q

5.5.1 Bioinformatics approach

Adventitious, possibly non-specific, proteases in the Golgi were thought to be responsible for the production of ATF6-P (Nadanaka 2007), but the consistent size of the cleavage product infers specificity of recognition for cleavage within the lumenal domain. *In silico* analysis of the lumenal domain can be used to identify potential cleavage sites; thereby narrowing the list of candidate proteases. The lumenal domain spans 271 amino acids from 399E to 670Q, however the range of amino acids where cleavage can potentially occur can be reduced. ATF6-P is larger than the intermediate formed from the cleavage by S1P. Therefore, Protease Q must cleave at a site beyond L419 – the last amino acid in the S1P cleavage site; this narrows the range by at least 20 amino acids (Figure 5-2). Additionally, the estimated size of ATF6-P can allow for the

exclusion of extreme C-terminal residues further reducing the possible range for potential cleavage sites.

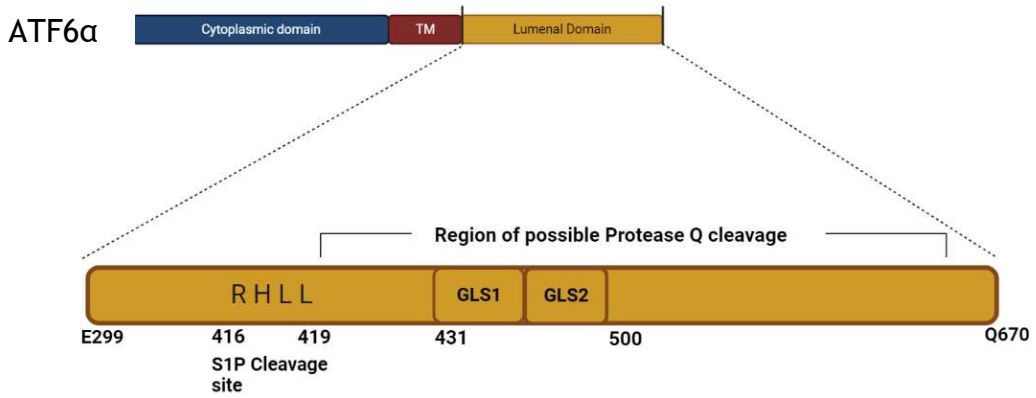

Figure 5-2 Domain structure and proteolytic cleavage sites in ATF6α lumenal domain. Figure shows the three domains of ATF6α (top) and calls out the structure of the lumenal domain to highlight the region potentially available for Protease Q cleavage based on the relative size of ATF6-P (Created with BioRender.com).

Two web-based resources have been identified for this analysis: iProt-sub (Song, Wang et al. 2018) and PROSPER (Song, Tan et al. 2012). PROSPER (PROtease substrate SPecificity servER), predicts potential cleavage sites for over 20 protease families curated within the MEROPS database using machine learning algorithms based on 4 sequence and structural characteristics (Song, Tan et al. 2012). IProt-sub, PROSPER'S contemporary, improves on the accuracy by training the machine learning algorithm to predict based on 11 characteristics and further benefits from accessing an expanded database (Song, Wang et al. 2018). Nevertheless, the experimental substrate validation built into PROSPERS' validation algorithm preserves its usefulness. Hits from these servers can be further assessed based on whether their location overlaps with ATF6-P formation, the position of the predicted cleavage sequence and the number of cleavage sites in the ATF6α lumenal domain.

5.5.2Mass spectrometry

The exact size of ATF6-P can be determined by MALDI-TOF mass spectrometry. Furthermore, comparison of trypsin digested spectrums of ATF6-P and ATF6WT can be useful because the presence of unique peptides that are present in

ATF6WT but absent from ATF6-P will reveal portions of the lumenal domain that are beyond the Protease Q cleavage site. Alignments of the unique peptides with the full sequence may also allow more precise identification of the cleavage site, but this depends on the position of the Protease Q site relative to the surrounding trypsin cleavage sites.

ATF6α is cleaved by Protease Q when S1P is bypassed. The scenarios in which this is possible can be classified based on whether S1P is functional. In unstressed ERp18 KO cells, for example, functional S1P is bypassed to produce ATF6-P; if the cells are stressed canonical cleavage is achieved. Inhibitors which inactivate S1P can also lead to the formation of ATF6-P during stress. The standing hypothesis is that the ATF6-P formed in the different scenarios is the same. To test this, the sizes and mass spectra of ATF6-P isolated from various scenarios will be compared. ATF6-P_1 will be isolated from HEK293 cells overexpressing ATF6-S1P treated with DTT. In this case S1P will be functional but unable to cleave ATF6 due to the mutation in the S1P cleavage site. ATF6-P_2 will be isolated from HEK293 cells overexpressing ATF6WT treated with S1P inhibitor and DTT. In this case, S1P is not functional. ATF6-P_3 will be isolated from unstressed ERp18KO cells overexpressing ATF6WT with functional S1P. If the spectra for ATF6-P_{1-3} are the same, it will indicate that there is a single site cleaved by Protease Q. If spectra are different, it will suggest that Protease Q is not solely responsible for cleavage. To control for this, experiments can be designed to investigate each scenario independently.

5.5.3 Experimental validation of proteases

*In silico a*nalysis of ATF6α sequence returned 16 and 6 hits from iProt-sub and PROSPER respectively; this included cathepsins, caspases, calpains, matrix metallopeptidases, kallikrein-related peptidases, elastases, granzymes and Furin (see Table 7-1 for complete list). When they are assessed based on sub-cellular location and number of [predicted] lumenal cleavage sites, Furin stands out as the most likely candidate. Lysosomal enzymes cathepsin D and L, which traverse the secretory pathway, can also be considered. Furin is a type 1 transmembrane protein that is localised to the trans-Golgi. It contains a subtilisin-like catalytic domain that cleaves substrates, which are usually pro-proteins, at sequences containing clusters of basic amino acids (Thomas 2002). Different strategies for

experimental validation of these results can be applied. Lysosomal proteases can be inhibited by using NH_4Cl, which prevents acidification of the lysosomes, or leupeptin which is known to specifically inhibit cathepsins L among others (Seglen, Grinde et al. 1979). Monitoring the effect of these inhibitors on ATF6-P formation can be used to rule out the cathepsins D and L as likely candidates and possibly provide suitable negative controls for other candidates. In the case of Furin, the bioengineered inhibitor α1-antitrypsin Portland with high selectivity for Furin can be used to determine its involvement (Jean, Stella et al. 1998).

5.6 Where does Protease Q cleavage occur?

The determination of the cellular compartment in which the cleavage occurs is important in identifying the protease responsible. Brefeldin A-mediated merging the Golgi and ER in cells that express a mutant of ATF6α that does not leave the ER under stress resulted in canonical cleavage. However, no ATF6-P was formed in the absence of stress indicating that cleavage occurs post ER - possibly in the Golgi (Oka, van Lith et al. 2019). This essentially rules out the possibility of this reaction (Protease Q cleavage) occurring in the ER. Furthermore, proteases such as S1P are synthesised in the ER as inactive proenzymes and then transported to the Golgi where they are activated (Espenshade, Cheng et al. 1999); thus, it is not likely that protease Q is active in the ER.

To investigate the localisation of ATF6-P, ERp18KO cells (which consistently produce ATF6-P) will be sedimented through a sucrose gradient to separate the ER from Golgi. Proteins from these fractions can then be resolved by SDS-PAGE and immunoblotted with ATF6 antibodies to determine which fraction contains ATF6-P. The fractions will also be immunoblotted with antibodies for ER- and Golgi – specific proteins to determine the fraction enriched for each of these two organelles. In unstressed cells, it is expected that most of the ATF6α will not be trafficked and therefore the ER should contain the monomer and dimer forms of ATF6α but should not contain ATF6-P. The form of ATF6α which escapes the ER and is trafficked to the Golgi will be cleaved to form ATF6-P. It is therefore expected that the Golgi-enriched fraction would contain ATF6-P along with the form that is transported to the Golgi. Experiments involving separation of the ER and Golgi using sucrose gradients usually show that more ER sediments in the denser fractions while more Golgi is found in the lighter

fractions. Between the two extremes of the densest and lightest fractions, there is a continuum of decreasing ER and increasing Golgi enrichment from the denser to lighter fractions. Therefore, a profile of the ratio-metric comparison between the relative quantities of ATF6-P and ATF6α found in the ER-enriched and the Golgi-enriched fractions could be generated to interpret results. To improve quantification, synthesis of new ATF6α will be halted by treatment with cycloheximide. The profile from ERp18KO cells will be compared to unstressed ERp18WT cells. The presence of ERp18 in the cell reduces but does not completely halt [abnormal] trafficking when ATF6α is over-expressed which leads to the formation of some ATF6-P. The profile for these cells therefore should show less ATF6-P in the Golgi-enriched fractions.

Dithiothreitol (DTT)-induced ER stress causes rapid trafficking of ATF6α through reduction of proteins in the ER. Coupling DTT treatment with S1P inhibition will lead to increased trafficking of ATF6α as well as the amount of ATF6-P produced giving a different ratio-metric profile. These results can be replicated by DTT treatment of ERp18KO or ERp18WT cells expressing ATF6-S1P. Because DTT changes the oligomeric status of ATF6α that leaves the ER, the profile produced may not accurately reflect what happens when the ER is not reduced. Thapsigargin (TG) induces the UPR by affecting ER calcium balance. Profiles obtained from cells treated with TG to induce the UPR will be more representative of normal ER redox balance given that it does not change the oligomeric status of ATF6α.

Whether Protease Q and S1P are in the same compartment is an important question to be addressed because this could give some indication of whether ATF6-P is formed later in the secretory pathway. To address this, sucrose gradient fractions will be immunoblotted with antibodies to S1P and ATF6 to determine the extent to which S1P colocalises with ATF6-P. This may not provide a definitive answer because it is unlikely that the cis and trans Golgi will be fully differentiated. However, the degree of colocalization of ATF6-P with S1P will at least provide some indication of whether S1P and protease Q are spatially separated.

5.7 Does oligomeric status affect cleavage?

Enzyme-substrate specificity is rarely determined by the sheer ability of a protease to recognise specific peptide bonds within the substrate sequence but may be regulated through the action of non-catalytic domains within the protease itself, interaction with other proteins or cofactors, or a specific form of the substrate (López-Otín and Bond 2008). Before it can be cleaved by S1P, mammalian SREBP, which is involved in lipid homeostasis, forms a complex with its molecular escort SCAP (Sakai, Nohturfft et al. 1997, Sakai, Nohturfft et al. 1998). In yeast, the cleavage of SREBP is carried out by Rhomboid protease Rbd2 which requires cdc48 (Hwang, Ribbens et al. 2016). In the case of [human] ATF6α, its oligomeric status influences its cleavage by S1P leading to the question of whether this is also the case for Protease Q.

To address this, the formation of ATF6-P in cells expressing various mutants of ATF6α will be followed. The double cysteine mutant of ATF6, ATF6-DM, will be used to examine the formation of ATF6-P from monomer substrate; the C467A mutant will be used to examine the formation from dimer 618 (618D) and the C618A mutant will be used to examine the formation from dimer 467 (467D). Stable cell lines must be utilised as existing data does not show the formation of ATF6-P by transient transfection with the ATF6α mutants (Oka, van Lith et al. 2019). These results will be compared with formation from ATF6-WT. The interrogation will be qualitative i.e., do these mutants form ATF6-P when S1P is inhibited? The inability of any of these mutants to form ATF6-P might indicate oligomeric limitation of cleavage by Protease Q.

An alternative approach to determine the importance of oligomeric status will be to look at the lumenal domain produced from ATF6-P formation. The lumenal domain produced from canonical ATF6α processing has been isolated as a dimer when NH_4Cl is used to prevent lysosomal degradation (Chapter 3 & (Oka, Pierre et al. 2022)). A similar approach can be used to isolate the lumenal domain of ATF6-P. ATF6WT cells will be treated with NH_4Cl before inducing the UPR with TG while inhibiting S1P. The lumenal domain product can then be immunoprecipitated with anti V5 and analysed under non-reducing conditions to assess whether it is in monomeric or dimeric form.

5.8 Using protease inhibitors to identify the family that contains Protease Q

Mammalian proteases are classed as metalloproteases, serine, cysteine, aspartate and threonine proteases, based on the catalytic mechanism (López-Otín and Bond 2008). Protease inhibitors for classes as well as individual proteases are readily available (listed in Table 7-2). Inhibitors will be utilised to determine the class to which Protease Q belongs. ATF6WT cells will be treated with class specific inhibitors, individually or in combination, to determine which ones abolish the formation of ATF6-P. Several experiments will be set up each using four class inhibitors with a different inhibitor omitted. Adding S1P inhibitor to the cocktail and inducing the UPR with thapsigargin will generate ATF6-P. For example, treating cells with a combination of Aprotinin, E-64 and Pepstatin will inhibit serine, cysteine and aspartic proteases. If ATF6-P formation is unaffected, this would suggest that a metalloprotease is responsible. This can then be confirmed if treatment with a metalloprotease inhibitor, on its own or in combination with other inhibitors, abolishes ATF6-P formation. The formation of ATF6-P will be followed by radiolabelling newly synthesised ATF6α. Initial accumulation of radiolabelled ATF6-P followed by decreased levels during the chase period will indicate inhibitors that block Protease Q activity. The inhibitor(s) that do not affect Protease Q should produce similar levels to untreated ATF6WT cells throughout the pulse and chase.

The lack of selectivity of broad-spectrum class inhibitors warrants a more surgical approach utilising more specific inhibitors. For example, the rhomboids are a relatively uncharacterised family of serine proteases that utilises a different catalytic mechanism and may not be affected by certain serine protease inhibitors. In fact, drosophila Rhomboid-1 was shown to be sensitive to 3,4-dichloroisocoumarin (DCI) and tosyl phenylalanine chloromethyl ketone (TPCK) (Urban, Lee et al. 2001) Rhomboids are conserved in prokaryotes and eukaryotes and are involved in diverse functions including cell signalling, regulated intramembrane proteolysis and protein degradation (Bergbold and Lemberg 2013). Additionally, members have been found in the secretory pathway and rhomboids can cleave without prior trimming as required by S2P (Lemberg, Menendez et al. 2005). This evidence suggests that they could be

involved in non-canonical processing of ATF6α. The use of inhibitors that affect rhomboids will allow the determination of whether Protease Q is a member of this family. A similar approach can be applied generally to other families suspected to contain Protease Q.

5.9 Treatment of expected results

These methods seek to identify Protease Q through combined systematic exclusion of other proteases based on several factors: size, location, cleavage site recognition, substrate oligomeric status and sensitivity to inhibitors. Due to limited knowledge about ATF6-P formation, confirming its location is an important starting point because it permits the contextual interpretation of suspect proteases derived from computational analyses and the exclusion of proteases that do not spatially overlap with ATF6-P. *In silico* analysis of ATF6α identified 19 proteases, from four sub-cellular locations, that can [theoretically] cleave the lumenal domain to produce ATF6-P. Stringent exclusion based on location leaves Furin as the only likely candidate because it resides in the Golgi. However, several other candidates traverse the secretory pathway and can be given some consideration bearing in mind that the results are theoretical. There are several options whereby the necessary experimental verification of these results can be obtained.

Firstly, by comparing the sequence of the cleaved ATF6-P terminus, determined by mass spectrometry, to the cleavage/recognition sequences of candidate proteases. Secondly, protease inhibitors can be engaged to experimentally verify the involvement of the identified potential proteases and if this produces positive results, proteases can be overexpressed in cells expressing ATF6α to further confirm the results. Overexpression of candidate proteases will also address the question of whether the effects observed with the inhibitors are a result of specific cleavage or due to pleiotropic effects caused by the inhibitor. Since it is possible that inhibitors may not completely abolish ATF6-P formation, their effect can be quantified based on the ratio-metric quantification of ATF6-P developed to verify the location of cleavage. This can also be achieved by quantification using a pulse-chase experiment.

Computational identification of candidate proteases, though useful, can be limited by the coverage of the data contained in the database utilised. The MEROPS database is extensive but must be continually updated as research into proteases continues. As such, recently discovered proteases and catalytic mechanisms are not included. The conserved catalytic activities of the different classes of proteases presents an opportunity to apply open screening of proteases using class-specific inhibitors. In addition to reducing the possibility space of candidates, this method can potentially target members with similar catalytic mechanisms that have not been included in the database thus, complementing computational analysis. Importantly, it can be progressively adapted to target narrow selections of proteases; however, this is limited by selectivity of inhibitors for their targets. The preference of Protease Q for a specific oligomeric form of ATF6α will be important in different stages of this project. In the initial stages, the preferred oligomeric status of the substrate can be leveraged to maximise the production of ATF6-P for subsequent experiments. In the latter stages, it may be a means of distinguishing between closely functionally and mechanistically related proteases.

Chapter 6. Discussion

6.1 Overview

The results presented in this thesis provide insight into mechanisms involved in the early stages of activation of the UPR sensor ATF6α. We sought to investigate the role of redox modulation of ATF6α during activation and interrogated the function of the small PDI-like protein, ERp18, in the process. ATF6α is known to be repressed by interaction with a complex containing BiP (Shen, Snapp et al. 2005). BiP release and a shift in the redox state of the lumenal cysteines prelude ATF6α trafficking to, and subsequent cleavage in, the Golgi leading to activation (Shen, Chen et al. 2002, Sato, Nadanaka et al. 2011).

We showed that, during ER stress, the principal form of ATF6α changes from the disulfide bonded monomer to 467D, a dimer stabilised by a C467-C467 disulfide. This change was observed during non-reductive stress induced by calcium depletion and reductive stress induced with DTT indicating the mechanism is not stressor dependent (Chapter 3). Given that intramolecular disulfide reduction is a prerequisite to dimerisation, this result provides evidence for additional regulatory modifications, in addition to reduction, that are necessary for ATF6α trafficking and subsequent activation while maintaining the previously described importance of reduction (Nadanaka, Okada et al. 2007). We also showed that 467D trafficked to the Golgi and was cleaved by S1P to yield a dimeric lumenal domain. Trafficking of ATF6α dimer is novel and is suggestive of specialised roles for the monomer, in retention, and 467D in trafficking.

The activation of ATF6α is impaired in the absence of ERp18 suggesting dysregulated trafficking and/or recognition which results in aberrant proteolytic processing (Oka, van Lith et al. 2019). Our experiments with ERp18 showed that its reductase activity antagonised the monomer to 467D redox shift in the presence of ER stress. Therefore, ERp18 was shown to be directly involved in regulating ATF6α exit from the ER. We attempted to identify residues within ERp18 that contributed to substrate binding but were unsuccessful. On the premise that investigating ATF6α dysregulation may provide further insight into regulatory mechanisms, we presented a proposal of experiments which can be used to discover the identity, localisation and function of the protease involved in the formation of ATF6-P in cells lacking ERp18.

6.2 Mechanism of ATF6α activation

6.2.1 Roles for ATF6α redox forms

Larger amounts of the ATF6α monomer are present in the resting cell compared to the dimers 467D and 618D. During ER stress, reducing amounts of monomer coupled with increases in 467D provide evidence that the monomer is actively retained in the ER and thus might be the major sub-population that is stably engaged by a regulatory complex (Shen, Chen et al. 2002). Additionally, in line with previous findings (Oka, Pierre et al. 2022), our data indicated that 467D functions as the preferred trafficking-competent form of ATF6α. This is supported by the identification of 467D with observed hyperglycosylation, a modification carried out by Golgi-localised enzymes, when intramembrane proteolysis is inhibited, and identification of lumenal domain dimer, produced from S1P cleavage (Chapter 3). Our data did not identify a role for dimer 618D and there is no significant change in the relative amount of 618D with the onset of ER stress.

ATF6α monomer and 467D likely exist in a state of dynamic equilibrium. In the absence of ER stress, the equilibrium shifts toward the monomer and ATF6α is retained in the ER. ER stress causes the equilibrium to shift toward the dimer by challenging the stability of the regulatory complex which maintains ATF6α in an inactive state. Complex dissociation leads to the release of monomers permitting the subsequent dimerisation to form 467D (Figure 6-1). Thus, ER stress functions as a switch that modulates the balance between retention- and export-competent forms of ATF6α.

6.2.2 Stress detection and trafficking

6.2.2.1 ATF6α regulatory complex

Stress detection remains an important feature of UPR transducer response. In the case of IRE1α and PERK, activation is initiated by release from BiP NBD when their lumenal domains and BiP SBD detect stress by direct interaction with unfolded proteins (Kopp, Larburu et al. 2019). ATF6α is repressed by stable interactions between its lumenal domain and BiP SBD as part of a regulatory

complex stabilised by yet unidentified factors. These accessory factors made the complex resistant to ATP induced dissociation which suggested the possible

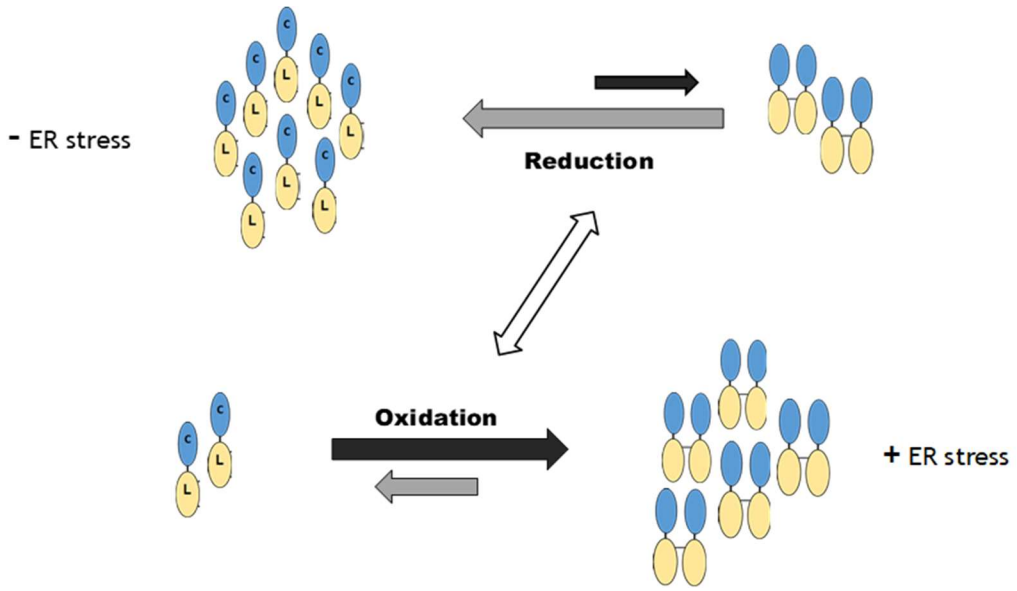

Figure 6-1 Dynamic Equilibrium between ATF6α monomer and 467D.
Equilibrium between the monomer and 467D is modulated by the ER stress. In the absence of ER stress, the monomer is the prominent species. In the presence of ER stress 467D accumulates and eventually exits the ER.

involvement of a nucleotide exchange inhibitor (NEI) (Shen, Snapp et al. 2005). We hypothesised that the NEI, MANF, which has been shown to stabilise BiP-substrate complexes by inhibiting nucleotide exchange, is UPR-upregulated and protects cells against ER stress, might be involved (Apostolou, Shen et al. 2008, Yan, Rato et al. 2019, Arrieta, Blackwood et al. 2020). We therefore investigated whether MANF interacts with BiP as part of the ATF6α regulatory complex. Our results confirmed the interaction of MANF with BiP, in line with previous reports (Glembotski, Thuerauf et al. 2012, Yan, Rato et al. 2019). The results also demonstrated interaction between MANF and the lumenal domain of ATF6 (ATF6LD) *in vivo* indicating it might participate in regulation (Chapter 4). However, time constraints did not allow the procedural and technical optimisations necessary to fully interrogate interactions between MANF and full length ATF6α. Nonetheless, a lysis protocol was developed to be utilised for future experiments some of which are proposed in section 6.4.2.1.

UPR stress detection is dependent on the detection of unfolded proteins. BiP senses and responds, through conformational changes, to unfolded proteins as a chaperone and UPR repressor (Marcinowski, Rosam et al. 2013, Carrara, Prischi et al. 2015). Therefore, it may be able to mediate stress detection of the ATF6α regulatory complex. However, being bound to ATF6LD, BiP SBD would be occupied and would not be available to directly interact with unfolded proteins. Thus, it is reasonable to postulate that stress detection might be carried out by a cofactor of BiP or at an alternative domain. MANF has been shown to display chaperone activity based on its conserved cysteines and thus can detect unfolded proteins (Arrieta, Blackwood et al. 2020). If it is involved in the ATF6α regulatory complex, it may also participate in binding unfolded proteins. It could, in response to the accumulation of misfolded proteins, disengage BiP to bind unfolded proteins which would permit nucleotide exchange and the release of ATF6α.

Considering that BiP dissociation is active rather than passive, the regulatory complex is likely to include factors that promote nucleotide exchange and not rely solely on NEI disengagement (Shen, Snapp et al. 2005). Therefore, an alternative mechanism might involve another BiP cofactor or cochaperone as a stress detector during and after NEI disengagement. The J proteins are likely candidates since they have been shown to bind to, and mediate signals between, BiP NBD and SBD, a function which is reliant on their ability to detect unfolded proteins (Kityk, Kopp et al. 2018).

The exact mechanism by which the complex is destabilised is still an open question. While modulation of the redox status of the cysteines is implicated (Nadanaka, Yoshida et al. 2006), such a change is responsive, and the mechanism and events that occur prior to this remains unclear. In addition to sensing unfolded proteins, stress detection may involve and/or initiate molecular rearrangement which provides the access to C467 required for dimerisation. Interestingly, in the oxidised monomer, this cysteine overlaps with the more prominent lumenal BiP binding site which has been shown to be necessary for stress detection (Shen, Snapp et al. 2005). Thus, reduction of the intramolecular disulfide (producing the reduced monomer) likely predisposes BiP release (Shen, Chen et al. 2002, Nadanaka, Yoshida et al. 2006).

When the UPR is induced by reductive ER stress, 618D is quickly reduced. This evidence demonstrated that C618 is more susceptible to reduction by DTT than C467 suggesting that it might be more exposed (Nadanaka, Okada et al. 2007). In addition, the fact that C467 is likely hidden through association with BiP, suggests that C618 is more likely to be the target of the initial nucleophilic attack during disulfide reduction. In the enzyme catalysed reaction, the nucleophilic attack on one of the bonded sulfur atoms by a free $-S^-$ group, leads to the formation of a transient mixed disulfide intermediate in which the substrate is bound to the reductase. Mutating one of the active site cysteines to alanine produces a CXXA substrate trapping mutant that can stabilise the intermediate in order to identify the enzyme and substrate. ER reductases ERp18 and PDIR are both capable of reducing ATF6α, however, experiments using the substrate trapping mutant of each enzyme have shown that mixed disulfide formation is biased toward C467, in the case of ERp18, and C618, in the case of PDIR (Oka, van Lith et al. 2019). Thus, PDIR is likely the reductase responsible for the reduction of ATF6α intramolecular disulfide through nucleophilic attack on C618. Indeed, the importance of PDIR reduction in ATF6α release, and trafficking, has been previously demonstrated (Higa, Taouji et al. 2014).

PDIR bias for C618 also supposes its ability to reduce 618D, the dimer stabilised by a C618-C618 intermolecular disulfide. Experiments with ATF6 single cysteine mutants demonstrate trafficking and cleavage in the absence of 467D albeit to a lesser extent as compared to when 467D is present (Chapter 3). The absence of Golgi-localised modification of 618D and observance of monomeric ATF6LD are indicative of cleaved monomer. While our data do not describe a role for 618D, its persistence during non-reductive ER stress, achieved through Ca^{2+} depletion, might suggest that it acts as a reserve pool of ATF6α that may be activated during prolonged ER stress.

6.2.2.2 Trafficking of ATF6α

Intramolecular disulfide reduction is followed by formation of the trafficking competent 467D through the formation of a C467-C467 disulfide. In the absence of stress, similar amounts of 467D and 618D are often seen which might suggest equivalent rates of formation, assuming dynamic exchange among the three

forms of ATF6α. In stressed cells, the formation of 467D increases causing it to accumulate (CH. 3 fig. 1). This is reasonable given that dimer formation is facilitated by an intermediary non-covalent association between monomers through an arrangement of monomers which is thought to sterically favour the formation of 467D (Koba, Jin et al. 2020). Thus, the accumulation of 467D could be due to more efficient formation of the C467-C467 disulfide coupled with stress dependent up-regulation of the oxidase catalysing this reaction. Identification of the oxidase involved in dimer formation would help to better understand this transition.

Trafficking of 467D raises the question of the monomer and how it traffics. Previous studies have identified the monomer in post ER compartments and trafficking vesicles (Nadanaka, Okada et al. 2007, Schindler and Schekman 2009). It might be worth considering the possibility of the packaging of non-covalently linked dimers into COPII vesicles for trafficking. The absence of the stabilising C467-C467 disulfide would allow for spontaneous dissociation which might explain the presence of the monomer.

6.2.3 The role of ERp18 in ATF6α regulation

ERp18 was previously implicated in the regulation of ATF6α trafficking. Since it was a reductase, it was identified as potential candidate for producing the reduced monomer which, at the time, was shown to be the trafficked species (Nadanaka, Okada et al. 2007, Koba, Jin et al. 2020). However, this model would not account for increased trafficking in the absence of ERp18 since it meant that a substitute reductase was more efficient, which is unlikely. It also would have meant that the substitute would be active when ATF6α expression exceeded the capacity of endogenous ERp18 since overexpression of ATF6α also led to trafficking in unstressed cells (Oka, van Lith et al. 2019).

In Chapter 4 we interrogated the role of ERp18 in ATF6α regulation by overexpressing the *wild type* (ERp18WT), a catalytically inactive mutant (ERp18CS) and two potential binding mutants (ERp18S136D & Y137T) in cells overexpressing ATF6α. The results demonstrated the involvement of ERp18 in reducing the disulfide present in 467D: overexpression of catalytically active ERp18 decreased the amount of 467D identified during ER stress. By

antagonising the redox shift, ERp18 regulated trafficking of ATF6α during ER stress. This model of ATF6α regulation adequately addresses the unanswered questions in the previous model. In the absence of ERp18 (or the catalytically inactive mutant), formation of the trafficking competent dimer of ATF6α (467D) is unhindered and exits the ER. Similarly, when ATF6α expression exceeds the catalytic capacity of endogenous levels of ERp18, dimers formed are trafficked.

This model also addresses the lack of trafficking of ATF6α in the absence of stress as dimers formed are immediately reduced to the monomer for retention. However, this raises the question of BiP regulation of ATF6α which should prevent dimer formation. The persistence of small amounts of 467D in unstressed cells could suggest that BiP transiently interacts with a small pool of ATF6α that can dimerise when BiP cycles off (Gething 1999). If ERp18 is absent, this pool is packaged and trafficked to the Golgi unhindered. However, ATF6-P formed by non-canonical proteolytic processing, persists longer than ATF6-N. Sustained trafficking of such a pool, in the absence of ERp18, coupled with inefficient degradation might explain the persistence of ATF6-P as compared to ATF6-N (Oka, van Lith et al. 2019). The presence of ER stress, through BiP release, increases the pool of ATF6α available for dimerisation and subsequent trafficking.

It is also unclear how some 467D escape ERp18 reduction. The trafficking of ATF6α when it is overexpressed in cells with endogenous ERp18 might suggest a simple mechanism driven by the substrate exceeding enzyme catalytic capacity. This is supported, in part, by the recent findings that overcrowding at ER exit sites drives cargo sorting and trafficking (Gomez-Navarro, Melero et al. 2020). However, it is challenged by the fact that trafficking can occur in the absence of stress. Furthermore, aberrant processing enabled by escape of S1P cleavage implicates conformational specificity (Oka, van Lith et al. 2019). Given that 467D should be trafficked, aberrant cleavage might suggest the existence of another step, apart from dimerisation, that might regulate recognition of ATF6α. Considering that aberrant cleavage occurs in the absence of ER stress and limited availability of ERp18 might suggest a stress-dependent mechanism which may or may not include a role for ERp18 reduction of 467D. Several groups have reported changes of the redox environment of the ER during stress and that proteins, such as Ero1, are redox responsive (Hwang, Sinskey et al. 1992, Baker,

Chakravarthi et al. 2008, Avezov, Cross et al. 2013, Bulleid and van Lith 2014). Thus, it is possible that conformational changes that determine specificity might be triggered by redox changes during stress. Alternatively, S1P bypass could occur due to mistargeting of trafficking vesicles. Traffic from the ER can be targeted to different parts of the Golgi. S1P has been shown to reside in the *cis*-Golgi (Espenshade, Cheng et al. 1999, Chen, Zhang et al. 2021). Recognition of cargo is important for correct targeting. Therefore, faulty recognition of ATF6α at the stage of trafficking could target ATF6α to the medial- or trans-Golgi which would bypass S1P cleavage. However, the mechanistic details would need to be experimentally determined.

6.3 Model of ATF6α activation

Our findings present important mechanistic details about how the activation of ATF6α is regulated up to and including the point of ER exit. Based on these findings, the following model of ATF6α regulation is proposed:

In the unstressed cell, ATF6α monomers are retained primarily by stable interaction with BiP. Monomers, that transiently associate with BiP, may form trafficking competent 467D but these are quickly reduced by ERp18 and recaptured by BiP. It is possible that dimerisation hides BiP binding sites, allowing the dimers to escape capture while monomerisation re-exposes BiP binding sequences enabling retention. In the presence of ER stress, reduction of the intramolecular disulfide by PDIR causes release of ATF6α monomers that stably associate with BiP. This causes a significant increase in the amount of disulfide stabilised 467D formed through the transient association of monomers. Therefore, 467D in excess of the catalytic activity of ERp18 is packaged into COPII vesicles and transported to the Golgi for cleavage (Figure 6-2).

6.4 Conclusion and future work

6.4.1 Conclusions

The importance of changes in the redox and oligomeric status of ATF6α in determining whether it is retained in the ER or trafficked to the Golgi for activation was demonstrated. ER stress regulates the equilibrium between the oxidised monomer retained by BiP and the 467D which is trafficked.

Dimerisation has previously been shown to be important in the activation of PERK and Ire1α (Kopp, Larburu et al. 2019). Reduction of the intramolecular disulfide by PDIR promotes trafficking while reduction of the C467-C467 disulfide by ERp18 promotes retention. Hence, reduction (and the reduced monomer) stands at the crossroad between the retention-competent oxidised monomer, and the trafficking-competent 467D. Redox changes elicited by ER stress may provoke conformational changes within the lumenal domain that favour the release of BiP and association of monomers and regulate the activity of the oxidase that creates the 467D disulfide. These conformational changes might also contribute to ATF6α recognition by S1P. Together, these changes represent auxiliary regulatory mechanisms that reconcile the reported insufficiency of stress-dependent reduction to cause activation.

Identifying the redox switch as a novel and regulatory mechanism is an important but small step toward elucidating how ATF6α functions. In the next section we propose some experiments that would serve to answer some of the outstanding questions.

6.4.2 Future work

6.4.2.1 ATF6α regulatory complex

The observed interactions between MANF/BiP and MANF/ATF6LD suggests the involvement of MANF in ATF6 regulation. Time constraints meant that we were not able to interrogate the interaction with full length ATF6α, however, we have optimised the lysis step of the immunoprecipitation protocol to facilitate this. Additionally, a cell line overexpressing MANF in the absence of endogenous ATF6α was established. Thus, the question of the involvement of a BiP-MANF complex which regulates ATF6α can be addressed. MANF/ATF6KO cells can be transfected with ATF6wt DNA and co-immunoprecipitation can be used to determine the interaction. The stability of the interaction in the presence of ER stress can confirm its involvement in regulation. The absence of endogenous ATF6α would facilitate the determination of differences in regulation that may exist among the redox forms of ATF6α by transfection with single mutants.

6.4.2.2 Trafficking of ATF6α

During ATF6α activation, the transition from monomer to 467D is an important prelude to ER exit that is regulated by ERp18 reduction (Chapter 3). However, some mechanistic details are yet to be determined including the identity of the oxidase catalysing the M → 467D shift and how its activity regulated and tuned and balanced with ERp18 reductase activity. Several trafficking deficient ATF6α mutants associated with achromatopsia have been identified (Chiang, Chan et al. 2017). Comparative studies with these mutants can help to elucidate mechanisms involved in regulation and trafficking.

6.4.2.3 Verification of ERp18 binding peptide

The fact that ERp18Y137T mutant affects *in vitro* reductase activity suggests that it is involved in substrate binding and may contribute, at least in part, to ATF6α interaction. Several other hydrophobic residues within the same region, Y139, F140 Y141 & V142, have been identified which define a hydrophobic stretch of amino acids that may be involved in binding. Of these Y141 has been proposed to be involved in the reaction mechanism (Rowe, Ruddock et al. 2009) while the side chains of F140, and V142 are oriented along a similar plane to Y137 pointing toward the active site. Sequential mutations of these residues can be carried out to determine their effect on the ATF6 interaction and phenotype. Furthermore, biophysical techniques such as isothermal titration calorimetry or biolayer interferometry can be used to quantify changes in binding affinity among mutants. In addition, techniques to determine the folding status of the protein are required to determine structural integrity of the mutants.

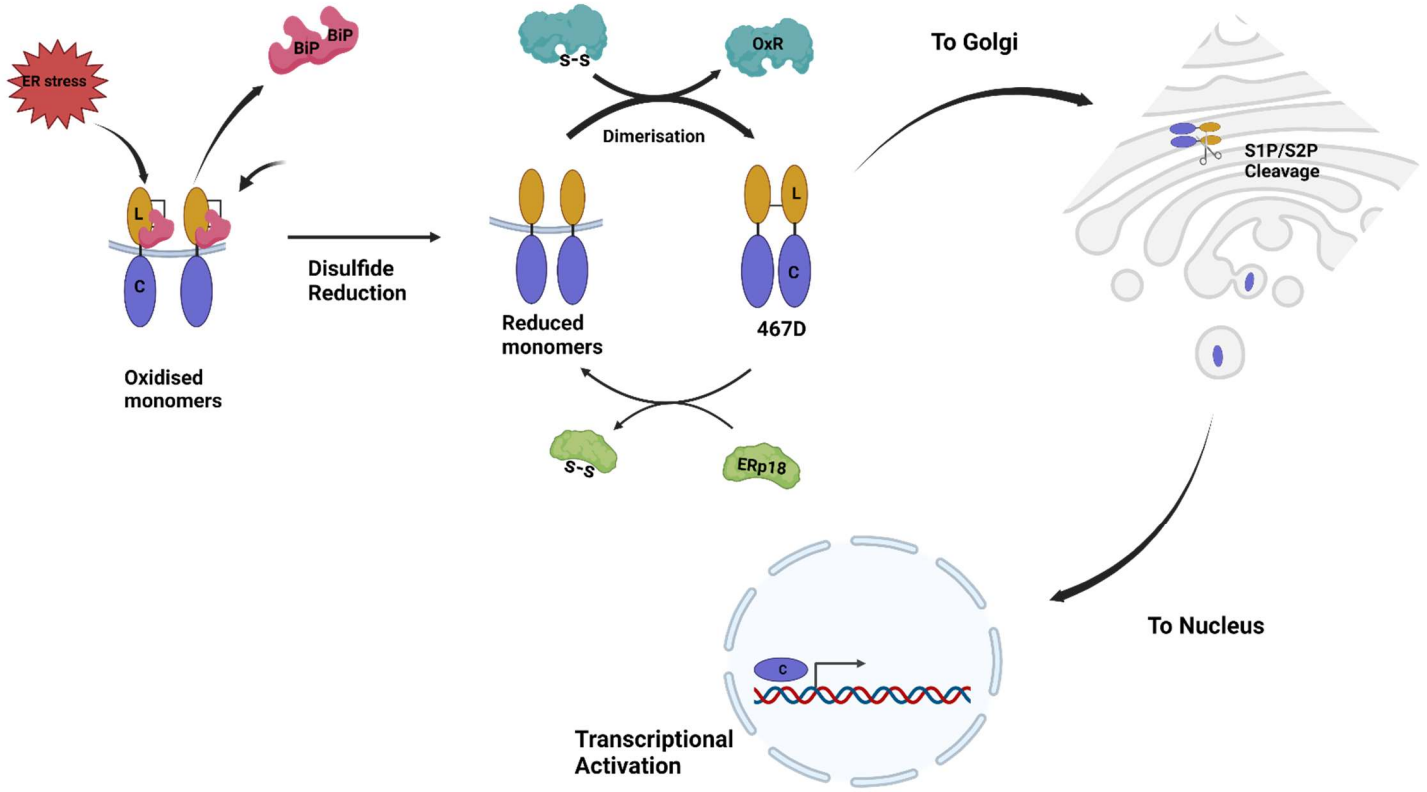

Figure 6-2 Model of ERp18-dependent regulation of ATF6
Oxidised monomer is retained in the ER by association with BiP. ER stress causes BiP release and reduction of the intramolecular disulfide by PDIR. Reduced monomers are linked by a disulfide forming 467D. Some dimers are engaged by ERp18 and reduced. Others escape ERp18 activity and are trafficked to the Golgi for proteolytic processing The released transcription factor translocates to the Nucleus to regulate transcription (Created with BioRender.com).

Chapter 7. Appendices

Table 7-1 Proteases predicted to cleave within the lumenal domain of ATF6α by PROSPER and iPROT-sub based on MEROPS database.

Protease	*MEROPS ID*	*Server*	*No. of lumenal cleavage sites*	*Position*	*Known function*	*Sub-cellular location*
cathepsin G	*S01.133*	*PROSPER*	*12*		*Cleaves complement C3*	*Lysosomes. CSM*
Elastase-2	*S01.131*	*Both*	*13(1*)*	*534*	*Modifies the function of white blood cells*	*Cytoplasmic vesicle*
Furin	*S08.071*	*iProt*	*1*	*550*	*Mediates TGFB1 activation*	*Trans-Golgi, CSM*
Granzyme A	*S01.135*	*iProt*	*1*	*449*	*Activates caspase-independent cell death*	*Cytoplasmic granule*
Granzyme B	*S01.010*	*iProt*	*3*	*428, 448, 564*	*This enzyme is necessary for target cell lysis in cell-mediated immune responses.*	*Cytoplasmic granules of T-lymphocytes*
Kallikrein-related Peptidase 4	*S01.251*	*iProt*	*1*	*561*	*Has a major role in enamel formation*	*Secreted*
Kallikrein-related Peptidase 5	*S01.017*	*iProt*	*1*	*624*	*May be involved in desquamation.*	*secreted*
Calpain-1	*C02.001*	*Both*	*1*	*531*	*Calcium-regulated non-lysosomal proteolysis of substrates involved in*	*Cytoplasm & CSM*

					cytoskeletal remodelling and signal transduction.	
Calpain-2	*C02.002*	*iProt*	*1*	*662*	*Calcium-regulated non-lysosomal proteolysis of substrates involved in cytoskeletal remodelling and signal transduction.* *Involved in the activation cascade of caspases responsible for apoptosis execution*	*Cytoplasm & CSM* *cytoplasm*
Caspase-3	*C14.003*	*iProt*	*1*	*431*		
Protease	***MEROPS ID***	***Server***	***No. of lumenal cleavage sites***	***Position***	***Known function***	***Sub-cellular location***
Caspase-6	*C14.005*	*iProt*	*8*		*Involved in the activation cascade of caspases responsible for apoptosis execution* *Thiol protease involved in osteoclastic bone resorption.*	*cytoplasm* *secreted*
Caspase-7	*C14.004*	*iProt*	*1*	*431*		
Caspase-8	*C14.009*	*iProt*	*1*	*431*		
cathepsin K	*C01.036*	*PROSPER*	*8*			
Cathepsin L	*C01.032*	*iProt*	*1*	*461*	*Possibly involved in degradation of proteins in lysosomes*	*lysosomes*
Cathepsin D	*A01.009*	*iProt*	*1*	*542*	*Acid protease active in intracellular protein breakdown.*	*lysosomes*

matrix metallopeptidase-2	*M10.003*	*PROSPER*	*1*	*403*	*involved in diverse functions such as remodelling of the vasculature*	*Extracellular matrix*
matrix metallopeptidase-3	*M10.005*	*PROSPER*	*2*	*598, 668*	*degrades fibronectin, laminin, gelatins, collagens and cartilage proteoglycans.*	*Extracellular matrix*
matrix metallopeptidase-9	*M10.004*	*PROSPER*	*12*		*May play an essential role in local proteolysis of the extracellular matrix and in leukocyte migration.*	*Extracellular matrix*

(1) - a single cleavage site was predicted by iPROT-sub while PROSPER predicted 12.* *Table 1 cont'd*

Table 7-2 Protease inhibitors.

	Inhibits	Reversibility
AEBSF	serine proteases	irreversible
Aprotinin	serine proteases	reversible
Batimastat	metalloproteases	reversible
DCI	serine proteases	
E-64	cysteine proteases	irreversible
EDTA/EGTA	metalloproteases	reversible
GM 6001	matrix metalloproteinases	reversible
Leupeptin	serine/cysteine proteases	reversible
Pepstatin	aspartic proteases	reversible
PMSF	serine proteases	irreversible

List of References

Acosta-Alvear, D., G. E. Karagöz, F. Fröhlich, H. Li, T. C. Walther and P. Walter (2018). "The unfolded protein response and endoplasmic reticulum protein targeting machineries converge on the stress sensor IRE1." Elife **7**.
Acosta-Alvear, D., Y. Zhou, A. Blais, M. Tsikitis, N. H. Lents, C. Arias, C. J. Lennon, Y. Kluger and B. D. Dynlacht (2007). "XBP1 controls diverse cell type- and condition-specific transcriptional regulatory networks." Mol Cell **27**(1): 53-66.
Adachi, Y., K. Yamamoto, T. Okada, H. Yoshida, A. Harada and K. Mori (2008). "ATF6 is a transcription factor specializing in the regulation of quality control proteins in the endoplasmic reticulum." Cell Struct Funct **33**(1): 75-89.
Alanen, H. I., R. A. Williamson, M. J. Howard, A. K. Lappi, H. P. Jantti, S. M. Rautio, S. Kellokumpu and L. W. Ruddock (2003). "Functional characterization of ERp18, a new endoplasmic reticulum-located thioredoxin superfamily member." J Biol Chem **278**(31): 28912-28920.
Almanza, A., A. Carlesso, C. Chintha, S. Creedican, D. Doultsinos, B. Leuzzi, A. Luís, N. McCarthy, L. Montibeller, S. More, A. Papaioannou, F. Püschel, M. L. Sassano, J. Skoko, P. Agostinis, J. de Belleroche, L. A. Eriksson, S. Fulda, A. M. Gorman, S. Healy, A. Kozlov, C. Muñoz-Pinedo, M. Rehm, E. Chevet and A. Samali (2019). "Endoplasmic reticulum stress signalling - from basic mechanisms to clinical applications." Febs j **286**(2): 241-278.
Anfinsen, C. B. (1973). "Principles that Govern the Folding of Protein Chains." Science **181**(4096): 223.
Apostolou, A., Y. Shen, Y. Liang, J. Luo and S. Fang (2008). "Armet, a UPR-upregulated protein, inhibits cell proliferation and ER stress-induced cell death." Experimental Cell Research **314**(13): 2454-2467.
Appenzeller-Herzog, C., J. Riemer, B. Christensen, E. S. Sørensen and L. Ellgaard (2008). "A novel disulphide switch mechanism in Ero1α balances ER oxidation in human cells." The EMBO Journal **27**(22): 2977-2987.
Appenzeller-Herzog, C., J. Riemer, E. Zito, K.-T. Chin, D. Ron, M. Spiess and L. Ellgaard (2010). "Disulphide production by Ero1α–PDI relay is rapid and effectively regulated." The EMBO Journal **29**(19): 3318-3329.
Araki, K., S.-i. Iemura, Y. Kamiya, D. Ron, K. Kato, T. Natsume and K. Nagata (2013). "Ero1-α and PDIs constitute a hierarchical electron transfer network of endoplasmic reticulum oxidoreductases." Journal of Cell Biology **202**(6): 861-874.
Arrieta, A., E. A. Blackwood, W. T. Stauffer, M. Santo Domingo, A. S. Bilal, D. J. Thuerauf, A. N. Pentoney, C. Aivati, A. V. Sarakki, S. Doroudgar and C. C. Glembotski (2020). "Mesencephalic astrocyte-derived neurotrophic factor is an ER-resident chaperone that protects against reductive stress in the heart." J Biol Chem **295**(22): 7566-7583.
Atkins, C., Q. Liu, E. Minthorn, S. Y. Zhang, D. J. Figueroa, K. Moss, T. B. Stanley, B. Sanders, A. Goetz, N. Gaul, A. E. Choudhry, H. Alsaid, B. M. Jucker, J. M. Axten and R. Kumar (2013). "Characterization of a novel PERK kinase inhibitor with antitumor and antiangiogenic activity." Cancer Res **73**(6): 1993-2002.
Avezov, E., B. C. S. Cross, G. S. Kaminski Schierle, M. Winters, H. P. Harding, E. P. Melo, C. F. Kaminski and D. Ron (2013). "Lifetime imaging of a fluorescent protein sensor reveals surprising stability of ER thiol redox." Journal of Cell Biology **201**(2): 337-349.

Baker, K. M., S. Chakravarthi, K. P. Langton, A. M. Sheppard, H. Lu and N. J. Bulleid (2008). "Low reduction potential of Ero1α regulatory disulphides ensures tight control of substrate oxidation." The EMBO Journal **27**(22): 2988-2997.
Bannykh, S. I., T. Rowe and W. E. Balch (1996). "The organization of endoplasmic reticulum export complexes." J Cell Biol **135**(1): 19-35.
Barlowe, C. (2003). "Signals for COPII-dependent export from the ER: what's the ticket out?" Trends in Cell Biology **13**(6): 295-300.
Behnke, J., M. J. Feige and L. M. Hendershot (2015). "BiP and Its Nucleotide Exchange Factors Grp170 and Sil1: Mechanisms of Action and Biological Functions." Journal of Molecular Biology **427**(7): 1589-1608.
Bellucci, A., L. Navarria, M. Zaltieri, E. Falarti, S. Bodei, S. Sigala, L. Battistin, M. Spillantini, C. Missale and P. Spano (2011). "Induction of the unfolded protein response by α-synuclein in experimental models of Parkinson's disease." J Neurochem **116**(4): 588-605.
Benedetti, R., M. A. Romeo, A. Arena, M. S. Gilardini Montani, L. Di Renzo, G. D'Orazi and M. Cirone (2022). "ATF6 prevents DNA damage and cell death in colon cancer cells undergoing ER stress." Cell Death Discov **8**(1): 295.
Bergbold, N. and M. K. Lemberg (2013). "Emerging role of rhomboid family proteins in mammalian biology and disease." Biochim Biophys Acta **1828**(12): 2840-2848.
Bertelsen, E. B., L. Chang, J. E. Gestwicki and E. R. Zuiderweg (2009). "Solution conformation of wild-type E. coli Hsp70 (DnaK) chaperone complexed with ADP and substrate." Proc Natl Acad Sci U S A **106**(21): 8471-8476.
Bertolotti, A., Y. Zhang, L. M. Hendershot, H. P. Harding and D. Ron (2000). "Dynamic interaction of BiP and ER stress transducers in the unfolded-protein response." Nat Cell Biol **2**(6): 326-332.
Betzer, C., L. B. Lassen, A. Olsen, R. H. Kofoed, L. Reimer, E. Gregersen, J. Zheng, T. Calì, W. P. Gai, T. Chen, A. Moeller, M. Brini, Y. Fu, G. Halliday, T. Brudek, S. Aznar, B. Pakkenberg, J. P. Andersen and P. H. Jensen (2018). "Alpha-synuclein aggregates activate calcium pump SERCA leading to calcium dysregulation." EMBO Rep **19**(5).
Brehme, M. and C. Voisine (2016). "Model systems of protein-misfolding diseases reveal chaperone modifiers of proteotoxicity." Dis Model Mech **9**(8): 823-838.
Bulleid, N. J. and L. Ellgaard (2011). "Multiple ways to make disulfides." Trends in Biochemical Sciences **36**(9): 485-492.
Bulleid, Neil J. and M. van Lith (2014). "Redox regulation in the endoplasmic reticulum." Biochemical Society Transactions **42**(4): 905-908.
Burré, J., M. Sharma and T. C. Südhof (2018). "Cell Biology and Pathophysiology of α-Synuclein." Cold Spring Harb Perspect Med **8**(3).
Cao, S. S. and R. J. Kaufman (2013). "Targeting endoplasmic reticulum stress in metabolic disease." Expert Opinion on Therapeutic Targets **17**(4): 437-448.
Cao, X., S. Lilla, Z. Cao, M. A. Pringle, O. B. V. Oka, P. J. Robinson, T. Szmaja, M. van Lith, S. Zanivan and N. J. Bulleid (2020). "The mammalian cytosolic thioredoxin reductase pathway acts via a membrane protein to reduce ER-localised proteins." J Cell Sci **133**(8).
Carlsson, L. and E. Lazarides (1983). "ADP-ribosylation of the Mr 83,000 stress-inducible and glucose-regulated protein in avian and mammalian cells: modulation by heat shock and glucose starvation." Proceedings of the National Academy of Sciences **80**(15): 4664-4668.
Carrara, M., F. Prischi, P. R. Nowak and M. M. Ali (2015). "Crystal structures reveal transient PERK luminal domain tetramerization in endoplasmic reticulum stress signaling." The EMBO Journal **34**(11): 1589-1600.

Carrara, M., F. Prischi, P. R. Nowak, M. C. Kopp and M. M. Ali (2015). "Noncanonical binding of BiP ATPase domain to Ire1 and Perk is dissociated by unfolded protein CH1 to initiate ER stress signaling." Elife **4**.
Chambers, J. E., K. Petrova, G. Tomba, M. Vendruscolo and D. Ron (2012). "ADP ribosylation adapts an ER chaperone response to short-term fluctuations in unfolded protein load." Journal of Cell Biology **198**(3): 371-385.
Chen, S., P. Novick and S. Ferro-Novick (2013). "ER structure and function." Current Opinion in Cell Biology **25**(4): 428-433.
Chen, X. and J. R. Cubillos-Ruiz (2021). "Endoplasmic reticulum stress signals in the tumour and its microenvironment." Nat Rev Cancer **21**(2): 71-88.
Chen, X., J. Shen and R. Prywes (2002). "The luminal domain of ATF6 senses endoplasmic reticulum (ER) stress and causes translocation of ATF6 from the ER to the Golgi." J Biol Chem **277**(15): 13045-13052.
Chen, X., J. Zhang, P. Liu, Y. Wei, X. e. Wang, J. Xiao, C.-c. Wang and L. Wang (2021). "Proteolytic processing of secretory pathway kinase Fam20C by site-1 protease promotes biomineralization." Proceedings of the National Academy of Sciences **118**(32): e2100133118.
Chevet, E., C. Hetz and A. Samali (2015). "Endoplasmic Reticulum Stress–Activated Cell Reprogramming in Oncogenesis." Cancer Discovery **5**(6): 586-597.
Chiang, W. C., P. Chan, B. Wissinger, A. Vincent, A. Skorczyk-Werner, M. R. Krawczyński, R. J. Kaufman, S. H. Tsang, E. Héon, S. Kohl and J. H. Lin (2017). "Achromatopsia mutations target sequential steps of ATF6 activation." Proc Natl Acad Sci U S A **114**(2): 400-405.
Christianson, J. C. and P. Carvalho (2022). "Order through destruction: how ER-associated protein degradation contributes to organelle homeostasis." Embo j **41**(6): e109845.
Cosson, P. and F. Letourneur (1994). "Coatomer Interaction with Di-Lysine Endoplasmic Reticulum Retention Motifs." Science **263**(5153): 1629-1631.
Credle, J. J., P. A. Forcelli, M. Delannoy, A. W. Oaks, E. Permaul, D. L. Berry, V. Duka, J. Wills and A. Sidhu (2015). "α-Synuclein-mediated inhibition of ATF6 processing into COPII vesicles disrupts UPR signaling in Parkinson's disease." Neurobiol Dis **76**: 112-125.
Das, I., A. Krzyzosiak, K. Schneider, L. Wrabetz, M. D'Antonio, N. Barry, A. Sigurdardottir and A. Bertolotti (2015). "Preventing proteostasis diseases by selective inhibition of a phosphatase regulatory subunit." Science **348**(6231): 239-242.
Delépine, M., M. Nicolino, T. Barrett, M. Golamaully, G. Mark Lathrop and C. Julier (2000). "EIF2AK3, encoding translation initiation factor 2-α kinase 3, is mutated in patients with Wolcott-Rallison syndrome." Nature Genetics **25**(4): 406-409.
Doyle, K. M., D. Kennedy, A. M. Gorman, S. Gupta, S. J. M. Healy and A. Samali (2011). "Unfolded proteins and endoplasmic reticulum stress in neurodegenerative disorders." Journal of Cellular and Molecular Medicine **15**(10): 2025-2039.
Dröse, S. and K. Altendorf (1997). "Bafilomycins and concanamycins as inhibitors of V-ATPases and P-ATPases." Journal of Experimental Biology **200**(1): 1-8.
Duran-Aniotz, C., V. H. Cornejo, S. Espinoza, Á. O. Ardiles, D. B. Medinas, C. Salazar, A. Foley, I. Gajardo, P. Thielen, T. Iwawaki, W. Scheper, C. Soto, A. G. Palacios, J. J. M. Hoozemans and C. Hetz (2017). "IRE1 signaling exacerbates Alzheimer's disease pathogenesis." Acta Neuropathologica **134**(3): 489-506.
Ellgaard, L., N. McCaul, A. Chatsisvili and I. Braakman (2016). "Co- and Post-Translational Protein Folding in the ER." Traffic **17**(6): 615-638.

Ellgaard, L. and L. W. Ruddock (2005). "The human protein disulphide isomerase family: substrate interactions and functional properties." EMBO Rep **6**(1): 28-32.
Espenshade, P. J., D. Cheng, J. L. Goldstein and M. S. Brown (1999). "Autocatalytic Processing of Site-1 Protease Removes Propeptide and Permits Cleavage of Sterol Regulatory Element-binding Proteins." Journal of Biological Chemistry **274**(32): 22795-22804.
Espenshade, P. J., D. Cheng, J. L. Goldstein and M. S. Brown (1999). "Autocatalytic Processing of Site-1 Protease Removes Propeptide and Permits Cleavage of Sterol Regulatory Element-binding Proteins*." Journal of Biological Chemistry **274**(32): 22795-22804.
Fagone, P. and S. Jackowski (2009). "Membrane phospholipid synthesis and endoplasmic reticulum function." Journal of Lipid Research **50**: S311-S316.
Farhan, H. and C. Rabouille (2011). "Signalling to and from the secretory pathway." Journal of Cell Science **124**(2): 171-180.
Fath, S., J. D. Mancias, X. Bi and J. Goldberg (2007). "Structure and Organization of Coat Proteins in the COPII Cage." Cell **129**(7): 1325-1336.
Feldman, H. C., M. Tong, L. Wang, R. Meza-Acevedo, T. A. Gobillot, I. Lebedev, M. J. Gliedt, S. B. Hari, A. K. Mitra, B. J. Backes, F. R. Papa, M. A. Seeliger and D. J. Maly (2016). "Structural and Functional Analysis of the Allosteric Inhibition of IRE1α with ATP-Competitive Ligands." ACS Chem Biol **11**(8): 2195-2205.
Feng, Y.-X., D. X. Jin, E. S. Sokol, F. Reinhardt, D. H. Miller and P. B. Gupta (2017). "Cancer-specific PERK signaling drives invasion and metastasis through CREB3L1." Nature Communications **8**(1): 1079.
Ford, C., A. Parchure, J. von Blume and C. G. Burd (2021). "Cargo sorting at the trans-Golgi network at a glance." Journal of Cell Science **134**(23).
Gardner, B. M. and P. Walter (2011). "Unfolded proteins are Ire1-activating ligands that directly induce the unfolded protein response." Science **333**(6051): 1891-1894.
Gething, M.-J. (1999). "Role and regulation of the ER chaperone BiP." Seminars in Cell & Developmental Biology **10**(5): 465-472.
Ghemrawi, R. and M. Khair (2020). "Endoplasmic Reticulum Stress and Unfolded Protein Response in Neurodegenerative Diseases." Int J Mol Sci **21**(17).
Ghosh, R., K. Colon-Negron and F. R. Papa (2019). "Endoplasmic reticulum stress, degeneration of pancreatic islet β-cells, and therapeutic modulation of the unfolded protein response in diabetes." Mol Metab **27s**(Suppl): S60-s68.
Gitler, A. D., B. J. Bevis, J. Shorter, K. E. Strathearn, S. Hamamichi, L. J. Su, K. A. Caldwell, G. A. Caldwell, J. C. Rochet, J. M. McCaffery, C. Barlowe and S. Lindquist (2008). "The Parkinson's disease protein alpha-synuclein disrupts cellular Rab homeostasis." Proc Natl Acad Sci U S A **105**(1): 145-150.
Gleeson, P. A. (1998). "Targeting of proteins to the Golgi apparatus." Histochem Cell Biol **109**(5-6): 517-532.
Glembotski, C. C., D. J. Thuerauf, C. Huang, J. A. Vekich, R. A. Gottlieb and S. Doroudgar (2012). "Mesencephalic Astrocyte-derived Neurotrophic Factor Protects the Heart from Ischemic Damage and Is Selectively Secreted upon Sarco/endoplasmic Reticulum Calcium Depletion." Journal of Biological Chemistry **287**(31): 25893-25904.
Gomez-Navarro, N., A. Melero, X.-H. Li, J. Boulanger, W. Kukulski and E. A. Miller (2020). "Cargo crowding contributes to sorting stringency in COPII vesicles." Journal of Cell Biology **219**(7): e201806038.
Greenman, C., P. Stephens, R. Smith, G. L. Dalgliesh, C. Hunter, G. Bignell, H. Davies, J. Teague, A. Butler, C. Stevens, S. Edkins, S. O'Meara, I. Vastrik, E. E. Schmidt, T. Avis, S. Barthorpe, G. Bhamra, G. Buck, B. Choudhury, J. Clements,

J. Cole, E. Dicks, S. Forbes, K. Gray, K. Halliday, R. Harrison, K. Hills, J. Hinton, A. Jenkinson, D. Jones, A. Menzies, T. Mironenko, J. Perry, K. Raine, D. Richardson, R. Shepherd, A. Small, C. Tofts, J. Varian, T. Webb, S. West, S. Widaa, A. Yates, D. P. Cahill, D. N. Louis, P. Goldstraw, A. G. Nicholson, F. Brasseur, L. Looijenga, B. L. Weber, Y. E. Chiew, A. DeFazio, M. F. Greaves, A. R. Green, P. Campbell, E. Birney, D. F. Easton, G. Chenevix-Trench, M. H. Tan, S. K. Khoo, B. T. Teh, S. T. Yuen, S. Y. Leung, R. Wooster, P. A. Futreal and M. R. Stratton (2007). "Patterns of somatic mutation in human cancer genomes." Nature **446**(7132): 153-158.
Griffiths, G. and K. Simons (1986). "The trans Golgi Network: Sorting at the Exit Site of the Golgi Complex." Science **234**(4775): 438-443.
Haas, I. G. and M. Wabl (1983). "Immunoglobulin heavy chain binding protein." Nature **306**(5941): 387-389.
Hanson, S. R., E. K. Culyba, T.-L. Hsu, C.-H. Wong, J. W. Kelly and E. T. Powers (2009). "The core trisaccharide of an N-linked glycoprotein intrinsically accelerates folding and enhances stability." Proceedings of the National Academy of Sciences **106**(9): 3131-3136.
Harding, H. P., Y. Zhang and D. Ron (1999). "Protein translation and folding are coupled by an endoplasmic-reticulum-resident kinase." Nature **397**(6716): 271-274.
Hartl, F. U. (1996). "Molecular chaperones in cellular protein folding." Nature **381**(6583): 571-579.
Hay, B. A., B. Abrams, A. Y. Zumbrunn, J. J. Valentine, L. C. Warren, S. F. Petras, L. D. Shelly, A. Xia, A. H. Varghese, J. L. Hawkins, J. A. Van Camp, M. D. Robbins, K. Landschulz and H. J. Harwood, Jr. (2007). "Aminopyrrolidineamide inhibitors of site-1 protease." Bioorg Med Chem Lett **17**(16): 4411-4414.
Hayashi, T., R. Rizzuto, G. Hajnoczky and T.-P. Su (2009). "MAM: more than just a housekeeper." Trends in Cell Biology **19**(2): 81-88.
Haze, K., T. Okada, H. Yoshida, H. Yanagi, T. Yura, M. Negishi and K. Mori (2001). "Identification of the G13 (cAMP-response-element-binding protein-related protein) gene product related to activating transcription factor 6 as a transcriptional activator of the mammalian unfolded protein response." Biochem J **355**(Pt 1): 19-28.
Haze, K., H. Yoshida, H. Yanagi, T. Yura and K. Mori (1999). "Mammalian transcription factor ATF6 is synthesized as a transmembrane protein and activated by proteolysis in response to endoplasmic reticulum stress." Mol Biol Cell **10**(11): 3787-3799.
Helenius, A. and M. Aebi (2001). "Intracellular functions of N-linked glycans." Science **291**(5512): 2364-2369.
Hellman, M., U. Arumäe, L.-y. Yu, P. Lindholm, J. Peränen, M. Saarma and P. Permi (2011). "Mesencephalic Astrocyte-derived Neurotrophic Factor (MANF) Has a Unique Mechanism to Rescue Apoptotic Neurons." Journal of Biological Chemistry **286**(4): 2675-2680.
Herbach, N., B. Rathkolb, E. Kemter, L. Pichl, M. Klaften, M. H. de Angelis, P. A. Halban, E. Wolf, B. Aigner and R. Wanke (2007). "Dominant-Negative Effects of a Novel Mutated Ins2 Allele Causes Early-Onset Diabetes and Severe ß-Cell Loss in Munich Ins2C95S Mutant Mice." Diabetes **56**(5): 1268-1276.
Higa, A., S. Taouji, S. Lhomond, D. Jensen, M. E. Fernandez-Zapico, J. C. Simpson, J. M. Pasquet, R. Schekman and E. Chevet (2014). "Endoplasmic reticulum stress-activated transcription factor ATF6alpha requires the disulfide isomerase PDIA5 to modulate chemoresistance." Mol Cell Biol **34**(10): 1839-1849.

Holmer, L. and H. J. Worman (2001). "Inner nuclear membrane proteins: functions and targeting." Cell Mol Life Sci **58**(12-13): 1741-1747.
Hoozemans, J. J., E. S. van Haastert, P. Eikelenboom, R. A. de Vos, J. M. Rozemuller and W. Scheper (2007). "Activation of the unfolded protein response in Parkinson's disease." Biochem Biophys Res Commun **354**(3): 707-711.
Hudson, D. A., S. A. Gannon and C. Thorpe (2015). "Oxidative protein folding: From thiol–disulfide exchange reactions to the redox poise of the endoplasmic reticulum." Free Radical Biology and Medicine **80**: 171-182.
Hwang, C., A. J. Sinskey and H. F. Lodish (1992). "Oxidized Redox State of Glutathione in the Endoplasmic Reticulum." Science **257**(5076): 1496-1502.
Hwang, J., D. Ribbens, S. Raychaudhuri, L. Cairns, H. Gu, A. Frost, S. Urban and P. J. Espenshade (2016). "A Golgi rhomboid protease Rbd2 recruits Cdc48 to cleave yeast SREBP." The EMBO journal **35**(21): 2332-2349.
Iddon, C. R., J. Wilkinson, A. J. Bennett, J. Bennett, A. M. Salter and J. A. Higgins (2001). "A role for smooth endoplasmic reticulum membrane cholesterol ester in determining the intracellular location and regulation of sterol-regulatory-element-binding protein-2." Biochem J **358**(Pt 2): 415-422.
Imperiali, B. and S. E. O'Connor (1999). "Effect of N-linked glycosylation on glycopeptide and glycoprotein structure." Curr Opin Chem Biol **3**(6): 643-649.
Iurlaro, R. and C. Muñoz-Pinedo (2016). "Cell death induced by endoplasmic reticulum stress." Febs j **283**(14): 2640-2652.
Jean, F., K. Stella, L. Thomas, G. Liu, Y. Xiang, A. J. Reason and G. Thomas (1998). "alpha1-Antitrypsin Portland, a bioengineered serpin highly selective for furin: application as an antipathogenic agent." Proc Natl Acad Sci U S A **95**(13): 7293-7298.
Jeong, W., D. Y. Lee, S. Park and S. G. Rhee (2008). "ERp16, an endoplasmic reticulum-resident thiol-disulfide oxidoreductase: biochemical properties and role in apoptosis induced by endoplasmic reticulum stress." J Biol Chem **283**(37): 25557-25566.
Jha, B. K., I. Polyakova, P. Kessler, B. Dong, B. Dickerman, G. C. Sen and R. H. Silverman (2011). "Inhibition of RNase L and RNA-dependent Protein Kinase (PKR) by Sunitinib Impairs Antiviral Innate Immunity*." Journal of Biological Chemistry **286**(30): 26319-26326.
Kaufman, R. J. (1999). "Stress signaling from the lumen of the endoplasmic reticulum: coordination of gene transcriptional and translational controls." Genes Dev **13**(10): 1211-1233.
Kim, Y. E., M. S. Hipp, A. Bracher, M. Hayer-Hartl and F. U. Hartl (2013). "Molecular chaperone functions in protein folding and proteostasis." Annu Rev Biochem **82**: 323-355.
Kityk, R., J. Kopp and M. P. Mayer (2018). "Molecular Mechanism of J-Domain-Triggered ATP Hydrolysis by Hsp70 Chaperones." Mol Cell **69**(2): 227-237.e224.
Knarr, G., M. J. Gething, S. Modrow and J. Buchner (1995). "BiP binding sequences in antibodies." J Biol Chem **270**(46): 27589-27594.
Koba, H., S. Jin, N. Imada, T. Ishikawa, S. Ninagawa, T. Okada, T. Sakuma, T. Yamamoto and K. Mori (2020). "Reinvestigation of Disulfide-bonded Oligomeric Forms of the Unfolded Protein Response Transducer ATF6." Cell Struct Funct **45**(1): 9-21.
Kopp, M. C., N. Larburu, V. Durairaj, C. J. Adams and M. M. U. Ali (2019). "UPR proteins IRE1 and PERK switch BiP from chaperone to ER stress sensor." Nat Struct Mol Biol **26**(11): 1053-1062.

Kozutsumi, Y., M. Segal, K. Normington, M.-J. Gething and J. Sambrook (1988). "The presence of malfolded proteins in the endoplasmic reticulum signals the induction of glucose-regulated proteins." Nature **332**(6163): 462-464.
Krzyzosiak, A., A. Sigurdardottir, L. Luh, M. Carrara, I. Das, K. Schneider and A. Bertolotti (2018). "Target-Based Discovery of an Inhibitor of the Regulatory Phosphatase PPP1R15B." Cell **174**(5): 1216-1228.e1219.
Laufen, T., M. P. Mayer, C. Beisel, D. Klostermeier, A. Mogk, J. Reinstein and B. Bukau (1999). "Mechanism of regulation of hsp70 chaperones by DnaJ cochaperones." Proc Natl Acad Sci U S A **96**(10): 5452-5457.
Lee, K. P., M. Dey, D. Neculai, C. Cao, T. E. Dever and F. Sicheri (2008). "Structure of the dual enzyme Ire1 reveals the basis for catalysis and regulation in nonconventional RNA splicing." Cell **132**(1): 89-100.
Lee, M. C. S., E. A. Miller, J. Goldberg, L. Orci and R. Schekman (2004). "BI-DIRECTIONAL PROTEIN TRANSPORT BETWEEN THE ER AND GOLGI." Annual Review of Cell and Developmental Biology **20**(1): 87-123.
Lemberg, M. K., J. Menendez, A. Misik, M. Garcia, C. M. Koth and M. Freeman (2005). "Mechanism of intramembrane proteolysis investigated with purified rhomboid proteases." The EMBO Journal **24**(3): 464-472.
Lemberg, M. K. and K. Strisovsky (2021). "Maintenance of organellar protein homeostasis by ER-associated degradation and related mechanisms." Mol Cell **81**(12): 2507-2519.
Li, W. W., S. Alexandre, X. Cao and A. S. Lee (1993). "Transactivation of the grp78 promoter by Ca2+ depletion. A comparative analysis with A23187 and the endoplasmic reticulum Ca(2+)-ATPase inhibitor thapsigargin." J Biol Chem **268**(16): 12003-12009.
Liu, C. Y., M. Schröder and R. J. Kaufman (2000). "Ligand-independent Dimerization Activates the Stress Response Kinases IRE1 and PERK in the Lumen of the Endoplasmic Reticulum*." Journal of Biological Chemistry **275**(32): 24881-24885.
Lohman, J. R. and S. J. Remington (2008). "Development of a Family of Redox-Sensitive Green Fluorescent Protein Indicators for Use in Relatively Oxidizing Subcellular Environments." Biochemistry **47**(33): 8678-8688.
López-Otín, C. and J. S. Bond (2008). "Proteases: multifunctional enzymes in life and disease." The Journal of biological chemistry **283**(45): 30433-30437.
Lv, X., J. Li, C. Zhang, T. Hu, S. Li, S. He, H. Yan, Y. Tan, M. Lei, M. Wen and J. Zuo (2017). "The role of hypoxia-inducible factors in tumor angiogenesis and cell metabolism." Genes Dis **4**(1): 19-24.
Malhotra, J. D., H. Miao, K. Zhang, A. Wolfson, S. Pennathur, S. W. Pipe and R. J. Kaufman (2008). "Antioxidants reduce endoplasmic reticulum stress and improve protein secretion." Proceedings of the National Academy of Sciences **105**(47): 18525-18530.
Marciniak, S. J., J. E. Chambers and D. Ron (2022). "Pharmacological targeting of endoplasmic reticulum stress in disease." Nat Rev Drug Discov **21**(2): 115-140.
Marciniak, S. J., C. Y. Yun, S. Oyadomari, I. Novoa, Y. Zhang, R. Jungreis, K. Nagata, H. P. Harding and D. Ron (2004). "CHOP induces death by promoting protein synthesis and oxidation in the stressed endoplasmic reticulum." Genes Dev **18**(24): 3066-3077.
Marcinowski, M., M. Rosam, C. Seitz, J. Elferich, J. Behnke, C. Bello, M. J. Feige, C. F. Becker, I. Antes and J. Buchner (2013). "Conformational selection in substrate recognition by Hsp70 chaperones." J Mol Biol **425**(3): 466-474.

Matus, S., L. H. Glimcher and C. Hetz (2011). "Protein folding stress in neurodegenerative diseases: a glimpse into the ER." Curr Opin Cell Biol **23**(2): 239-252.
Maurel, M., E. Chevet, J. Tavernier and S. Gerlo (2014). "Getting RIDD of RNA: IRE1 in cell fate regulation." Trends in Biochemical Sciences **39**(5): 245-254.
Maurel, M., J. Obacz, T. Avril, Y.-P. Ding, O. Papadodima, X. Treton, F. Daniel, E. Pilalis, J. Hörberg, W. Hou, M.-C. Beauchamp, J. Tourneur-Marsille, D. Cazals-Hatem, L. Sommerova, A. Samali, J. Tavernier, R. Hrstka, A. Dupont, D. Fessart, F. Delom, M. E. Fernandez-Zapico, G. Jansen, L. A. Eriksson, D. Y. Thomas, L. Jerome-Majewska, T. Hupp, A. Chatziioannou, E. Chevet and E. Ogier-Denis (2019). "Control of anterior GRadient 2 (AGR2) dimerization links endoplasmic reticulum proteostasis to inflammation." EMBO Molecular Medicine **11**(6): e10120.
Mezzacasa, A. and A. Helenius (2002). "The Transitional ER Defines a Boundary for Quality Control in the Secretion of tsO45 VSV Glycoprotein." Traffic **3**(11): 833-849.
Moenner, M., O. Pluquet, M. Bouchecareilh and E. Chevet (2007). "Integrated endoplasmic reticulum stress responses in cancer." Cancer Res **67**(22): 10631-10634.
Mohtar, M. A., L. Hernychova, J. R. O'Neill, M. L. Lawrence, E. Murray, B. Vojtesek and T. R. Hupp (2018). "The Sequence-specific Peptide-binding Activity of the Protein Sulfide Isomerase AGR2 Directs Its Stable Binding to the Oncogenic Receptor EpCAM." Mol Cell Proteomics **17**(4): 737-763.
Nadanaka, S., T. Okada, H. Yoshida and K. Mori (2007). "Role of disulfide bridges formed in the luminal domain of ATF6 in sensing endoplasmic reticulum stress." Mol Cell Biol **27**(3): 1027-1043.
Nadanaka, S., H. Yoshida and K. Mori (2006). "Reduction of disulfide bridges in the lumenal domain of ATF6 in response to glucose starvation." Cell Struct Funct **31**(2): 127-134.
Neurath, H. and K. A. Walsh (1976). "Role of proteolytic enzymes in biological regulation (a review)." Proceedings of the National Academy of Sciences **73**(11): 3825.
Nishitoh, H., M. Saitoh, Y. Mochida, K. Takeda, H. Nakano, M. Rothe, K. Miyazono and H. Ichijo (1998). "ASK1 is essential for JNK/SAPK activation by TRAF2." Mol Cell **2**(3): 389-395.
Nohturfft, A., R. A. DeBose-Boyd, S. Scheek, J. L. Goldstein and M. S. Brown (1999). "Sterols regulate cycling of SREBP cleavage-activating protein (SCAP) between endoplasmic reticulum and Golgi." Proc Natl Acad Sci U S A **96**(20): 11235-11240.
Oka, O. B., M. van Lith, J. Rudolf, W. Tungkum, M. A. Pringle and N. J. Bulleid (2019). "ERp18 regulates activation of ATF6alpha during unfolded protein response." EMBO J **38**(15): e100990.
Oka, O. B., M. van Lith, J. Rudolf, W. Tungkum, M. A. Pringle and N. J. Bulleid (2019). "ERp18 regulates activation of ATF6α during unfolded protein response." The EMBO Journal **38**(15): e100990.
Oka, O. B., H. Y. Yeoh and N. J. Bulleid (2015). "Thiol-disulfide exchange between the PDI family of oxidoreductases negates the requirement for an oxidase or reductase for each enzyme." Biochem J **469**(2): 279-288.
Oka, O. B. V., A. S. Pierre, M. A. Pringle, W. Tungkum, Z. Cao, B. Fleming and N. J. Bulleid (2022). "Activation of the UPR sensor ATF6α is regulated by its redox-dependent dimerization and ER retention by ERp18." Proceedings of the National Academy of Sciences **119**(12): e2122657119.

Oku, Y., M. Kariya, T. Fujimura, J. Hoseki and Y. Sakai (2021). "Homeostasis of the ER redox state subsequent to proteasome inhibition." Scientific Reports **11**(1): 8655.
Okumura, M., H. Kadokura and K. Inaba (2015). "Structures and functions of protein disulfide isomerase family members involved in proteostasis in the endoplasmic reticulum." Free Radic Biol Med **83**: 314-322.
Oslowski, C. M. and F. Urano (2011). "Measuring ER stress and the unfolded protein response using mammalian tissue culture system." Methods in enzymology **490**: 71-92.
Oyadomari, S., A. Koizumi, K. Takeda, T. Gotoh, S. Akira, E. Araki and M. Mori (2002). "Targeted disruption of the Chop gene delays endoplasmic reticulum stress–mediated diabetes." The Journal of Clinical Investigation **109**(4): 525-532.
Pandey, V. K., A. Mathur and P. Kakkar (2019). "Emerging role of Unfolded Protein Response (UPR) mediated proteotoxic apoptosis in diabetes." Life Sci **216**: 246-258.
Papa, F. R. (2012). "Endoplasmic reticulum stress, pancreatic ß-cell degeneration, and diabetes." Cold Spring Harb Perspect Med **2**(9): a007666.
Parveen, A., M. S. Akash, K. Rehman and W. W. Kyunn (2016). "Dual Role of p21 in the Progression of Cancer and Its Treatment." Crit Rev Eukaryot Gene Expr **26**(1): 49-62.
Pobre, K. F. R., G. J. Poet and L. M. Hendershot (2019). "The endoplasmic reticulum (ER) chaperone BiP is a master regulator of ER functions: Getting by with a little help from ERdj friends." J Biol Chem **294**(6): 2098-2108.
Poothong, J., P. Sopha, R. J. Kaufman and W. Tirasophon (2010). "Domain compatibility in Ire1 kinase is critical for the unfolded protein response." FEBS Lett **584**(14): 3203-3208.
Potelle, S., A. Klein and F. Foulquier (2015). "Golgi post-translational modifications and associated diseases." J Inherit Metab Dis **38**(4): 741-751.
Preissler, S., C. Rato, Y. Yan, L. A. Perera, A. Czako and D. Ron (2020). "Calcium depletion challenges endoplasmic reticulum proteostasis by destabilising BiP-substrate complexes." eLife **9**: e62601.
Preissler, S., L. Rohland, Y. Yan, R. Chen, R. J. Read and D. Ron (2017). "AMPylation targets the rate-limiting step of BiP's ATPase cycle for its functional inactivation." Elife **6**.
Presley, J. F., N. B. Cole, T. A. Schroer, K. Hirschberg, K. J. M. Zaal and J. Lippincott-Schwartz (1997). "ER-to-Golgi transport visualized in living cells." Nature **389**(6646): 81-85.
Prischi, F., P. R. Nowak, M. Carrara and M. M. Ali (2014). "Phosphoregulation of Ire1 RNase splicing activity." Nat Commun **5**: 3554.
Qin, J., G. M. Clore, W. M. Kennedy, J. R. Huth and A. M. Gronenborn (1995). "Solution structure of human thioredoxin in a mixed disulfide intermediate complex with its target peptide from the transcription factor NF kappa B." Structure **3**(3): 289-297.
Rabhi, N., E. Salas, P. Froguel and J.-S. Annicotte (2014). "Role of the Unfolded Protein Response in ß Cell Compensation and Failure during Diabetes." Journal of Diabetes Research **2014**: 795171.
Rana, S. V. S. (2020). "Endoplasmic Reticulum Stress Induced by Toxic Elements-a Review of Recent Developments." Biol Trace Elem Res **196**(1): 10-19.
Reily, C., T. J. Stewart, M. B. Renfrow and J. Novak (2019). "Glycosylation in health and disease." Nature Reviews Nephrology **15**(6): 346-366.
Ri, M., E. Tashiro, D. Oikawa, S. Shinjo, M. Tokuda, Y. Yokouchi, T. Narita, A. Masaki, A. Ito, J. Ding, S. Kusumoto, T. Ishida, H. Komatsu, Y. Shiotsu, R. Ueda,

T. Iwawaki, M. Imoto and S. Iida (2012). "Identification of Toyocamycin, an agent cytotoxic for multiple myeloma cells, as a potent inhibitor of ER stress-induced XBP1 mRNA splicing." Blood Cancer J **2**(7): e79.
Rowe, M. L., L. W. Ruddock, G. Kelly, J. M. Schmidt, R. A. Williamson and M. J. Howard (2009). "Solution Structure and Dynamics of ERp18, a Small Endoplasmic Reticulum Resident Oxidoreductase." Biochemistry **48**(21): 4596-4606.
Rowe, M. L., L. W. Ruddock, G. Kelly, J. M. Schmidt, R. A. Williamson and M. J. Howard (2009). "Solution structure and dynamics of ERp18, a small endoplasmic reticulum resident oxidoreductase." Biochemistry **48**(21): 4596-4606.
Ruggiano, A., O. Foresti and P. Carvalho (2014). "Quality control: ER-associated degradation: protein quality control and beyond." J Cell Biol **204**(6): 869-879.
Ruiz-Canada, C., D. J. Kelleher and R. Gilmore (2009). "Cotranslational and posttranslational N-glycosylation of polypeptides by distinct mammalian OST isoforms." Cell **136**(2): 272-283.
Sakai, J., A. Nohturfft, D. Cheng, Y. K. Ho, M. S. Brown and J. L. Goldstein (1997). "Identification of Complexes between the COOH-terminal Domains of Sterol Regulatory Element-binding Proteins (SREBPs) and SREBP Cleavage-Activating Protein." Journal of Biological Chemistry **272**(32): 20213-20221.
Sakai, J., A. Nohturfft, J. L. Goldstein and M. S. Brown (1998). "Cleavage of Sterol Regulatory Element-binding Proteins (SREBPs) at Site-1 Requires Interaction with SREBP Cleavage-activating Protein: EVIDENCE FROM IN VIVO COMPETITION STUDIES." Journal of Biological Chemistry **273**(10): 5785-5793.
Sato, B. K., D. Schulz, P. H. Do and R. Y. Hampton (2009). "Misfolded Membrane Proteins Are Specifically Recognized by the Transmembrane Domain of the Hrd1p Ubiquitin Ligase." Molecular Cell **34**(2): 212-222.
Sato, Y., S. Nadanaka, T. Okada, K. Okawa and K. Mori (2011). "Luminal domain of ATF6 alone is sufficient for sensing endoplasmic reticulum stress and subsequent transport to the Golgi apparatus." Cell Struct Funct **36**(1): 35-47.
Sawaya, M. R., S. Sambashivan, R. Nelson, M. I. Ivanova, S. A. Sievers, M. I. Apostol, M. J. Thompson, M. Balbirnie, J. J. W. Wiltzius, H. T. McFarlane, A. Ø. Madsen, C. Riekel and D. Eisenberg (2007). "Atomic structures of amyloid cross-β spines reveal varied steric zippers." Nature **447**(7143): 453-457.
Schindler, A. J. and R. Schekman (2009). "In vitro reconstitution of ER-stress induced ATF6 transport in COPII vesicles." Proceedings of the National Academy of Sciences **106**(42): 17775-17780.
Schröder, M. (2006). "The unfolded protein response." Molecular Biotechnology **34**(2): 279-290.
Schroder, M. and R. J. Kaufman (2005). "The mammalian unfolded protein response." Annu Rev Biochem **74**: 739-789.
Schröder, M. and R. J. Kaufman (2006). "Divergent roles of IRE1alpha and PERK in the unfolded protein response." Curr Mol Med **6**(1): 5-36.
Seglen, P. O., B. Grinde and A. E. Solheim (1979). "Inhibition of the lysosomal pathway of protein degradation in isolated rat hepatocytes by ammonia, methylamine, chloroquine and leupeptin." Eur J Biochem **95**(2): 215-225.
Shamu, C. E. and P. Walter (1996). "Oligomerization and phosphorylation of the Ire1p kinase during intracellular signaling from the endoplasmic reticulum to the nucleus." The EMBO Journal **15**(12): 3028-3039.
Shen, J., X. Chen, L. Hendershot and R. Prywes (2002). "ER stress regulation of ATF6 localization by dissociation of BiP/GRP78 binding and unmasking of Golgi localization signals." Dev Cell **3**(1): 99-111.

Shen, J., E. L. Snapp, J. Lippincott-Schwartz and R. Prywes (2005). "Stable binding of ATF6 to BiP in the endoplasmic reticulum stress response." Mol Cell Biol **25**(3): 921-932.
Short, B., A. Haas and F. A. Barr (2005). "Golgins and GTPases, giving identity and structure to the Golgi apparatus." Biochimica et Biophysica Acta (BBA) - Molecular Cell Research **1744**(3): 383-395.
Sisinni, L., M. Pietrafesa, S. Lepore, F. Maddalena, V. Condelli, F. Esposito and M. Landriscina (2019). "Endoplasmic Reticulum Stress and Unfolded Protein Response in Breast Cancer: The Balance between Apoptosis and Autophagy and Its Role in Drug Resistance." Int J Mol Sci **20**(4).
Siwecka, N., W. Rozpędek-Kamińska, A. Wawrzynkiewicz, D. Pytel, J. A. Diehl and I. Majsterek (2021). "The Structure, Activation and Signaling of IRE1 and Its Role in Determining Cell Fate." Biomedicines **9**(2).
Song, J., H. Tan, A. J. Perry, T. Akutsu, G. I. Webb, J. C. Whisstock and R. N. Pike (2012). "PROSPER: An Integrated Feature-Based Tool for Predicting Protease Substrate Cleavage Sites." PLOS ONE **7**(11): e50300.
Song, J., Y. Wang, F. Li, T. Akutsu, N. D. Rawlings, G. I. Webb and K.-C. Chou (2018). "iProt-Sub: a comprehensive package for accurately mapping and predicting protease-specific substrates and cleavage sites." Briefings in Bioinformatics **20**(2): 638-658.
Stanley, P. (2011). "Golgi glycosylation." Cold Spring Harbor perspectives in biology **3**(4): a005199.
Steiner, D. F. (2000). "New aspects of proinsulin physiology and pathophysiology." J Pediatr Endocrinol Metab **13**(3): 229-239.
Støy, J., E. L. Edghill, S. E. Flanagan, H. Ye, V. P. Paz, A. Pluzhnikov, J. E. Below, M. G. Hayes, N. J. Cox, G. M. Lipkind, R. B. Lipton, S. A. W. Greeley, A.-M. Patch, S. Ellard, D. F. Steiner, A. T. Hattersley, L. H. Philipson, G. I. Bell and n. null (2007). "Insulin gene mutations as a cause of permanent neonatal diabetes." Proceedings of the National Academy of Sciences **104**(38): 15040-15044.
Swain, J. F., G. Dinler, R. Sivendran, D. L. Montgomery, M. Stotz and L. M. Gierasch (2007). "Hsp70 Chaperone Ligands Control Domain Association via an Allosteric Mechanism Mediated by the Interdomain Linker." Molecular Cell **26**(1): 27-39.
Szegezdi, E., S. E. Logue, A. M. Gorman and A. Samali (2006). "Mediators of endoplasmic reticulum stress-induced apoptosis." EMBO Rep **7**(9): 880-885.
Szegezdi, E., D. C. Macdonald, N. C. T, S. Gupta and A. Samali (2009). "Bcl-2 family on guard at the ER." Am J Physiol Cell Physiol **296**(5): C941-953.
Tavender, T. J. and N. J. Bulleid (2010). "Peroxiredoxin IV protects cells from oxidative stress by removing H2O2 produced during disulphide formation." Journal of Cell Science **123**(15): 2672-2679.
Thomas, G. (2002). "Furin at the cutting edge: from protein traffic to embryogenesis and disease." Nature reviews. Molecular cell biology **3**(10): 753-766.
Thompson, N. and W. Wakarchuk (2022). "O-glycosylation and its role in therapeutic proteins." Biosci Rep **42**(10).
Thuerauf, D. J., L. Morrison and C. C. Glembotski (2004). "Opposing roles for ATF6alpha and ATF6beta in endoplasmic reticulum stress response gene induction." J Biol Chem **279**(20): 21078-21084.
Torres, S. E., C. M. Gallagher, L. Plate, M. Gupta, C. R. Liem, X. Guo, R. Tian, R. M. Stroud, M. Kampmann, J. S. Weissman and P. Walter (2019). "Ceapins block

the unfolded protein response sensor ATF6α by inducing a neomorphic inter-organelle tether." Elife **8**.
Tsaytler, P., H. P. Harding, D. Ron and A. Bertolotti (2011). "Selective inhibition of a regulatory subunit of protein phosphatase 1 restores proteostasis." Science **332**(6025): 91-94.
Tsuru, A., Y. Imai, M. Saito and K. Kohno (2016). "Novel mechanism of enhancing IRE1α-XBP1 signalling via the PERK-ATF4 pathway." Sci Rep **6**: 24217.
Urano, F., X. Wang, A. Bertolotti, Y. Zhang, P. Chung, H. P. Harding and D. Ron (2000). "Coupling of stress in the ER to activation of JNK protein kinases by transmembrane protein kinase IRE1." Science **287**(5453): 664-666.
Urban, S., J. R. Lee and M. Freeman (2001). "Drosophila Rhomboid-1 Defines a Family of Putative Intramembrane Serine Proteases." Cell **107**(2): 173-182.
Voeltz, G. K., M. M. Rolls and T. A. Rapoport (2002). "Structural organization of the endoplasmic reticulum." EMBO Rep **3**(10): 944-950.
Walter, P. and D. Ron (2011). "The Unfolded Protein Response: From Stress Pathway to Homeostatic Regulation." Science **334**(6059): 1081-1086.
Walter, P. and D. Ron (2011). "The unfolded protein response: from stress pathway to homeostatic regulation." Science **334**(6059): 1081-1086.
Wang, J., K. A. Pareja, C. A. Kaiser and C. S. Sevier (2014). "Redox signaling via the molecular chaperone BiP protects cells against endoplasmic reticulum-derived oxidative stress." Elife **3**: e03496.
Wang, J. and C. S. Sevier (2016). "Formation and Reversibility of BiP Protein Cysteine Oxidation Facilitate Cell Survival during and post Oxidative Stress." J Biol Chem **291**(14): 7541-7557.
Wang, M. and R. J. Kaufman (2016). "Protein misfolding in the endoplasmic reticulum as a conduit to human disease." Nature **529**(7586): 326-335.
Watson, P., A. K. Townley, P. Koka, K. J. Palmer and D. J. Stephens (2006). "Sec16 Defines Endoplasmic Reticulum Exit Sites and is Required for Secretory Cargo Export in Mammalian Cells." Traffic **7**(12): 1678-1687.
Wei, J. and L. M. Hendershot (1995). "Characterization of the nucleotide binding properties and ATPase activity of recombinant hamster BiP purified from bacteria." J Biol Chem **270**(44): 26670-26676.
Westermark, P., K. H. Johnson, T. D. O'Brien and C. Betsholtz (1992). "Islet amyloid polypeptide--a novel controversy in diabetes research." Diabetologia **35**(4): 297-303.
Wilson, J. and T. Hunt (2002). Molecular biology of the cell: a problems approach. Molecular biology of the cell: a problems approach**:** 4th. ed-4th. ed.
Xu, Y., M. Cai, Y. Yang, L. Huang and Y. Ye (2012). "SGTA Recognizes a Noncanonical Ubiquitin-like Domain in the Bag6-Ubl4A-Trc35 Complex to Promote Endoplasmic Reticulum-Associated Degradation." Cell Reports **2**(6): 1633-1644.
Yamaguchi, H. (2002). "Chaperone-Like Functions of N-Glycans in the Formation and Stabilization of Protein Conformation." Trends in Glycoscience and Glycotechnology **14**(77): 139-151.
Yan, Y., C. Rato, L. Rohland, S. Preissler and D. Ron (2019). "MANF antagonizes nucleotide exchange by the endoplasmic reticulum chaperone BiP." Nature Communications **10**(1): 541.
Yang, J., Y. Zong, J. Su, H. Li, H. Zhu, L. Columbus, L. Zhou and Q. Liu (2017). "Conformation transitions of the polypeptide-binding pocket support an active substrate release from Hsp70s." Nat Commun **8**(1): 1201.

Ye, J., R. B. Rawson, R. Komuro, X. Chen, U. P. Davé, R. Prywes, M. S. Brown and J. L. Goldstein (2000). "ER stress induces cleavage of membrane-bound ATF6 by the same proteases that process SREBPs." Mol Cell **6**(6): 1355-1364.
Yoshida, H., T. Okada, K. Haze, H. Yanagi, T. Yura, M. Negishi and K. Mori (2000). "ATF6 activated by proteolysis binds in the presence of NF-Y (CBF) directly to the cis-acting element responsible for the mammalian unfolded protein response." Mol Cell Biol **20**(18): 6755-6767.
Youle, R. J. and A. Strasser (2008). "The BCL-2 protein family: opposing activities that mediate cell death." Nat Rev Mol Cell Biol **9**(1): 47-59.
Zhu, X., X. Zhao, W. F. Burkholder, A. Gragerov, C. M. Ogata, M. E. Gottesman and W. A. Hendrickson (1996). "Structural analysis of substrate binding by the molecular chaperone DnaK." Science **272**(5268): 1606-1614.